Intensified Post-Combustion Carbon Capture using a Pilot Scale Rotating Packed Bed and Monoethanolamine Solutions

---

By

Toluwanimi Oluwatomiwo Kolawole

Thesis submitted in partial fulfilment for the degree of PhD in the Faculty of Science, Agriculture and Engineering of Newcastle University

School of Engineering

July,2019

Abstract

Post-combustion carbon capture with the rotating packed bed (RPB) is an alternative way of industrial carbon capture that offer considerable advantages in comparison to conventional absorption columns. Due to the enhancement of mass transfer by harnessing high gravity (HIGEE) forces within the RPB, absorbers that are more compact can be designed for CO_2 capture. This will result in significant cost savings in size and space required. This thesis deals with the experimental study of three different RPB gas-flow modes (counter-current, co-current and cross-flow) for CO_2 capture with aqueous monoethanolamine (MEA) solutions.

A systematic study was carried out on a newly constructed RPB to determine the performance of each gas-flow contact mode for CO_2 absorption from simulated flue gas. The important operation parameters for the CO_2 absorption experiments were the rotational speed, liquid-gas (L/G) ratios and the MEA concentration that were varied within the typical industrial range for CO_2 scrubbing from flue gas. In addition, the gas phase was saturated, as would be the case for industrial flue gas. The performance of the RPB configurations was evaluated with respect to overall gas mass transfer coefficients (K_Ga), the CO_2 capture efficiency, height of transfer unit (HTU) and the pressure drop. Furthermore, a commercial scale-up design using the experimental results was carried out to determine the absorber sizes of the RPB configuration to be deployed for an industrial CO_2 capture case study.

The results clearly show that the each of the variables influenced CO_2 capture efficiency, overall mass transfer coefficient and HTU values. It was also found that the gas flow mode of the RPB had an effect on the liquid flow properties within the RPB. It also influenced the effective contact between the liquid and gas thereby affecting the mass transfer performance. An important conclusion from the experimental study is that the counter-current showed the best performance for mass transfer, CO_2 capture efficiency and HTU due to it being the RPB mode that best harnessed the HIGEE forces within the RPB. This is because it possesses the greatest driving force for mass transfer and better liquid-gas contact due to the counter-current contact of the liquid and gas. The cross-flow RPB also displayed the best performance with respect to pressure drop and better performance than the co-current RPB did.

The experimental results were utilized for sizing a RPB absorber for an intensified CO_2 capture demonstration plant from industrial flue gas. The design results showed that the

counter-current RPB was the preferable design with respect to deriving maximum mass transfer advantages for commercial deployment but it has the drawback of high pressure drop. The cross-flow had the most compact RPB absorber size and provided the lowest pressure and power consumption. This shows that the cross-flow RPB is a viable alternative to the counter-current RPB for commercial CO_2 carbon capture. However, designing a cross-flow RPB is more challenging.

Dedication

To my heavenly Father,

The eternal king, immortal, invisible, the Almighty only wise God and saviour, Jesus Christ

All to Him I owe

To Him be honour and glory forever and ever.

Amen

Acknowledgement

I wish to express my deepest gratitude to my supervisor, Dr. Jonathan Lee for his excellent supervision and support throughout my doctorate degree. I wish to thank the technical staff: Michael Percival, Rob Dixon, Ian Ditchburn, Ian Strong, and Brian Grover for their invaluable help with the experimental facility and their support to help complete this work. I also wish to recognize the important contributions made by Dr Pierrot Attidekou, Dr. James Hendry, James Bates, Laura O'Neill and Augustine Chantrelle to my work.

I wish to express my deepest gratitude to my dear parents; Mr and Mrs Kolawole for their generous financial support to enable me to undertake this program and their constant prayers, love and encouragement that saw me through this program. I also wish to thank my two sisters, Boluwajo and Boluwarin for their love, encouragement and support. I am deeply grateful to my uncles, Mr Akintunde Ojo and Mr Boluwarin Ojo and their families as well as my aunt, Mrs Eunice Akinbami for supporting me all along the way.

I like to extend my deep appreciation to the members of my local church, Deeper Life Bible Church, my youth group; New Life Youth and especially to my local pastor, Pastor Sam Ohiomokhare and his wife.I am also grateful to my dear friends who have been incredibly supportive of my research throughout my stay in Newcastle: Kemi, Xenia, Komo, Believe, Henry, Chukwuma, Sahr and many others too numerous to mention.

Table of Contents

List of Figures

List of Tables

List of Symbols

Uppercase Latin symbols

Symbol	**Meaning**	**Unit**
$K_G a_e$	Overall gas mass transfer coefficient	s^{-1}
A	Cross-sectional area	m^2
D	Diffusivity	$m^2\ s^{-1}$
E	Enhancement	
C	Molar Concentration	mol dm^{-1}
F	Force	N
G′	Molar gas flow rate	mol s^{-1}
L′	Molar liquid flow rate	mol s^{-1}
H	Henry's constant	Pa m^3 mol^{-1}
H	Height	m
L	Torque arm length	m
L	Liquid flow rate	$m^3\ s^{-1}$
P	Pressure	Pa
P	Power	W
*P**	Equilibrium partial pressure	Pa
ΔP	Pressure drop across the packing	Pa m^{-1}
R	Radius	m
S	Stripping factor	
T	Temperature	K
Q_G	Gas volumetric flow rate	m^3/s
V	Volume	m^3
Z	Axial length	m

Lowercase Latin symbol

Symbol	**Meaning**	**Unit**
r_o	Outer radius	m
r_i	Inner radius	m
a_e	Interficial surface area	$m^2\ m^{-3}$
p	Partial pressure	Pa
x	Liquid Mole Fraction	
$y_{co2,\,in}$	Inlet gas feed CO_2 concentration	
$y_{co2,\,out}$	Outlet gas feed CO_2 concentration	

$\boldsymbol{p}$	Liquid jet to exit gas kinetic energy ratio	
g	Gravitational acceleration	m s^{-2}

Greek symbols

Symbol	Meaning	Unit
ω	Angular velocity	rad s^{-1}
$\boldsymbol{ø}$	Cavity zone contribution	
$\boldsymbol{\mu_{gas}}$	Gas viscosity	Pa s
ϵ	porosity	
$\boldsymbol{\beta}$	Rotational speed	rpm
$\cap_{\boldsymbol{fan}}$	Fan efficiency	%
$\boldsymbol{\rho_G}$	Gas density	kg m^{-3}
$\boldsymbol{\rho_L}$	Liquid density	kg m^{-3}

Abbreviations

Abbreviation	Meaning
AEEA	Aminoethylethanolamine
MEA	Monoethanolamine
DEA	Diethanolamine
RPB	Rotating packed bed
PCC	Post-combustion carbon capture
RPB	Rotating packed bed
MDEA	N-methyldiethanolamine
IEAGHG	International Energy Agency Greenhouse Gas Program
GHG	Greenhouse gases
CCS	Carbon capture and storage
PZ	Piperazine
AMP	2-Amino-2-methyl-1-propanol
MDEA	Methyldiethanolamine
NTU	Number of transfer unit
HTU	Height of transfer units

Chapter 1. Introduction

1.1 Mitigating global anthropogenic CO_2 emissions

Global warming due to anthropogenic CO_2 emissions poses long-term risk to the planet (Eldardiry and Habib, 2018). The negative impact of global warming is demonstrated by extreme weather events, worsening droughts and floods, rising sea levels and adverse effects on marine species (Rafiee *et al.*, 2018). Recognising the urgency of reversing rising CO_2 emissions globally and its effects on climate, national governments adopted the Paris Agreement in 2015 under the United Nations Framework Convention on Climate Change (UNFCC) to limit global average temperature rise to below 2^{o}C above pre-industrial age levels (IEA/OECD, 2016). Combating CO_2 emissions requires various abatement strategies such as switching to renewable energy, carbon capture and storage (CCS), reducing global energy consumption and switching to less carbon-intensive fuels among others (Eldardiry and Habib, 2018).

The growth in the use of fossil fuels for electricity generation especially in rapidly developing countries has significantly contributed to the increase in CO_2 emissions (Greenblatt *et al.*, 2017; Aghaie *et al.*, 2018). The use of fossil fuels such as coal and natural gas for electricity generation contributes over 70% of the total global CO_2 emissions (Olivier *et al.*, 2016). Coal-fired power plants alone account for close to one-third of the CO_2 emissions from power generation (Olivier *et al.*, 2016; Aghaie *et al.*, 2018). Fossil fuels are widely used for electricity generation because they are cheap, abundantly available, widely distributed geographically and easily exploitable with existing technology (Florin and Fennell, 2010; Greenblatt *et al.*, 2017). Although other alternative energy sources such as renewable energy have shown great potential to replace fossil fuels, they are not yet fully reliable and in some areas not able to effectively compete with cheap fossil fuels (IEA/OECD, 2016). Moreover, energy systems made up of 100% renewable energy sources are not yet feasible in the short to medium term globally (IEA/OECD, 2016). This makes the use of fossil fuels for electricity generation likely to continue for the near future even as efforts continue towards a full transition from fossil fuels to renewable sources. As a result, there have been intensive research

efforts geared towards reducing CO_2 emissions from existing and future power plants (Garg *et al.*, 2018).

CCS technology has been identified by IEA (2016) to be the most effective approach for mitigating CO_2 emissions from existing power plants. This is also supported by Aghaie *et al.* (2018) and Eldardiry and Habib (2018) who suggested that CCS is the most viable approach to reduce CO_2 emissions from existing fossil-fuel power plants. This is because it can be retrofitted easily to the existing infrastructure causing minimum disruption (Eldardiry and Habib, 2018). CCS may also be the most feasible option to reduce CO_2 emissions from industries such as iron and steel smelting, cement production, natural gas processing and petrochemical refining that produce considerable CO_2 emissions (IEAGHG, 2014). Consequently, the deployment of CCS is considered vital to reduce CO_2 emissions from power plants and other industrial plants (Karimi and Khalilpour, 2015). Furthermore, several studies have suggested that the Paris Agreement target to keep global atmospheric temperature well below 2 °C will not be realized without the deployment of large-scale CCS technologies (IPCC, 2014; Rogelj *et al.*, 2016; Peters *et al.*, 2017). In addition to existing CCS facilities, it is estimated that around 2500 large-scale CCS facilities will be needed globally by 2040 to reach the emission targets of the agreement (GCCSI, 2017).

1.2 Approaches to CO_2 capture

CCS is made of up of three major parts: capturing CO_2, transporting it and injecting it into storage sites for long-term storage (Eldardiry and Habib, 2018). The process of capturing CO_2 can be grouped into three broad categories which are capturing CO_2 before fuel combustion (pre-combustion capture), after combustion (post-combustion capture) or combustion in a pure stream of O_2 (oxy-fuel capture) (Rafiee *et al.*, 2018).

1.2.1 Pre-combustion capture

In this approach, CO_2 emission is prevented during combustion (Leonard, 2013). The fossil fuel to be combusted is converted into CO_2 and H_2 via steam reforming or gasification process as shown in Figure 1.1. The CO_2 from the process is captured and the hydrogen used as fuel to generate electricity. When gasification and electricity generation

from H_2 occur in the same process using gas and steam turbines, this is known as Integrated Gasification Combined Cycle (IGCC) (Pachauri and Reisinger, 2007).The CO_2 content produced as a result of this process is usually very significant and physical absorption /separation between H_2 and CO_2 can be applied. The high pressure of the CO_2 and H_2 stream results in CO_2 production at high pressure thereby reducing compression costs. However, it is technologically not applicable for retrofitting to existing power plants (Pachauri and Reisinger, 2007).

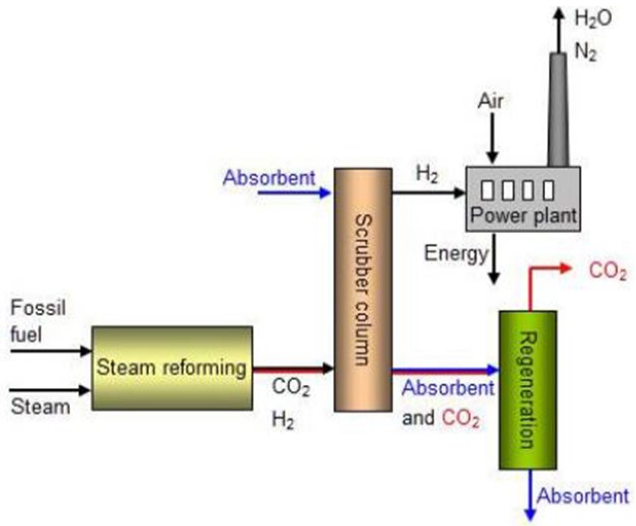

Figure 1.1: Schematic diagram of the pre-combustion capture (Leonard, 2013).

1.2.2 Oxy-fuel combustion capture

The oxy-fuel CO_2 capture as shown in Figure 1.2 is the combustion of fossil fuels in a pure stream of O_2 instead of air resulting in a flue gas of very high concentration of CO_2 and water vapour (Stanger *et al.*, 2015). This is because it is not diluted by the presence of N_2 in the air. An advanced form of oxy-combustion is chemical looping combustion (Leonard, 2013). This is a catalysed combustion with O_2 in which dual reactors are used for combustion (Buhre *et al.*, 2005). In the first reactor, a metal is oxidised with air, and the produced metal oxide is taken to a second reactor where it reacts with the fuel in a catalytic combustion (Toftegaard *et al.*, 2010). The fuel is oxidised and the metal oxide reduced (Normann *et al.*, 2009). The reaction in the first reactor is exothermic and the produced heat is used partially for power generation and partially recycled to the second

reactor with the metal oxide. The technology also eliminates direct contact between fuel and air using a metal oxide carrier such as oxides of iron, nickel or copper for oxygen transfer for fuel combustion (Florin and Fennell, 2010). The challenges with this approach include identifying suitable metals that can be an oxygen carrier, handling of solid streams as well as the limiting reaction kinetics of metal oxide reduction (Leonard, 2013).

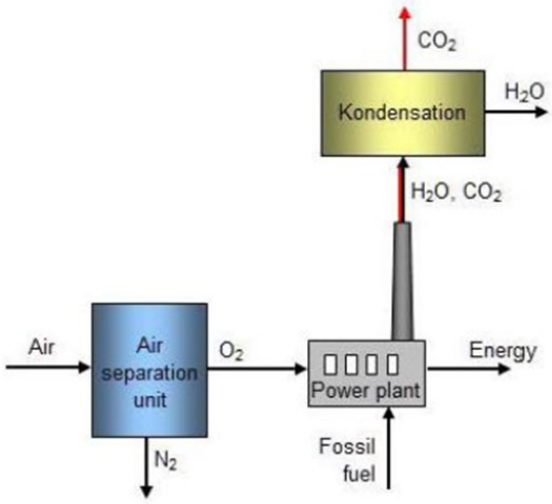

Figure 1.2: Simple schematic diagram of oxy-fuel CO_2 capture (Leonard, 2013).

1.2.3 Post-combustion capture

Post-combustion capture (PCC) involves the selective separation of CO_2 from flue gases (usually 5-15 vol% CO_2) after fossil fuel combustion (Yu *et al.*, 2012). It can be carried out using different methods such as physical absorption, chemical absorption, membrane separation, physical adsorption and chemical adsorption process. Physical absorption involves the use of physical solvents to capture CO_2 from a gas stream. The solvent absorbs CO_2 under high partial pressure and low temperature based on Henry's law (D'Alessandro *et al.*, 2010). They are suitable for capturing CO_2 from streams with high CO_2 partial pressure and are not economical for gas streams with less than 15 % vol CO_2 (Wang et al, 2011). The physical solvent is then desorbed at reduced pressure and increased temperature (Yu et al, 2012). Physical absorption has been extensively used in industry for years for various industrial processes such as natural gas sweetening,

synthesis and hydrogen gas production with high CO_2 contents (Yu et al, 2012). There are numerous types of physical absorbents processes such as Selexol (a mixture of dimethylethers of polyethylene glycol), rectinol (methanol), Purisol (N-methypyrrolidone), and Fluor process (propylene carbonate) amongst others. The Selexol and Rectinol process are used industrially in natural gas sweetening and synthesis gas treatment. The advantages of these processes are lower energy consumption in solvent regeneration, low toxicity and low corrosive solvents (Yu et al, 2012). An example of a physical absorbent that has recently generated research interest is ionic liquids. Ionic liquids have become very important physical solvents for CO_2 capture and have the potential to minimize energy requirements. Ionic liquids usually need to be designed for the specific task they are intended and although task specific ionic liquids for CO_2 absorption have been developed, they are very expensive and their manufacturing process is complex (Florin and Fennell, 2010).

Another PCC physical absorption separation process is the use of membrane separation technology that involves the selective permeation of flue gases through a material. The membrane separation process is driven by pressure difference achieved either via compression of the feed stream or creating a vacuum downstream. A number of material types such as metallic and ceramic membranes have a range of applications relevant to CO_2 capture systems (Florin and Fennell, 2010). Physical or chemical adsorption PCC involve a gas attaching to a solid surface known as the adsorbent. In the case of physical adsorption, the gas attaches to the solid surface in a physical process while it is chemical bound to the adsorptive surface in the chemical process. The adsorbent can then be regenerated either by application of heat (temperature swing adsorption) or reducing the pressure (pressure swing adsorption) (Wang *et al.*, 2011b). Physical adsorbents include zeolites, metal oxides, activated carbon, carbon molecular sieves and metal-organic frameworks (MOFs) (D'Alessandro *et al.*, 2010). Chemical adsorbents include amine-impregnated adsorbent and carbonaceous materials. (Florin and Fennell, 2010). While the adsorption process has the advantages of low energy penalty for stripping the captured CO_2, it is considered to be unsuitable for power plants as the low adsorption capacity of most available adsorbents will pose significant challenges at such a large scale (Wang *et al.*, 2011b).

Chemical absorption PCC as shown in Figure 1.3 involves the absorption of CO_2 from a flue gas stream using reactive solvents such as amines, sodium hydroxide and ammonia. The reaction of the reactive solvent and the CO_2 in the flue gas forms reaction products that can then be reversed by the application of heat or pressure. The solvent is thermally regenerated in a stripper to give a pure stream of CO_2 after which, the lean absorbent (absorbent from which CO_2 has been removed) is taken back to the absorber for another absorption cycle. However, the process comes with a high energy penalty as CO_2 regeneration after separation is energy intensive and accounts for about 75-80% of total costs (Florin and Fennell, 2010). The most industrially used solvent and widely recognised as the primary solvent for CO_2 capture is MEA.

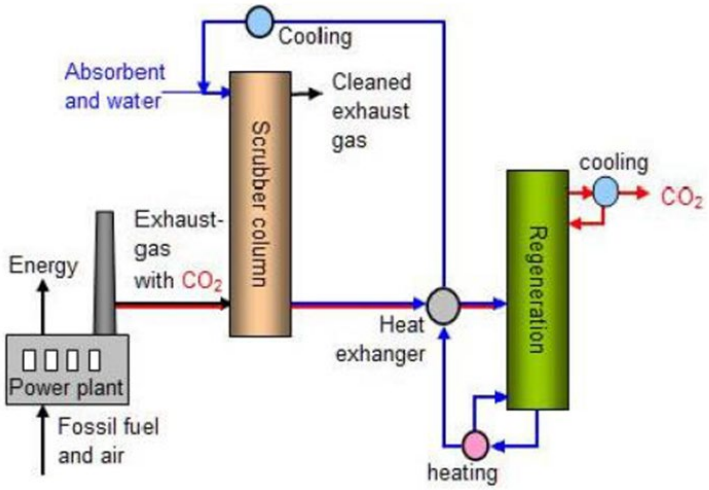

Figure 1.3: Simple schematic diagram of PCC with chemical absorption (Leonard, 2013).

Amine-based PCC process involves capturing CO_2 from flue gas using highly reactive aqueous amine solutions such as MEA. It is well known in the chemical industry for acid gas scrubbing and has been extensively studied for decades (Aghaie *et al.*, 2018). It is considered a mature technology and has been suggested to be ideally suited for flue gas conditions from fossil-fuel power plants (low CO_2 partial pressure) (Liu *et al.*, 2017). It can also be easily retrofitted without significant changes to the plant (McDonough, 2013). It also has the advantages of simple operation, high absorption efficiency and high economic value (Peng *et al.*, 2012). Moreover, it is appropriate for situations where large

volumes of gases have to be treated at atmospheric pressure such as those from fossil-fuel power plants (Chakravarti S. *et al.*, 2001).

1.3 Conventional PCC process

In conventional PCC process using MEA, pre-cooled flue gas from a power plant enters the absorber at near atmospheric pressure and the CO_2 is bound chemically to the chemical solvent in the absorber. This is usually done at temperatures between 40-60ºC. The 'rich' solvent containing the chemically bound CO_2 is then taken to a stripper to be regenerated. As illustrated in Figure 1.4, the lean solvent solution coming from the stripper is contacted in a counter-current mode with the flue gas, and the aqueous MEA solution (usually 30 wt%) chemically absorbs the CO_2 in the stream.

This absorption involves the reaction of CO_2 to form carbonate or bicarbonate and other chemical species. As this is an exothermic reaction, there is need for inter-stage cooling in the contact towers so as to maintain a high absorption efficiency (Sreenivasulu *et al.*, 2015). The rich solvent then exits at the bottom of the absorber and is pumped to the top of the stripper operating usually between 100-150˚C under a thermal swing operation. At the bottom of the stripper is the reboiler that generates steam to strip the CO_2 rich solvent as it flows down the stripper. The temperature swing reverses the CO_2 reaction with the solvent and returns the bound CO_2 molecules in the chemical solvent to the gas phase. As the regeneration process of the chemical solvent involves heating up to 100ºC-150ºC by supplying heat to the reboiler to reverse the reaction between CO_2 and MEA which usually results in a high thermal penalty. The CO_2 released is then compressed and transported while the regenerated solvent (lean) solution is returned back to the absorber column, passing through a heat exchanger to transfer heat to the rich solvent coming from the absorber (Wang *et al.*, 2015).

PCC is most commonly done with packed columns but there are other absorber configurations reported in literature for CO_2 absorption including, bubble columns, tray towers and RPBs. There has been extensive research work geared towards the development of efficient gas-liquid contactor configurations for CO_2 capture, solvent

systems and configurations of strippers where the objectives have been to achieve high capture efficiency and reduce energy penalty of the capture process to the minimum.

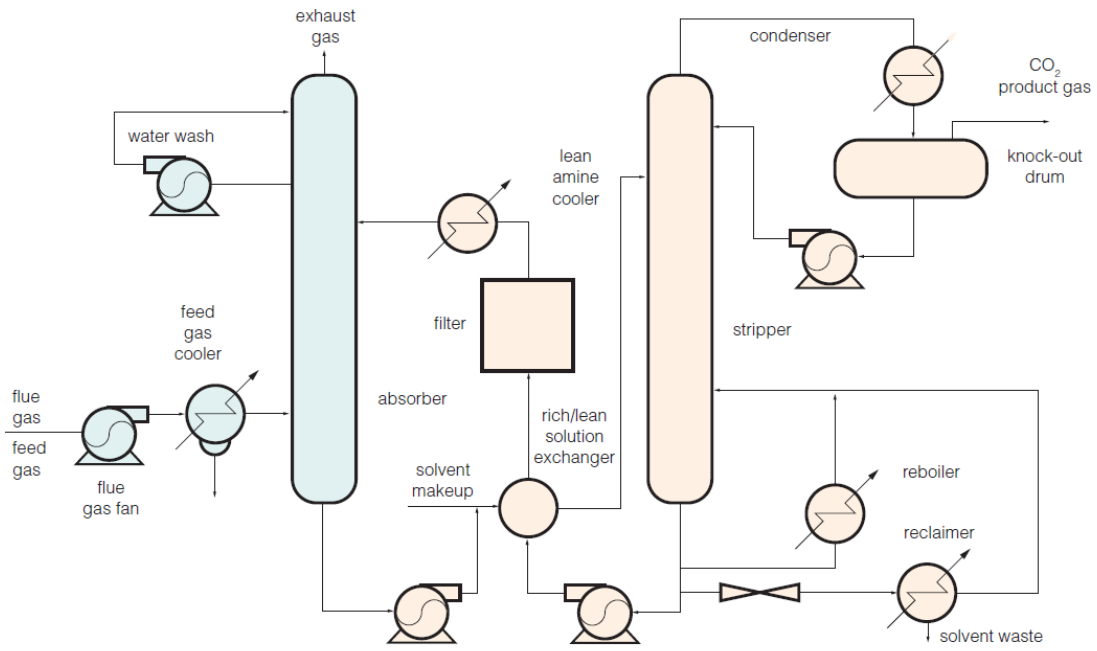

Figure 1.4: A process flow diagram of PCC process using aqueous MEA solutions in a conventional packed column (Davidson, 2007).

According to Sreenivasulu *et al.* (2015), the important factors that significantly influence efficiency of the carbon capture process are the composition of the flue gas, the flue gas temperature and the regeneration energy penalty during the desorption process. In addition, other factors that influence the CO_2 absorption process are the physical properties of the solvent, the gas and liquid flow rates, the partial pressure of CO_2, the total pressure of the system, temperature, the concentration of the solvent, the nature of the packing used and the CO_2 loading in the solvent.

PCC capture using MEA has been demonstrated in numerous pilot-plant scale projects and some commercial facilities such as the SaskPower Boundary Dam project in Saskatchewan, Canada (Yu *et al.*, 2012; IEAGHG, 2015). Despite the progress made in the commercial deployment of the technology, adoption has remained slow due to high capital and operational costs, corrosion issues and solvent losses due to degradation

(Rafiee *et al.*, 2018). The high capital costs are due to the large absorber sizes that result from the significant mass transfer resistances that need to be overcome in conventional gas-liquid contacting technologies such as packed columns. Furthermore, significant energy penalty is introduced when power plants are retrofitted with amine-based PCC process which can have an energy penalty in the range of 10-40% of the total electricity generated (Metz *et al.*, 2005). In a bid to lower capital costs from equipment sizes, process intensification (PI) has generated significant research interest to achieve costs reduction and make amine-based PCC more economically attractive.

1.4 Process intensification of PCC using the RPB

Process intensification (PI) as an approach is employed to reduce capital costs of chemical processes, enhance efficiency and safety without compromising capacity (Reay *et al.*, 2011). This is usually achieved via the improvement of heat and mass transfer by generating better contacts between fluids and increasing heat and mass transfer rates by harnessing fast mixing (Hassan-beck, 1997). There are various PI technologies such as spinning disk reactors, oscillatory baffled reactors, microchannel reactors, static mixers and high-gravity contactors (HIGEE). This equipment seeks to improve process performance by reducing equipment sizes using an intensified field such as centrifugal, electrical or microwave. Furthermore, they also integrate multiple processing tasks into a single unit (Wang *et al.*, 2015).

PI technologies vary in their functions and areas of applications and can be applicable for intensifying heat transfer or mass transfer. HIGEE contactors are an example of mass transfer intensification equipment that exploit high-gravity fields to intensify gas-liquid mass transfer (Cortes Garcia *et al.*, 2017). HIGEE contactors generate fields that are 100-1000 times the strength of terrestrial gravity in order to enhance the rate of mass transfer by 1-2 orders of magnitude. Under the influence of this high gravity field, the liquid within the HIGEE field flows as thin films and tiny droplets. This enhances gas-liquid contact and therefore mass transfer, due to the larger contact area and intensive mixing between the gas and liquid phases (Zhao *et al.*, 2016). This leads to potential equipment size reductions of up to 10 times in comparison to conventional columns for the same

process. The most common example of a HIGEE contactor is the rotating packed bed (RPB).

The RPB intensifies mass transfer by harnessing the idea that increasing the centrifugal acceleration of multiphase fluids would increase their slip velocity (Jassim, 2002). This is due to the dynamic behaviour of multiphase fluids being determined by the interphase buoyancy factor $\Delta\rho g$ (Ramshaw and Mallinson, 1981). This improves the flooding characteristics and interfacial shear stress and thereby increases the rate of interphase mass transfer (Jassim et al., 2007). RPBs have shown higher mass transfer results which is due to increased gas-liquid contact and high centrifugal fields generated within the RPB (Wang *et al.*, 2015). Therefore, it shows a lot of potential to reduce equipment sizes, save energy and lower capital costs for the amine-based PCC (Yu and Tan, 2013; Jiao *et al.*, 2017). Moreover, it can also potentially overcome viscosity issues that will arise from using higher concentration amine in conventional absorbers. This is because RPBs are usually constructed with stainless steel resistant to corrosion and rotate at high speeds which means higher amine solution strengths could be used without significantly impacting the rate of mass transfer (Jassim, 2002).

Although there has been considerable research interest in the application of RPBs for PCC in recent years, it has not been deployed industrially (Pan *et al.*, 2017). Currently, here are no commercial CO_2 capture projects using RPB absorbers reported in literature (Wang *et al.*, 2011a; Pan *et al.*, 2017; Xie *et al.*, 2019). Several reviews of the state of the technology have given the reason for this to include evaluation of RPB performance for PCC in terms of gas-flow configurations. Other reasons include carrying out experimental studies for a fully intensified PCC process that include the absorber, pressure drop, power consumption, systematic solvent screening for intensified PCC process, detailed techno-economic studies and simulation modules for commercial process simulators (Zhao *et al.*, 2010; Wang *et al.*, 2011a; Hu *et al.*, 2013; Wang *et al.*, 2015; Zhao *et al.*, 2016; Cortes Garcia *et al.*, 2017; Jiao *et al.*, 2017; Pan *et al.*, 2017). It is also important to determine the critical point for the trade-off between power consumption and increasing rotating speed for enhancing mass transfer in the RPB as power consumption would be critical for making the case for the advantage of

commercial scale RPBs over conventional PCC. Another challenge is the large variation that exists in literature on RPBs used for experimental studies (in terms of flow area and the radial centrifugal force). This makes the mass transfer coefficients usually reported in literature not comparable and of limited use for design for industrial deployment (Cortes Garcia *et al.*, 2017). Furthermore, experimental results reported in literature have not saturated the gas phase as would be expected in industrial flue gas but have only used dry gas.

1.5 Thesis aim and objectives

The detailed study of the performance of the three gas-flow contact mode in the RPB for CO_2 capture with respect to mass transfer and CO_2 capture efficiency is significant for the optimum design and scale-up of the RPB. At present, existing experimental RPB studies have not made a systematic comparison of the three RPB gas-flow modes. Although various studies have assisted in forming some understanding of the performance of these RPB modes, there are still some challenges that need to be overcome before accurate scale-up and industrial deployment of the RPB can be carried out. In particular, these include carrying out a comparative study of the three RPB configurations, using saturated gas phase as would be the case for industrial flue gas, investigating the pressure drop of the RPBs when used for CO_2 capture and not just dry pressure drop in the RPB. Such a study would contribute vital experimental data relevant for scaling-up the RPB commercial deployment.

The aim of this research work is to carry out a study to investigate the performance of a pilot-scale RPB in three gas-flow configurations (counter-current, co-current and cross-flow) for CO_2 absorption with aqueous MEA solutions.

The specific objectives are:

- To investigate the overall gas-side mass transfer, CO_2 capture and HTU performance of three RPB configurations by carrying out CO_2 absorption studies using aqueous MEA solutions at 30 wt%, 50 wt% and 70 wt%.

- To investigate the effects of rotational speed, liquid-gas ratio (L/G) by wt% and MEA solution concentration on CO_2 capture efficiency, overall gas –phase mass transfer, height of transfer unit (HTU) for the three different RPB gas flow configurations.
- To investigate the experimental pressure drop of the three RPB configurations during the CO_2 absorption mass transfer experiments.
- To estimate the absorber sizes for a potential CO_2 capture demonstration project using a RPB using the results of the performance study in this work.
- To evaluate the three RPB configuration for scale-up by comparing the performance of the three RPB configurations in terms of size, mass transfer and pressure drop.

1.6 Outline of the thesis

The thesis is divided into eight chapters. Chapter 1 introduces the challenge of global warming and climate change, CCS and the approaches to CO_2 capture as well as a detailed description of the PCC process. Also, the aim and objectives of the work are highlighted. In Chapter 2, the economic and technical considerations for the application of the RPB for CO_2 capture is provided as well as a detailed background of PCC and PCC technologies. In addition, an overview of the theory and applications of packed bed technologies, absorption mass transfer process and process intensification of CO_2 capture using RPBs is provided. The mechanism of the reaction of CO_2 with amine solutions at different strengths is also described as well as residence time in the RPB. A summary of the research gaps found in literature is provided that serves as the motivation for this study.

Chapter 3 describes the experimental facility and the three gas flow configurations used in this work as well as the experimental procedure for the absorption runs. This experimental facility is novel because it employs a humidifier to wet the gas phase. The experimental validation of the RPB is provided in Chapter 4. To validate the new facility, preliminary mass transfer absorption runs with aqueous MEA solutions (30wt %, 50wt%, 90 wt%) at 40^{o}C were measured. Troubleshooting the issues identified in the run was carried out. After this, CO_2 absorption experiments were conducted with the RPB in the counter-current gas-flow configuration using MEA solutions ranging from 30wt%-

70wt%. In chapter 5, the co-current RPB configuration is investigated for CO_2 absorption with MEA solutions at different concentrations. Chapter 6 presents the work done on the cross-flow RPB and presents the performance of the cross-flow RPB with respect to HTU mass transfer, CO_2 capture efficiency and pressure drop. A comparison of the three different RPB configurations and scale-up calculations for a full-scale RPB facility for PCC are presented in Chapter 7. Chapter 8 presents the conclusions drawn from the experimental studies done in the thesis and provides recommendations for future work.

Chapter 2. Literature review

2.1 Process intensification of CO_2 capture

2.1.1 Economic considerations of PI application for PCC

In recent years, there has been a growing demand for highly efficient and low-cost CO_2 capture technology within the context of global CO_2 emissions abatement (Xie *et al.*, 2019). Due to the limitation of the relatively slow mass transfer of the conventional PCC, the application of process intensification (PI) to PCC has been regarded as a promising alternative to the use of packed columns (Yan and Chen, 2010; Biliyok *et al.*, 2012; Xie *et al.*, 2019). The concept of PI was pioneered in the 1970s by Ramshaw and Mallinson (1981) at ICI with the aim of achieving size reduction for industrial process equipment. Reay (2008) defined PI as developments in engineering that result in substantial reduction in the size of units with more efficient operation, less environmental footprint and improved safety. This is driven by the goal of achieving capital cost reduction and other benefits such as process integration and inventory reduction achieved via a combination of intensified equipment and novel processing methods. In recent years, the reduction of capital and operating costs of CO_2 capture as well as reduced energy penalty have gained considerable attention (Songolzadeh *et al.*, 2014). Conventional CO_2 scrubbing with gas-liquid contactors such as packed columns and spray columns have required large absorber sizes due to low mass transfer efficiency and low throughput (Ma and Chen, 2016). Lawal *et al.* (2012) carried out a modelling study of a 500 MW sub-critical coal-fired power plant and their results showed that two absorbers of 27 m in packing height and 9 m in diameter were required to separate CO_2 from the flue gas stream. Due to high capital costs of constructing such large absorbers, applying PI to the PCC process has become very attractive because of its potential to save cost by reducing absorber sizes and space requirements.

Wang *et al.* (2015) suggested that the rotating packed bed (RPB) is the most suitable PI technology for intensification of PCC due to its high mass transfer performance compared to other mass transfer devices such as spinning disc reactors, static mixers, loop reactors among others. RPBs have been shown to significantly improve the rate of mass transfer between gas and liquid (Jassim, 2002; Ma and Chen, 2016) They also have

less equipment footprint, require less investment and can deal with highly concentrated amine-based solvents more efficiently (Xie *et al.*, 2019). Yu and Tan (2013) also demonstrated that RPBs have higher gas-liquid contact area and mass transfer for CO_2 capture. Zhao *et al.* (2016) suggested that the RPB have the potential to use high flow rates which would result in the enhancement of mass transfer. Another advantage is that the use of RPBs will reduce absorber sizes but not compromise production capacity (Jassim *et al.*, 2007). Wang *et al.* (2015) suggested that applying PI to PCC would improve the process dynamics which could mean cost reductions in other areas of the capture process including regeneration in addition to absorber size reduction.

Furthermore, Zhao *et al.* (2010) reported that RPBs could have height of transfer unit (HTU) as low as 1-2 cm and mass transfer rates of 1-3 orders of magnitude larger than conventional packed beds. This demonstrated that the mass transfer in the RPB was more efficient in comparison to conventional process. In terms of volume reduction, Cortes Garcia *et al.* (2017) suggested that the volume reduction that could be obtained for the RPB with respect to conventional absorber columns could be up to 10 times. This would be a significant saving in absorber construction materials with the RPB having a much more compact design (Zhao *et al.*, 2016). It is also possible to use higher concentration solvents in the RPB without any significant corrosion issues due to possibility of designing RPBs with stainless steel such that the size reduction offsets the increased material costs. It would also potentially reduce the liquid flows which will result in cost savings in terms of liquid holdup and energy for pumping (Wilcox *et al.*, 2014). All these considerations make the application of RPBs economically attractive for PCC.

2.1.2 Application of the RPB for PCC studies

Jassim *et al.* (2007) carried out a study on the absorption and desorption of CO_2 with a RPB using MEA solutions between of 30 wt %, 50 wt%, 75 wt%, and 100 wt%; solvent flow rates of 0.66 and 0.35 kg/s and a flue gas flow rate of 2.86 kmol/h. They reported that using MEA concentrations above 30% achieved higher CO_2 capture efficiency (the percentage of CO_2 removal between the inlet and outlet gas stream) and that no operational problems were observed in dealing with higher MEA concentrations. This clearly showed that it was possible to use RPBs for CO_2 absorption with highly

concentrated amine solutions with no significant negative effect. Conventional acid gas scrubbing process usually use aqueous amine concentrations between 30-40 wt%. Due to viscosity and corrosion considerations, the use of highly concentrations alkanolamines is avoided in conventional packed columns for CO_2 capture. Chiang *et al.* (2009) found in their work that mass transfer coefficient (K_Ga) decreased with viscosity by the exponent of 0.21-0.32. The mass transfer in an RPB is not as significantly affected by viscosity of the liquid as in conventional packed columns because of the acceleration of the liquid flow by the centrifugal force field. In a study carried out by Chen *et al.* (2005), they found that while liquid mass transfer coefficients decreased with increasing viscosity in the RPB, dropping from a K_La of 0.08 for a glycerol solution at 0.1cP solution to 0.01 K_La for a 40cP solution, there was still effective mass transfer resulting from centrifugal forces. It was also found that compared with packed columns, the influence of viscosity on the mass transfer coefficients was less in RPBs. In another study by Chiang *et al.* (2009) on the absorption of ethanol into water and glycerol/water solution in a RPB, it was found that despite the decrease in gas-phase mass transfer coefficient (K_Ga) with increasing liquid viscosity, there was still remarkable enhancement of mass transfer coefficient in the viscous media within the RPB in comparison to the conventional packed columns. RPBs therefore provide potential for using amine solvents at higher strengths as RPBs can be built from materials with greater resistance to corrosion and not be significantly affected by viscosity issues due to intense mixing in the RPB due to the application of HIGEE forces.

Yu *et al.* (2013) used concentrated aqueous piperazine (PZ) and diethylenetriamine (DETA) solutions in the RPB and their results indicated that increasing the concentration of PZ increased the CO_2 capture efficiency. Cheng and Tan (2006) observed that CO_2 removal efficiency could be adjusted by varying amine concentration, gas flow rates and amine solution. Similarly, in another investigation they carried out using 30 wt% MEA, aminoethylethanolamine (AEEA) and 2-amino-2-methyl-1-propanol (AMP) in a RPB, their findings showed that due to the short contact time in RPBs, only alkanolamines with high reactivity such as MEA, monomethylethanolamine (MMEA) and PZ should be utilized for CO_2 absorption (Cheng and Tan, 2009). This was further confirmed by study carried out by Cheng and Tan (2011) to investigate CO_2 removal from indoor air with an

alkanolamine. They used blends of PZ and MEA as well as AMP and MDEA and found that the blend of PZ-MDEA was not suitable for use for CO_2 absorption due to the low reactivity of MDEA. From their study, they also deduced that the solvent reactivity is a very important factor to consider when selecting solvents for use in the RPB. Moreover, Jassim *et al.* (2007) and Ma and Chen (2016) suggested that increasing the alkanolamine concentration increases the reaction rate and therefore absorption efficiency. This would suggest that the rate of CO_2 absorption in the RPB is strongly influenced by the alkanolamine solution concentration and that it would be preferable to use high concentration amines in RPBs due to the short contact times.

Tan and Chen (2006) in their work found out that the height of transfer unit (HTU) in the RPB were found to be lower than 1.0 cm in comparison to HTU of 40cm for the PCC in a packed column. This also demonstrated the significant improvement in mass transfer efficiency that can be obtained in the RPB. Jassim and co-workers also did a comparison study between a simulated stripper and the RPBs for desorption at 34 wt% MEA concentration showing that the using the RPB achieved a height and diameter reduction by factors of 8.4 and 11.3 respectively with respect to a conventional stripper. However, it is important to note that the liquid-gas ratios used by Jassim *et al.* (2007) in this work were very large (16 and 33) and are not practical due to the regeneration implications for using liquid flow rates that are that large.

2.2 Design characteristics of the RPB

2.2.1 Packed bed design

Veerapandian *et al.* (2017) described packed bed reactors as single state reactors that contain a packing material located in the discharge region of the reactor. The packing material can be either catalytic or non-catalytic. Packed beds are preferred for gas-liquid mass transfer processes because of their easier design and construction as well as the ease of their operation (Iranshahi *et al.*, 2018). Packed bed reactors are even more advantageous particularly for gas-phase reactions as minimizing the pressure drop is one of the most important concerns in the reactor design. According to Jassim *et al.* (2007) the first recorded development of the packed bed reactor was the work done by Chamber and Wall (1954) with mass transfer between the gas and liquid taking place in the

intermesh of the concentric rings. However, Cortes Garcia *et al.* (2017) has reported that a patent was filed by Elsenhans (1906)for a non-rotor stator rotating zigzag bed for purifying gases and a patent by Schmidt (1913) for a RPB with wire mesh packing. This shows that the concept of the RPB has been around for over a century. In the 1960s, Pilo and Dahlbeck (1960) obtained patents for rotating packed beds for gas absorption and desorption as well as distillation. The RPB has been successfully applied to de-aeration of brine, production of HOCl, the preparation of nanoparticles with new applications being continuously developed (Zhao *et al.*, 2010).

The RPB consists of a rotating part that consists of an annular rotor with a packed bed and a static housing with both parts connected with bearings and seals. The eye of the RPB is the empty centre of the rotor which contains the liquid distributor (Wenzel and Górak, 2018). The basic design of a RPB is shown in Figure 2.1 with the inner packing radius, r_i and outer packing radius, r_0 and the axial length or height, h. These three basic dimensions are fundamental to the design of the RPB in terms of achieving efficient absorption. (Agarwal *et al.*, 2010).

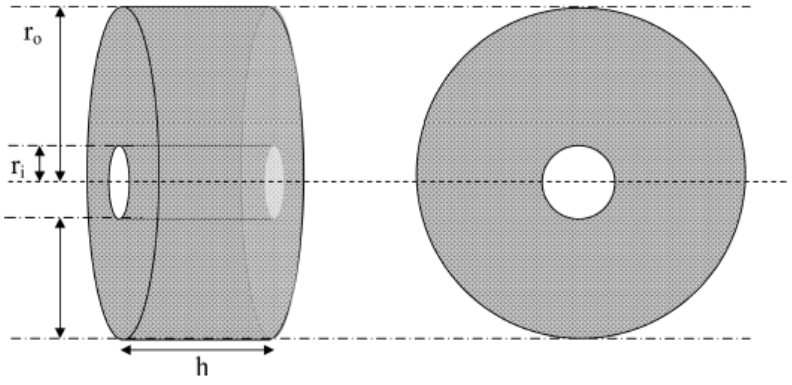

Figure 2.1: The basic design of a RPB (Agarwal *et al.*, 2010).

The inner radius of the RPB is where the liquid distributor sprays the liquid into the packing. The radial depth (r_o-r_i) and the axial height correspond to the height of the conventional packed column and its diameter respectively.

The top view of typical RPB as can be seen in Figure 2.2 shows that the liquid is injected from the liquid distributors onto the inner edge of the rotor and flows uniformly through the packing of the rotor. The liquid then leaves the rotor and sprays onto the rotor casing at the tip speed of the motor which is typically 40-60 ms^{-1} (Pan *et al.*, 2017). The gas can be introduced into the RPB to contact the liquid within the rotor in three different configurations that include counter-current (radially inwards, leaves via the rotor centre), co-current (radially outwards and leaves via the outer rotor) and cross-flow (upwards and leaves via the top of the rotor) as shown in Figure 2.3.

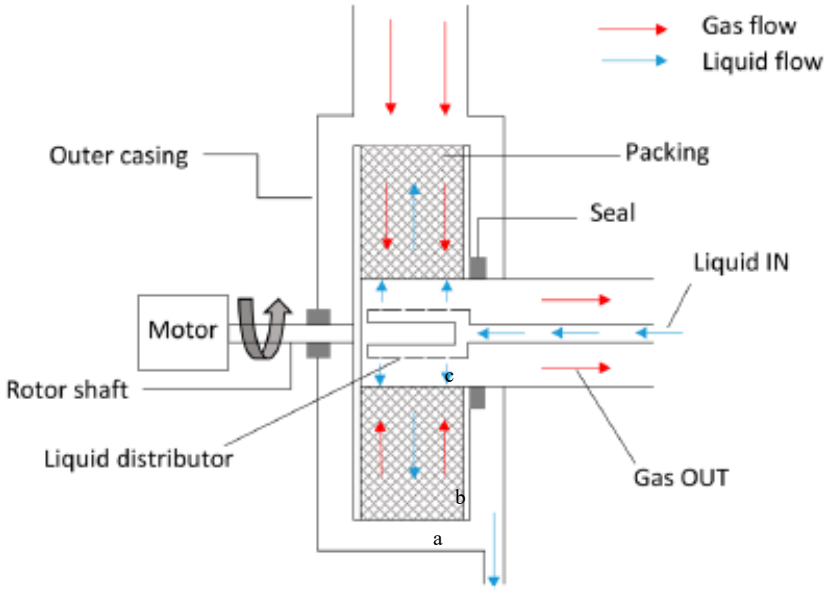

Figure 2.2: Top view of a RPB showing the liquid and gas flow.

According to Pan *et al.* (2017), the contact angles between gas and the liquid flows within the zone of packing for the counter-current, co-current and cross flow are 180°, 0° and 90° respectively. For any of the flow configurations, the characteristics of the packing within the RPB remain unchanged in the packing zone. The high gravity field within the RPB can be broadly divided into three zones. The first zone is the outer zone, the space between the machine casing and the outer periphery of the RPB. The solvent used within the RPB is thrown from the outer periphery of the packed bed onto the casing, therefore

forming tiny droplets. The second zone is within the rotor itself where the packing resides and it is in this region that the intensive mixing between the gas and liquid phases occurs. In addition, the interface between the gas and liquid are renewed very rapidly contributing to intensive mass transfer and reaction. The third zone is where the liquid is ejected from the liquid distributors before reaching the inner edge of the rotor. Structured packing such as stainless wires, expamet are usually used as packing for the RPB in CO_2 absorption although other packing designs such as blade packing, split packing, ball packing have been utilized for specialized applications of the RPB (Pan *et al.*, 2017).

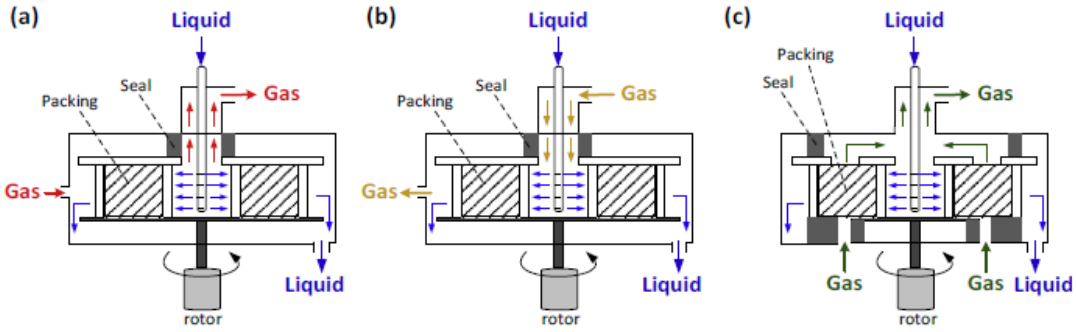

Figure 2.3: Different RPB configurations for contacting gas and liquid: (a) counter-current (b) co-current and (c) cross-flow (Pan *et al.*, 2017).

2.2.2 RPB flow characteristics

Zhao *et al.* (2016) suggested that notwithstanding the type of flow configuration used in a RPB, the intensification that can be observed in a RPB was highly dependent on the liquid flow pattern within the packing. The work done by Burns and Ramshaw (1996) found that there are three types of liquid flow within the rotating packed bed which are pore flow, droplet flow and film flow as shown in Figure 2.4. However, they also pointed out that due to some experimental constraints in their work, they were unable to perform the tests with counter-current gas flow and acknowledged this could make their results less relevant for the RPB operating in a counter-current gas flow. Notwithstanding the limitation of this work, other experimental studies performed after their work have largely been in support of their findings. Zhao *et al.* (2016) in their work identified a number of different liquid flow patterns existing in the RPB which are pore flow at

rotating speeds of 300-600 rpm, droplet flow at rotating speeds between 600-900 rpm and then film flow at higher rotational speeds.

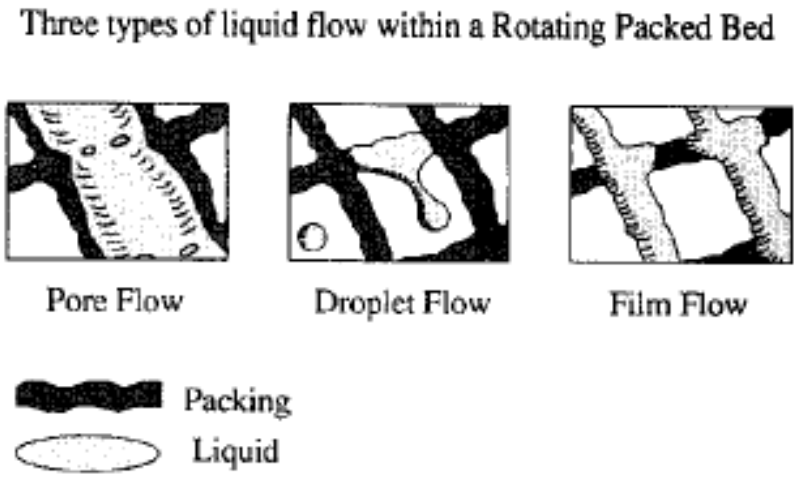

Figure 2.4: Types of liquid flow in a RPB (Burns and Ramshaw, 1996).

They suggested that liquid exist on the packing surface together with pore flow between 300-600 rpm while it coexists with droplet flow between 800-1000 rpm. The film thickness has also been shown in experimental studies to decrease as the rotational speed increases but then approaches a constant thickness at higher speeds. The intensification by HIGEE fields in the RPB are attributed to its effects on the gas-liquid contact boundary, viscosity, effects on flow pattern and intense microscopic mixing (Zhao *et al.*, 2016). The rotational speed in revolutions per minute (rpm) of the RPB is a parameter that is associated with the hyper-gravity factor within the RPB and is an indicator of the value of HIGEE field within the RPB. This so-called hyper-gravity factor was defined by Zhao *et al.* (2016) as the ratio of the centrifugal acceleration to gravitational acceleration anywhere within the HIGEE field in the RPB.

The formula for the angular velocity of the RPB is described as:

$$\beta = \frac{\omega^2 r}{g} = 900N^2 r/(\pi^2 g) \quad (2.1)$$

where $\beta(\frac{rad}{s})$ is the angular velocity, r (m) is the RPB radius, N(r/min) is the rotational speed and g (m/s^2) is the gravitational acceleration.

According to Agarwal *et al.* (2010), as the rotational speed is increased, the overall mass transfer coefficient increases and suggested the RPB should be operated at high rotational speed as possible and suggested that a design of 1500 rpm should be used for an industrial scale RPB units. However, Zhao *et al.* (2016) findings were in disagreement with the conclusions of Agarwal and co-workers as they found that the amount of hyper-gravity factor that can be obtained from increasing rotational speed has a critical value. They argued that a continuous increase in rotational speed shortens the liquid phase residence time within the packing and that past this critical point, some of the liquid escapes from the packing zone before reacting sufficiently thereby reversing the effect of the intensification supposed to be derived from increasing the hyper-gravity. This result in the CO_2 capture efficiency not increasing further beyond this critical point and could in fact decrease it. Moreover, increasing rotational speeds will mean an increase in power consumption therefore higher operating costs.

Pressure drop is also identified as one of the important indicators used in evaluating the performance of a RPB as it directly impacts on the choice of packing used and energy consumption of the RPB (Hu *et al.*, 2013). This will influence the selection of packing, structural design and the operating costs of the system (Zhao *et al.*, 2016). Although determining the effect of pressure drop in RPB is quite complex due to differences in the gas-liquid flow patterns, it is generally found that the gas pressure drop generally increases with increasing rotational speed and gas flow rates. However, the liquid flow rate does not seem to have any noticeable effect on pressure drop at higher rotational speeds. In 1990, Kumar and Rao published a study into pressure drop on a high-gravity gas-liquid contactor and stated that the pressure drop, ΔP across the rotor was mainly because of the centrifugal and frictional forces and to the gain of kinetic energy at the expense of pressure head.

Experimental studies in literature on the effect of increasing solvent concentration on CO_2 capture efficiency in the RPB generally show increasing CO_2 capture efficiency with

increasing solvent concentration. Generally, the increased reaction kinetics due to high concentration of the solvent enhances mass transfer and the liquid side forward reaction kinetics (Zhao *et al.*, 2016). Furthermore, the use of higher concentration MEA in the RPB is advantageous because of lower solvent flow rate and the higher driving force for mass transfer. However, one of the potential drawbacks from the use of higher concentration MEA could be the increased temperature bulge from the reaction heat at higher concentrations of MEA.

Moreover, the gas and liquid flow rates are important parameters in determining the handling capacity of a RPB that the mass transfer in the RPB also depends on (Gao *et al.*, 2016). Luo *et al.* (2012c) found that increasing gas-liquid ratio increased the effective interfacial area (a_e) within the RPB. This results in the gas-liquid interactions in the packing becoming intensified. The turbulent mixing of both liquid and gases produce smaller liquid droplets and thinner liquid films that enlarge the effective interfacial area.

2.2.3 Residence time in the RPB

Residence time distribution (RTD) is a useful tool that provides information on the fluid motion and mixing in a continuous flow system such as the RPB (Keyvani and Gardner, 1989). The stimulus-response technique is the method that has been used in literature for RTD studies in the RPB. A tracer is used as a stimulus that is put into the fluid entering into the RPB and the response is the time recorded for the tracer to enter and leave the RPB. Examples of tracers used include sodium chloride and other electrolytes that have been found to be suitable for aqueous systems due to having similar flow properties as the fluid being measured. They can also be distinguished in other characteristics from the fluid so the analytical instrument can pick them up.

Probes placed on the rotor at the inner and outer peripheries pick up the pulse signal of the tracer. This is measured by electro-conductivity meters and recorded by a computer. The residence time distribution (RTD) in the RPB has been studied by investigators such as Keyvani and Gardner (1989), Burns *et al.* (2000) and Guo *et al.* (2000) with the commonly used method being the tracer response technique. Keyvani and Gardner (1989) carried out their RTD experiments using concentrated $NaNO_3$ solutions charged to a

tracer inlet loop using simultaneous half turn of two shut-off valves, the tracer was introduced into the liquid stream inlet. They suggested that the mean residence time depended on rotational speed and liquid flowrate respectively and observed that the mean residence time decreases as the rotational speed increases or the liquid flowrate increases. However, the gas flow rate did not have significant effects on the residence time. The mean residence time varied from 0.4 to 1.8 seconds for accelerations of between 300 and 2800 m s^{-2} and superficial liquid flow velocities of between 0.9 and 3.6 cm s^{-1}. However, according to Bašić and Duduković (1995), the tracer response technique used by Keyvani and Gardner (1989) had some shortcomings which were the use of measurements taken at the rotor feed and exit points and the additional delays thereby incurred. They suggested that was not an accurate method. This was because the response times included transit times through parts of the rotor other than the packing that were not taken into consideration. This led Burns *et al.* (2000) to improve on the work of Keyvani and Gardner (1989) in their work by placing two sensors inside the packing. They found that the liquid residence times in the RPB were very short, with liquid typically moving through the packing at an average 1ms^{-1}. Guo *et al.* (2000) were also in agreement in their work and suggested that the average residence time of liquid in a RPB varies with liquid flow rate and rotating speed and ranged from 200 to 800 millisecond.

Another closely related parameter to the residence time in the RPB is the liquid holdup (ε_L) defined as the liquid volume per unit packing volume (Xie *et al.*, 2017). The relationship between the residence time of the liquid in the RPB and the liquid holdup can be expressed with the equation (Burns *et al.*, 2000):

$$t = \frac{\varepsilon_L}{U}(r_0 - r_1) \qquad (2.2)$$

Where r_0 and r_1 are radial positions of the outer and inner packing and U is the superifical liquid flow velocity and can be calculated by:

$$U = \frac{\mu_0 d}{2\pi r} \qquad (2.3)$$

Where μ_0 is the liquid jet velocity, dis the width of the nozzle and r is the mean packing radius.

2.2.4 RPB mass transfer equations

The mass transfer coefficient is generally considered one of the most important parameter in estimating the mass transfer area of a RPB (Guo *et al.*, 2014). The fluid dynamic behaviour in multiphase systems is determined by the interphase buoyancy factors ($\Delta\rho g$). For a scenario where $\Delta\rho g = 0$, for example in deep space, there will be no interphase slip velocity and the transfer process will be determined by surface tension forces only. However, if 'g' is increased such as by generating centrifugal field by rotation, larger interphase slip velocity can be achieved and the rate of interphase transfer will increase (Hassan-beck, 1997).

Considering a differential volume dV as shown in the Figure 2.5, the material balance across this differential volume can be mathematically expressed as:

$$\{mass\ in\} - \{mass\ out\} = rate\ of\ stripping \quad (2.4)$$

The differential volume is given as:

$$dV = 2\pi rh\ dr \quad (2.5)$$

The amount of liquid passing through the differential volume of the RPB is given as L moles/m^2 hr^{-1} and the rate of mass transfer of gas to liquid is given as:

$$d(Q_L c) = K_L a(c - c^*)dV \quad (2.6)$$

where a is the interfacial area per unit volume of the packing section, c and c* is the CO_2 bulk concentration in the aqueous phase and in equilibrium respectively, dV is the differential volume of the packing. If the equation 2.6 is integrated, the volume of the bed required for a given stripping for liquid-phase controlled mass transfer is obtained and mathematically expressed as:

$$V = \frac{Q_L}{K_L a} \int_{c_1}^{c_2} \frac{dc}{c - c^*} \quad (2.7)$$

The equation above can be expressed for dilute solutions in terms of liquid mole fraction in the equation expressed as (Hassan-beck, 1997):

$$V = \frac{Q_L}{K_L a} \int_{x_1}^{x_2} \frac{dx}{x - x^*} \qquad (2.8)$$

The above equation can then written in terms of the height of the bed as:

$$H = \frac{Q_L}{AK_L a} \int_{x_1}^{x_2} \frac{dx}{x - x^*} \qquad (2.9)$$

where A is the cross-sectional area.

This can be further simplified to give:

$$H = \frac{L}{\rho K_L a} \int_{x_1}^{x_2} \frac{dx}{x - x^*} \qquad (2.10)$$

The integral part of the equations $V = \frac{Q_L}{K_L a} \int_{x_1}^{x_2} \frac{dx}{x - x^*}$ and $H = \frac{Q_L}{AK_L a} \int_{x_1}^{x_2} \frac{dx}{x - x^*}$ is known as the number of transfer units (NTU) and the terms $\frac{Q_L}{AK_L a}$ or $\frac{L}{\rho K_L a}$ represent the height of transfer units (HTU) (Hassan-beck, 1997).

In a dilute solution with constant Henry's constants or equilibrium constants, the NTU for such system can be mathematically represented as:

$$NTU = \frac{S}{S-1} ln\left(\frac{\frac{x_{in}}{x_{out}}(S-1)+1}{S}\right) \qquad (2.11)$$

where S is the stripping factor which is defined as the ratio between the slopes of the equilibrium and operating lines

$$S = \frac{mG'}{L'} \qquad (2.12)$$

where G' and L' are the molar gas and liquid flow rates respectively and m is the equilibrium constant. The total height of the bed, H (m), can be obtained from the following equation:

$$H = HTU\ X\ NTU \quad (2.13)$$

The performance of the RPB is determined based on the packed height or radial depth (R_o-R_i) and the height of the transfer unit (HTU). Therefore, the number of transfer unit in a RPB can be expressed as:

$$NTU = \frac{R_o - R_i}{HTU} \quad (2.14)$$

Where R_o and R_i are the outside and inside radii of the bed

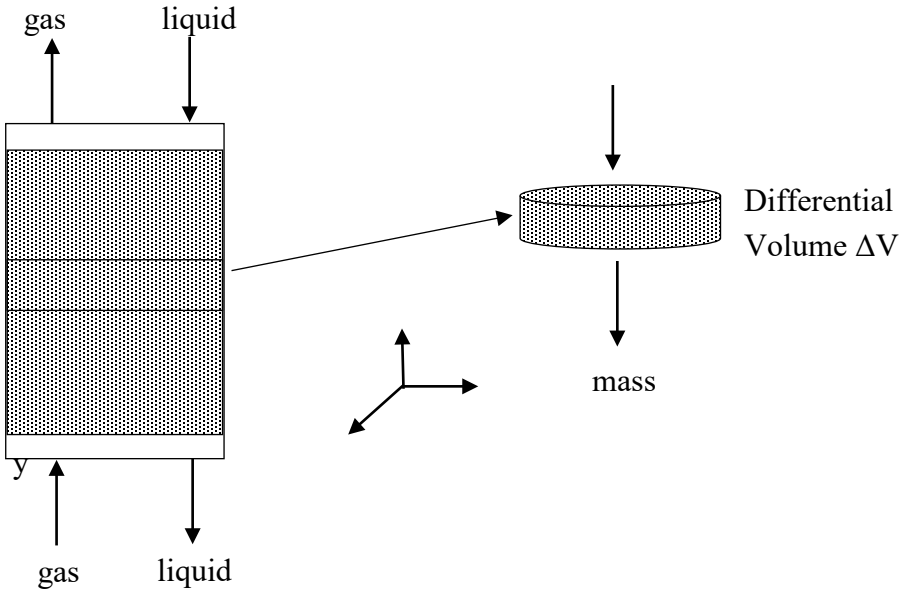

Figure 2.5: Mass balance schematic representation in the RPB.

2.3 Flow configurations of the RPB

2.3.1 Counter-current RPB

The so-called single-block counter-current RPB is the conventional design of the HIGEE gas-liquid contactor. However, there are different designs of the RPB with different mass transfer and hydraulic characteristics which are predominantly a function of the design of their rotors (Cortes Garcia *et al.*, 2017). The three main designs of the RPB are the counter-current, co-current and cross-flow RPBs. The counter-current RPB consists of a doughnut-shaped packed bed mounted between two discs that rotate coaxially with the rotor's axis of rotation. The liquid is then fed in from the centre of the rotor (as shown in

Figure 2.6) onto the packing and then flows outwards under the action of the high centrifugal acceleration being generated. The CO_2 is introduced into the RPB from the periphery and flows inwardly to the centre of the rotor. As centrifugal forces are generated from the rotation of the RPB rotor, this means that in the counter-current flow, the gas phase is being pushed against this force. It has been estimated that in a counter-current RPB, centrifugal pressure accounts for about 12-20% of the total pressure drop while frictional force accounted for 40-70% of the total pressure drop (Zhao *et al.*, 2016).

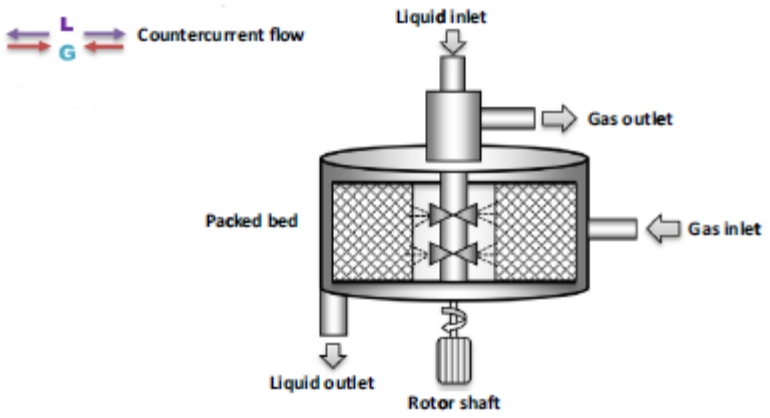

Figure 2.6: Schematic diagram of a counter-current RPB (Zhao *et al.*, 2016).

Inside the RPB, a high centrifugal acceleration environment generates high shear forces within the liquid and this results in very thin liquid films (Hassan-beck, 1997). These films can then yield very large surface area when fine packing is used. In addition, the centrifugal acceleration may result in the rapid and continuous renewal of interfacial surface for gas absorption. In addition to these, the turbulence generated by the gas entering into the RPB are such that the gas-liquid counter-current flow offers a very high mass transfer enhancement potential in the RPB compared to conventional packed beds. This also results in very low height of transfer units (HTUs) compared to conventional packed beds which can be attributed to the higher values of volumetric mass transfer coefficient (Hassan-beck, 1997).

The overall performance of the RPB in capturing CO_2 can be evaluated in terms of three key parameters that are the height of transfer units (HTU), CO_2 capture efficiency and the overall gas-phase mass transfer coefficient. These key parameters are in turn influenced by operating parameters such as rotational speeds, gas-liquid ratio, liquid distribution and flow regime within the RPB, temperature and solvent concentration. These operating conditions can be used to determine the optimal operating conditions, the power consumption and energy efficiency of the process and design parameters for scale up.

2.3.2 Co-current RPB

In a co-current flow RPB as shown in Figure 2.7, the gas flows outward from the inner edge of the RPB to the outer edge of the rotor driven by both the centrifugal force and pressure difference (Chu *et al.*, 2014). Chu *et al.* (2014) suggested that the co-current RPB has lower pressure drop in comparison to the counter-current RPB but at the expense of the mass transfer driving force. Due to the gas pressure drop being considered a critical parameter with important implications for power consumption of the CO_2 capture process, there has been renewed interest in investigating the application of co-current RPBs for CO_2 capture in recent years (Li *et al.*, 2013).

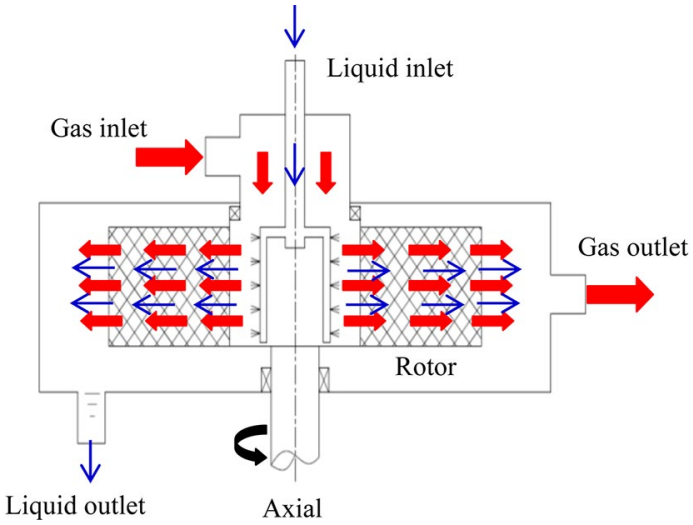

Figure 2.7: Schematic diagram of a co-current RPB (Chu *et al.*, 2014).

Li and Hao (2013) also reported in their work that co-current RPBs showed lower pressure drop in comparison to the counter-current RPBs. They carried out an investigation on a co-current RPB using a water-air system and showed that the gas pressure drop in the co-current RPB was significantly reduced with increasing rotor speed. Despite the potential merits of lower gas pressure drop in co-current RPBs and the potential for reduction in power consumption, there are few studies found in literature on experimental work done on applying it for CO_2 capture. A recent study using the co-current RPB was by Li *et al.* (2016) for treating VOC-containing waste gas fume exhaust from restaurant cooking with low pressure drops. A possible reason for the limited cases for the application of co-current RPBs might be its suggested possible shortcoming of a worse mass transfer performance in comparison to the counter-current rotating packed bed (Chu *et al.*, 2014). Notwithstanding, it could be argued it shows some promise for CO_2 capture in terms of lowering power consumption due to lower gas pressure drop. Nevertheless, there are no comparative study of the performance of the two RPBs as absorbers for CO_2 capture.

2.3.3 Cross-flow RPB

Figure 2.8 shows the basic structure of a cross-flow RPB. The gas flow in a cross-flow RPB differs from that of a counter-current RPB although the liquid flow regime is similar (Lin and Chen, 2011a). The liquid flows from the liquid distributor located in the centre of the cross-flow RPB and into the inner edge of the rotor packing and is thrown along the radial direction. On the other hand, the gas flow goes through the packing layers in the axial direction making the gas and liquid cross contact. The gas then leaves through the gas outlet pipe at the top of the RPB and the liquid leaves the RPB from the bottom of the RPB (Hu *et al.*, 2013).

Accordingly, the gas flow mechanism in a cross-flow RPB differs from that of the counter-current RPB although their liquid flow form remains similar. As a result, Hu *et al.* (2013) suggested that the characteristics of the fluid mechanics of counter-current RPBs can be applicable in cross-flow RPBs. The diameter of the cross-flow RPB packing rotor is greatly decreased such that the overall equipment volume is reduced resulting in size reduction and huge savings in equipment costs (Hu *et al.*, 2013). It also has the

advantage of no flooding and reduced diameter of the rotors although with the drawback of shorter contact time available for mass transfer, increased axial length and liquid entrainment (McDonough, 2013).

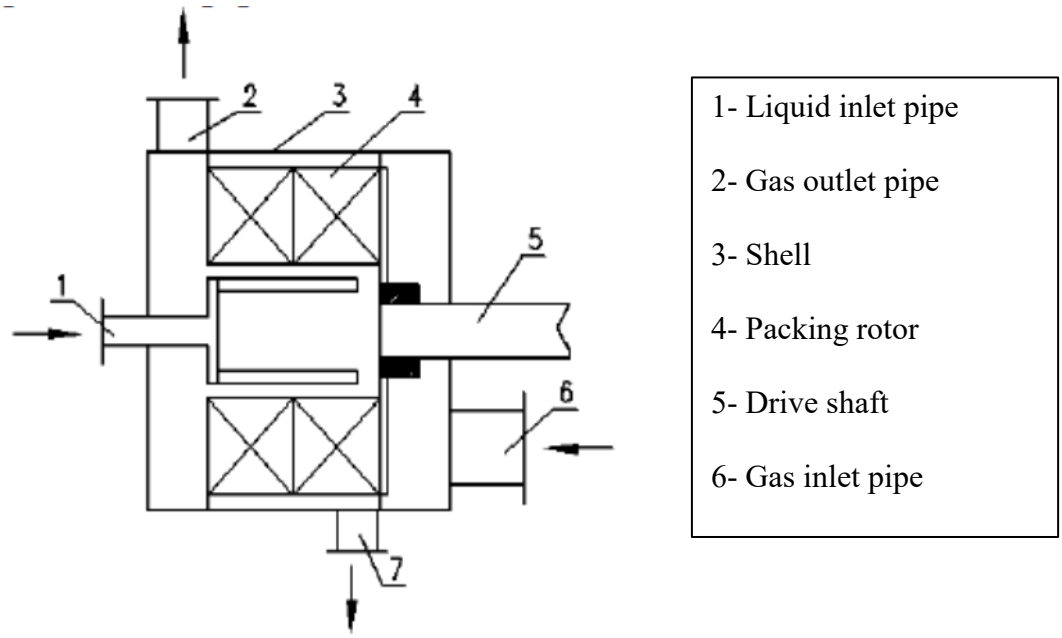

Figure 2.8: Schematic diagram of a cross-flow RPB (Hu *et al.*, 2013).

Guo *et al.* (1997) were the first to publish work in literature on the use of cross-flow RPBs and they investigated the hydrodynamics and mass transfer of a cross-flow RPB. According to Guo *et al.* (1997), the characteristics of the cross flow RPB are such that there is no limitation to the critical gas velocity and it can operate at very high gas velocities leading to significant reduction in the equipment size.

This is possible because the cross flow overcomes the drawback present in counter-current RPBs where a flooding limit is reached when working in the counter-current configuration which makes operating the RPB impossible because the liquid is prevented from flowing into the RPB. Jiao *et al.* (2010) also suggested that the having the RPB in the cross-flow configuration results in a reduction in pressure drop especially if used in a process with high gas flow rates such as gas absorption. It has also been shown from

other studies in literature that the use of cross-flow RPB will be more desirable for gaseous streams with higher flow rates as compared with the counter-current RPB where flooding may occur. Lin and Chen (2008) found that the $K_G a$ of the cross-flow RPB depended on the gas and liquid flow rates and indicated that the mass transfer in the liquid phase was more important that the gas-phase. Their results also showed that the $K_G a$ values were comparable to those of counter-current RPBs showing a great potential of the use of cross-flow RPBs for cost savings in terms of equipment sizes.

Lin and his co-workers were the first in literature to test the performance of a cross-flow RPB for capturing CO_2 capture experiment with alkanolamines. They conducted an investigation into CO_2 absorption using aqueous MEA solutions using MEA solutions at 0.2. 0.5. 0.7 and 1.0 mol/L and air stream between 1-10% CO_2 mole fraction using a cross-flow RPB of inner radius and outer radius of 2.4 cm and 4.4 cm respectively and an axial height of 12 cm. They found that their $K_G a$ values were 2.5 times higher than that of a similar sized counter-current RPB and concluded that the mass transfer performance of a cross-flow RPB was better than that of the counter-current RPB. This view was supported by the work carried out by Lin *et al.* (2006) into the performance of a pilot-scale cross-flow RPB in the removal of VOCs from waste gas streams. They found that the mass transfer efficiency of the cross-flow RPB was greater than that of a counter-current RPB.

Lin *et al.* (2010) investigated CO_2 removal in a cross-flow RPB using 30 wt% MEA and blended alkanolamine solutions containing MEA, piperazine (PZ), and 2-amino-2-methyl-1-propanol (AMP) to remove CO_2 from a 10 vol% CO_2 gas stream. According to their findings, they claimed that that the cross-flow RPB could be applicable to processes that required high gas-stream flow rates and high CO_2 concentrations as an alternative to counter-current RPBs. In addition, they suggested also found that there was less contact time in the cross flow RPB and therefore, only alkanolamines having high reaction rates should be used in the cross-flow RPBs. There are few reported work in literature that have investigated the application of cross-flow RPBs in capturing CO_2 using alkanolamines and been used to test alkanolamines only at lower concentrations. This makes them not fully understood with respect to CO_2 capture. Therefore, an experimental

study to investigate the use of high concentration MEA solutions in the cross-flow RPB would contribute to knowledge on the performance of the cross-flow RPB for CO_2 absorption.

2.4 CO_2 absorption and mass transfer process

2.4.1 CO_2 absorption reaction with MEA

The reactions of CO_2 with primary amines such as MEA is usually described by the formation of zwitterion intermediate first and then formation of a carbamate (Bishnoi and Rochelle, 2000; Vaidya and Kenig, 2007a). This is represented by:

$$\mathbf{CO_2 + R_1R_2 - NH \leftrightarrow R_1R_2 - NH^+COO^-}$$

$$\mathbf{R_1R_2 - NH^+COO^- + B \leftrightarrow R_1R_2 - NCOO^- + BH^+}$$

Here, B represents a basic compound that could be amine, OH^- or H_2O.

During the reaction of CO_2 with MEA, the CO_2 diffuses from the bulk gas phase to the gas-liquid interface and dissolves in the liquid amine solutions (Putta *et al.*, 2014). Several chemical reactions occur in the liquid solution and three different reaction mechanisms have been proposed for the reaction of CO_2 and MEA (Lv *et al.*, 2015). These are the zwitterion mechanism, single-step or termocular mechanism and the carbamic acid reaction route.

The zwitterion mechanism suggests that primary alkanolamines such as MEA will first react with CO_2 to form zwitterion intermediates which are then instantaneously neutralized by the base (such as amine, OH^- and H_2O) to form a carbamate. However, Da Silva and Svendsen (2004) argued that a single-step reaction mechanism would be more compatible for the reaction of primary alkanolamines with CO_2. The single-step mechanism also known as the termocular mechanism was first proposed by Crooks and Donnellan (1989). In this mechanism, bond formation and the transfer of proton to the base occur simultaneously that gives a third-order reaction. In this mechanism, the water molecule acts as a proton acceptor instead of MEA.

$$\mathbf{CO_2 + RNH_2 - B \leftrightarrow RNHCOO^- - BH^+}$$

The third mechanism involves the formation of carbamic acid in which the MEA first reacts with CO_2 to form carbamic acid and then catalyzed by another MEA to form carbamate (Arstad *et al.*, 2007)

$$\mathbf{CO_2 + RNH_2 \leftrightarrow RNHCOOH}$$

$$\mathbf{RNHCOOH \quad + RNH_2 \leftrightarrow RNHCOO^- + RNH_3{}^+}$$

According to Putta *et al.* (2016), most investigators of the CO_2 reaction mechanism with loaded MEA solutions generally assume that pseudo first order reactions kinetics using the two film theory to interpret experimental data. The zwitterion mechanism is the most commonly accepted of the mechanisms and MEA is known to generally have an overall second-order kinetics in aqueous solutions. Therefore the mechanism of the reaction will depend on the concentration of the amine in the liquid bulk (Vaidya and Kenig, 2007a).

The efficiency of the CO_2 absorption reaction with MEA is also directly influenced by the CO_2 partial pressure due to it being determinant of the driving force for mass transfer. Flue gas streams from power stations are usually at low partial pressure of CO_2 resulting in a diminshed driving force for separation (McDonough, 2013). As a result of this, a higher concentration of MEA is prefered for its separation. Aqeuous solutions of MEA (ranging from 30 wt% to 40wt%) have been a popular choice for CO_2 capture for many years due to its high reactivity that makes it effective capture CO_2 at low partial pressures. As a result, this MEA percentage strength is generally considered as a reference for solvent based capture plants using MEA as it is also relatively cheap and proven commericially (Dubois and Thomas, 2012).

However, major disadvantages are the considerable energy penalty of the process for solvent regeneration, low CO_2 loading, high equipment corrosion and oxidative degradation that leads to high solvent make-up rates. The typical values for the energy penalty for the absorption-desorption lie in the range of 0.37-0.5 MWh/tonne CO_2. The energy penalty can be lowered to a range of 0.19-0.2 MWh/ton CO_2 by using either novel solvents or solvent blends (Sreenivasulu *et al.*, 2015). Due to the low CO_2 concentrations in the flue gas (usually 7-14% for coal-fired plants and as low as 4% for gas-fired), the

associated regeneration energy required and cost for the capture to achieve the CO_2 concentration required for transport is greatly increased.

Significant research efforts have also been directed towards the reduction of operating costs and the energy penalty from stripping which contributes the most significant cost of the entire capture process by looking at other amine solvents and solvent blends that are potential candidates for CO_2 capture in the hopes of better performance than MEA in terms of solvent regeneration. These include PZ (piperazine), diethanolamine (DEA), AMP and MAPA blends, methyldiethanolamine (MDEA) and triethanolamine (TEA) (Bernhardsen and Knuutila, 2017). Some such as biphasic solvents have been shown to lower the electricity costs by less than 20% when compared to scenarios where MEA is used (Oko *et al.*, 2017).

2.4.2 Mass transfer models

To carry out an efficient absorption process, it is essential to provide a large surface area for contact between the gas and the liquid (Danckwerts, 1965). Packed columns are the conventional equipment used for gas-liquid contacting for CO_2 capture in industry (Shivhare *et al.*, 2013). During the gas absorption process, the mass transfer mechanism can be described as the soluble gas diffusing to the liquid surface and then dissolving in the liquid before passing into the liquid bulk (Jassim, 2002). The absorption of CO_2 into a reacting solvent usually involves the solvent flowing over the packing in a film that varies in thickness from point to point, velocity and its angle of inclination (Danckwerts, 1965). As the liquid flows over the packing, there are formed regions of the surface where the layer moves slowly or is completely at a standstill or forms thinner faster moving layer and the gas-liquid interface at these points become saturated with carbon dioxide (Eimer, 2014). Theoretical models have been developed to describe the hydrodynamics of the mass transfer at the gas-liquid interface.

Surface renewal models propose that parts of the liquid surface are being replenished or renewed from time to time by fresh liquid brought up from within the bulk layer (Horvath and Chatterjee, 2018). The freshly formed surfaces absorb rapidly, and the rate of absorption then declines progressively as concentration of solute in the neighbourhood of

the surface increases. In some cases, the liquid in the layer could be turbulent such that eddies renew the liquid on the surface while at other times, the surface layer may be undisturbed laminar flow (Chung *et al.*, 1971). The exception to this are in areas where discontinuities exist between pieces of packing and the liquid is thoroughly mixed (Perlmutter, 1961). The fresh liquid surface is renewed continually at the top of the packing, and then moves downwards absorbing the gas at a decreasing rate until a discontinuity is reached. This is then replenished once again by fresh liquid from the bulk layer (Perlmutter, 1961; Danckwerts, 1965).

A simpler version of the surface renewal model proposed by Higbie (1935) known as the penetration model assumes that every element of the liquid surface get exposed to the gas for equal time lengths before being renewed from within the bulk layer with fresh liquid. The two-film theory by Whitman (theoretical framework that contains the Higbie's penetration theory and Dankwert's surface renewal theory) assumes that liquid at the surface is in laminar flow parallel to the surface while the liquid below the surface is in turbulent motion.(Danckwerts and Kennedy, 1997). For physical absorption, it is assumed that the gas is absorbed into the liquid without any chemical reaction taking place between the gas and the liquid (Ying, 2013). The rate of the absorption of the gas into the liquid bulk is determined predominantly by the molecular diffusion in the surface layer. The effects of diffusion transport and turbulence are presumed to vary continuously with depth below the surface. However, the model is taken as a stagnant layer of effective thickness x_L over liquid of uniform composition and the film thickness assumed small enough that the absorption-process is treated as one of steady-state diffusion through the stagnant layer (Danckwerts and Kennedy, 1997).

The two film theory proposed by Lewis and Whitman (1924) indicates a model where the mass transfer of a gas to a given solvent happens across stagnant gas and liquid films that exists on either side of a gas-liquid interface (Wilcox *et al.*, 2014). The film model proposes a situation wherein the liquid flowing over the surface is continuously being mixed by the turbulence of the liquid flow (Danckwerts, 1965). An exception occurs in the immediate vicinity of the free surface where turbulence is supposed to be damped-out, resulting in a "stagnant film". A stagnant film is one across which dissolved

molecules of gas can pass only by molecular diffusion (for physical absorption) (Danckwerts, 1965). It is assumed for the two-film theory that the resistance to mass transfer is entirely within the thin gas and liquid films closely attached to the interface (Jassim, 2002).

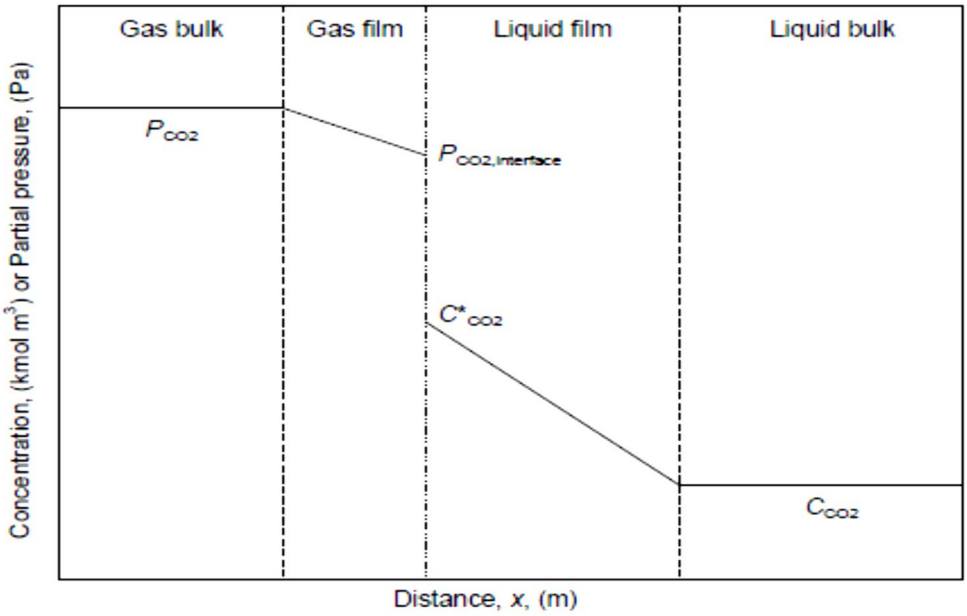

Figure 2.9: Diagram of the two-film model for the absorption of CO_2 in a liquid without chemical reaction (Ying, 2013).

The interface itself is assumed to contain no resistance and the interfacial equilibrium concentration of the gas and liquid phases are related by Henry's law (Wang *et al.*, 2018). For the case of CO_2 absorption in a liquid by physical absorption, the concentration profile of CO_2 in both gas and liquid phase using the two-film theory is shown in Figure 2.9. The liquid-film mass transfer coefficient for physical absorption, k_L is given as

$$R_0 = (C^* - C\ )k_L \qquad (2.15)$$

Where C* is liquid interface concentration and C is the bulk liquid concentration and k_L is the liquid phase mass transfer coefficient. The equation that describes k_L for the two-film theory is given by:

$$\frac{D}{x_L} \tag{2.16}$$

Where D is the diffusivity and the x_L is the depth of the liquid film.Therefore R_0 can be written as:

$$R_0 = \frac{D}{x_L}(C^* - C_0) \tag{2.17}$$

For the case where the CO_2 absorption is accompanied with a chemical reaction as shown in

Figure 2.10**,** the rate of absorption of CO_2 into a solvent is enhanced. In this case, CO_2 diffuses through the gas film, dissolves and then reacts with the alkanolamine solvent in a reaction zone within the liquid film. Due to the occurring chemical reaction, the amount of CO_2 within the liquid film increases while the amount of CO_2 in the gas phase reduces. Hence, fresh quantities of the solvent will diffuse from the liquid bulk to the interphase.

In the reaction zone, the concentration of the dissolved CO_2 and alkanolamine solvent are assumed to be negligible when the CO_2 loading is less than 0.3 mol CO_2/mol MEA and the reaction zone thickness assumed small when compared to the liquid film thickness (Dang and Rochelle, 2003). The reaction zone may be assumed to be at a distance X from the gas/liquid interface (Jassim, 2002). The magnitude of the distance X is dependent on the diffusivities of CO_2 and the solvent as well as the solvent concentration in the liquid solution. The reaction rate of absorption is gas film controlled if the CO_2 reacts at the surface of the liquid. However, if the reaction only occurs in a narrow zone within the liquid film, then the absorption rate is diffusion rate controlled in the liquid, as the reaction rate is much higher than diffusion rate. This corresponds to a fast pseudo-first order reaction that defines the rate of absorption of CO_2 into MEA solutions. The following show mathematically the basic mass transfer equation for CO_2 across an interface for a physical solvent is given by Lewis and Whitman (1924):

$$N_A = k_G(P_{AG} - P_{Ai}) = k_L^0(C_{Ai} - C_{AL}) \tag{2.18}$$

Where k_G and k_L are gas-film and liquid-film transfer coefficient respectively. The mass transfer resistance in both the liquid and gas phase are usually combined together as an over-all coefficient when Henry's law holds over the concentration range in which a gas

of intermediate solubility is being absorbed by a liquid and is described by the following expression (Lewis and Whitman, 1924):

$$\frac{1}{K_G} = \frac{1}{k_G} + \frac{H}{k_L^0}; and \ \frac{1}{K_L} = \frac{1}{k_L^0} + \frac{1}{Hk_G} \qquad (2.19)$$

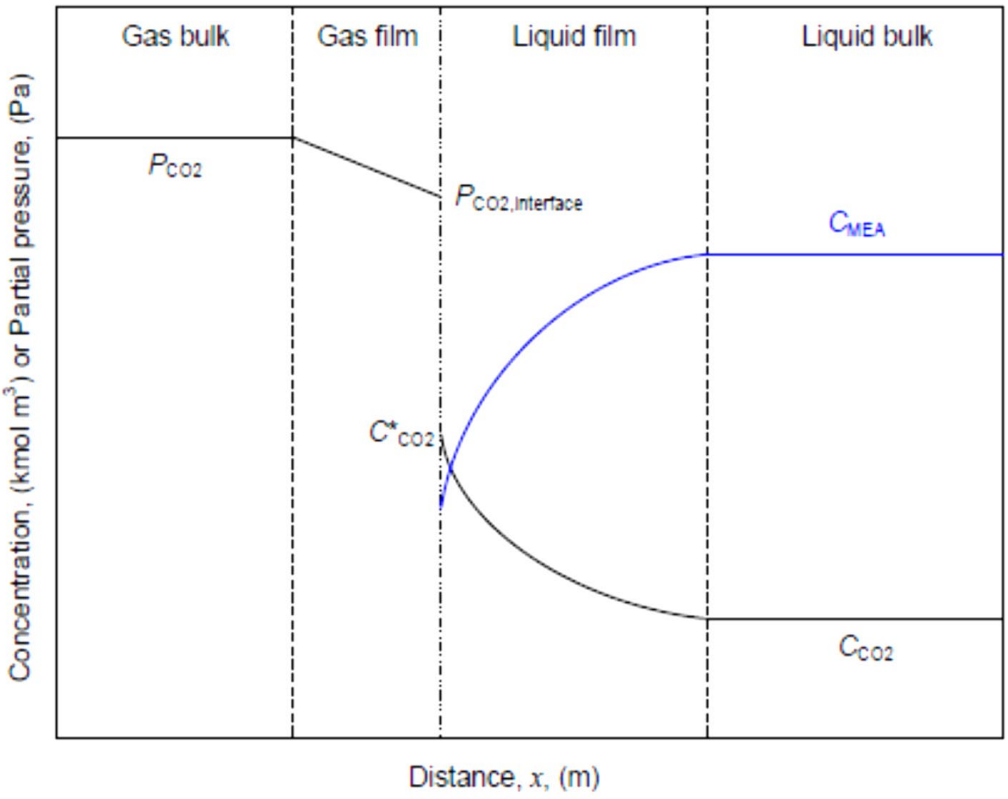

Figure 2.10: Diagram of the two-film model for the absorption of CO_2 in a liquid with chemical reaction (Ying and Eimer, 2013).

Where K_G and K_L are the overall gas-phase mass transfer coefficient and liquid phase mass transfer coefficient respectively, k_G is the individual gas-phase mass transfer coefficient and H is the Henry's constant.

In the case of the mass transfer enhanced with chemical reaction, the enhancement factor is introduced into the physical mass transfer equation to reflect the mass transfer acceleration in the liquid film by the chemical reaction and is given as (Jassim, 2002):

$$N_{AL(chemical)} = (k_{AL})_{chemical}\left(C_{AL}{}^{*} - C_{AL}\right) \quad (2.20)$$

And using the two-film theory to define the mas transfer coefficient, the following expression is obtained:

$$(k_{AL})_{chemical} = \frac{D_{AL}}{(\delta_L)_{chemical}} \quad (2.21)$$

The enhancement factor will then be the ratio of the physical and chemical molar fluxes defined as:

$$E = \frac{(k_{AL})_{chemical}}{(k_{AL})_{physical}} \quad (2.22)$$

Substituting into the chemical molar flux equation gives:

$$N_{AL(chemical)} = Ek_{AL_{chemical}}\left(C_{AL}{}^{*} - C_{AL}\right) \quad (2.23)$$

Where k_{AL} is the physical mass transfer coefficient. When this is written in terms of the overall mass transfer coefficient, it then becomes:

$$\frac{1}{K_G} = \frac{1}{k_G} + \frac{H}{k_L^0 E}; and\ \frac{1}{K_L} = \frac{1}{k_L^0 E} + \frac{1}{Hk_G} \quad (2.24)$$

E is the enhancement factor for the chemical reaction (for purely physical absorption process, the E is equal to unity) and H is the Henry's constant that is defined as:

$$p_{CO_2} = HC_{CO_2} \quad (2.25)$$

Such that p_{CO_2} is the partial pressure of CO_2 in equilibrium with the liquid phase at the gas-liquid interface and C_{CO2} is the CO_2 concentration in the solvent. The enhancement factor (E) is calculated
using:

$$E = \sqrt{M} \quad (2.26)$$

Where M is defined as (Danckwerts, 1971)

$$M = \frac{D_{CO_2} k_1}{(k_L^0)^2} \quad (2.27)$$

Where k_1 is the rate coefficient for the pseudo first order reaction

$$k_1 = k_2[MEA] \quad (2.28)$$

k_2 is the kinetic rate constant given for temperature range 298-313K. Mathematical limiting behaviour was developed by Astarita *et al.* (1983) for gas absorption process such as CO_2 absorption into aqueous amine solutions. For a gas-phase controlled absorption process, given as:

$$\frac{k_L}{Hk_G} \gg 1 \quad (2.29)$$

This means the solute gas (CO_2 in this case is very soluble in the aqueous amine solution and therefore the resistance is mainly in the gas film (low Henry's constant value). On the other hand, for a liquid phase control:

$$\frac{k_L}{Hk_G} \ll 1 \quad (2.30)$$

The mechanism of the transport of CO_2 from the gas to the liquid phase is commonly modelled using the two-film mass transfer theory due to its simplicity and the behaviour of the CO_2-MEA reaction that occurs within the liquid-film only (Khan *et al.*, 2011). Due the fast reaction of CO_2-MEA, the concentration of CO_2 reduces to zero in the liquid-film(Astarita, 1967)

2.5 Challenges of deploying of the RPB

In recent years, there have been increasing concern that despite the number of experimental studies existing in literature on the use of RPBs for PCC, the adoption of the RPB has been rather slow without any current commercial deployment (Wang *et al.*,

2015). Experimental studies, modelling work and reported industrial applications in literature on RPBs clearly show that the RPB has enormous potential due to its intensified gas-liquid mass transfer rates (Cortes Garcia *et al.*, 2017). Despite this, it has not been fully exploited for commercial PCC due to existing research gaps. An example of this is the large variation in RPB studies for intensified CO_2 capture. According to Cortes Garcia *et al.* (2017), these variations in RPBs experimental studies are usually in terms of flow area, alkanolamine concentration and RPB gas-flow configurations making the mass transfer coefficients usually reported in literature not very useful for industrial scale-up. The use of such studies becomes even more limited due to leaving out vital information such as the type of distributor, the packing used and the experimental conditions.

This also makes the comparative evaluation of the best flow configuration for a commercial scale RPB design difficult. This decision is important in identifying the appropriate flow geometry that has the right balance in terms of size and performance for an industrial scale intensified PCC design (Wang *et al.*, 2015). There are also other issues shortcomings of reported studies in literature such as the gas phase not being saturated as would be expected in CO_2 capture from flue gas (Lee *et al.*, 2017). The pressure drop of the RPB for CO_2 capture also needs to be investigated as it would have an effect on required energy for the CO_2 capture process (Cheng *et al.*, 2013). This is because the flow configuration of the RPB influences the pressure drop of the RPB (Chu *et al.*, 2014). According to Chu *et al.* (2014), gas pressure drop is a key factor in the scaling of RPBs for industrial applications. Therefore, experimental studies of the three RPB gas-flow configurations should be carried out to demonstrate the viability of the technology for industrial CO_2 capture.

2.6 Summary

The application of RPBs for CO_2 capture presents potential economic advantages in terms of mass transfer performance. The RPB shows great potential for capital costs reduction with respect to absorber sizes as well as operational costs. This has been demonstrated in various studies in literature. Due to the short residence times in the RPB, high concentration amine solutions are more suitable for the RPB to take advantage of the intensification due to the HIGEE forces. However, despite its advantages, there still

exists knowledge gaps that need to be filled for scale-up. Most studies available in literature have been carried out on RPBs of different sizes and characteristics making any meaningful comparison very difficult. There are no studies currently found in literature that have carried out a systematic investigation of the performance of three types of RPB gas-flow configurations with simulated industrial CO_2 capture. There was also no work found in literature so far where the gas phase was saturated. Therefore, carrying out such experimental study is very important. It will contribute relevant experimental data to scale-up and commercial deployment.

Chapter 3. Experimental facility

3.1 Description of the experimental facility

The experimental facility consisted of the RPB, solvent feed system, gas feed system, data collection system and the connecting pipework made up of joints, valves and fittings. The flowsheet of the experimental facility is shown in Figure 3.1. The materials used for the construction of the experimental facility were stainless steel, polypropylene, polyether ether ketone (PEEK) and Delrin. The selection of the materials was done considering factors such as material costs, availability, ease of machining and performance. The parts of the RPB were constructed with polypropylene and PEEK while the pipework was constructed with polypropylene. The choice of polypropylene for the RPB casing was because it was cheap, easy to work with and also chemically resistant to amine solutions (Burns *et al.*, 2000). The RPB rotor was constructed with PEEK because it offered better resistance to amine corrosion at high temperatures. The support base for the RPB was constructed with Delrin and it was chosen due to its mechanical strength and wear resistance.

The MEA solution was stored in a 300 L solvent feed tank and each experimental run was carried out twice using approximately 280 L of the prepared solution. A three-way valve installed in the pipework allowed the amine feed to be routed in two directions. The first valve turning allowed the feedstock to be recycled continuously into the feed tank. This ensured a well-mixed homogenous solution and that the inlet liquid feed temperature of the amine solution was 40 $^{\circ}$C before flowing into the RPB for the experimental run. The liquid feed temperature was chosen because this is the typical inlet flue gas temperature for conventional acid-gas scrubbing and CO_2 capture (Addington and Ness, 2010). The other valve turning allowed the prepared MEA solution to be fed into the RPB. The experimental facility was built inside a well-ventilated test bay with an air extraction system attached to the RPB. This ensured good venting of the outlet gas stream and maintained the CO_2 and MEA exposure levels well below the set allowable work exposure limits (WEL) by the Health and Safety Executive (5000 ppm) (HSE, 2018).

The RPB design also allowed the gas feed system to be switched such that experimental runs could be carried out in the counter-current, co-current and cross-flow configurations respectively as shown in Figure 3.2.

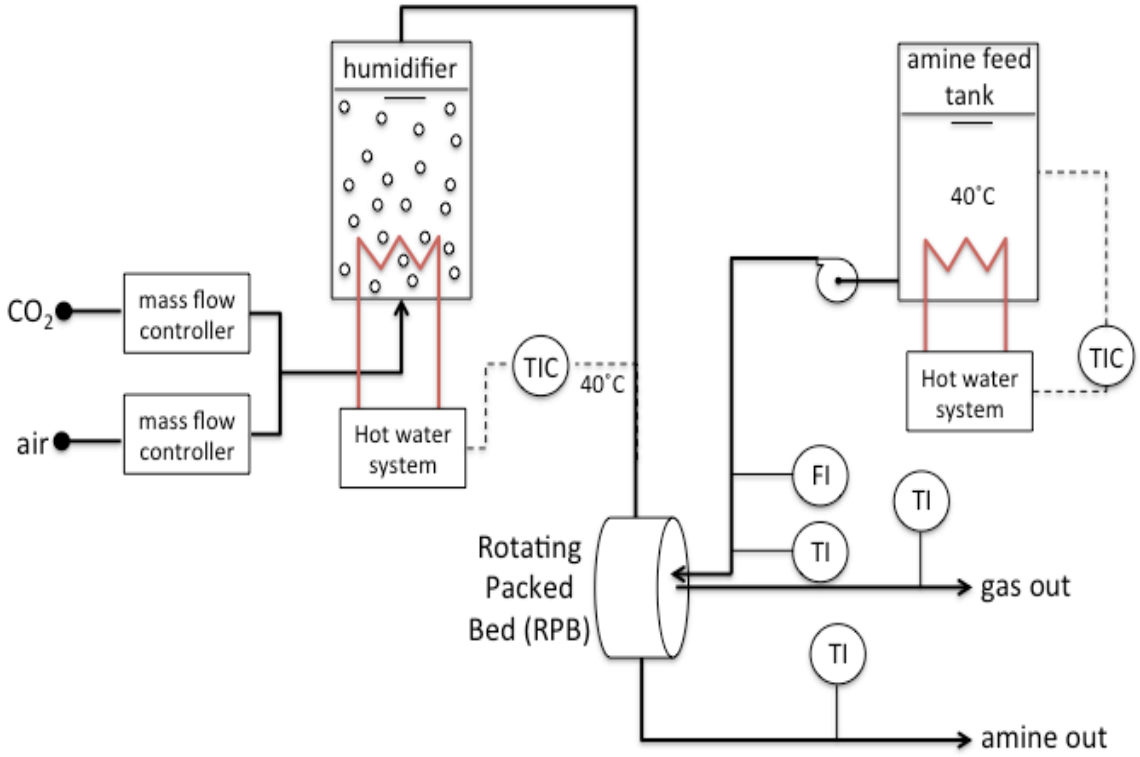

Figure 3.1: Flowsheet for the experimental pilot-plant rig (FI- Flow meter, TI- Temperature probe, TIC- External temperature control).

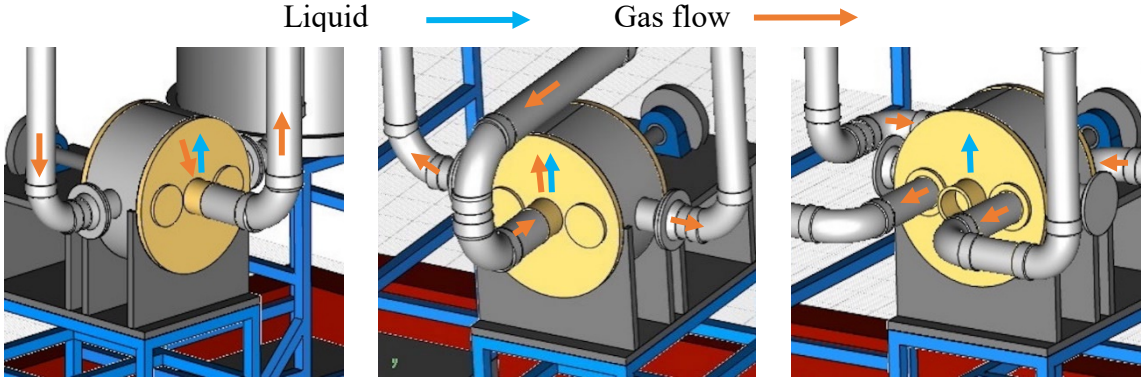

Figure 3.2: The three gas flow configurations of the experimental facility.

3.1.1 RPB rig

The RPB rig was made up of the rotor housing (casing), the rotor, the packing, liquid distributor, electric motor, support frame and the connected pipework. Figure 3.3 shows the rotor housed in the RPB casing with internal diameter of 360 mm. The front and back covers as well as the sides were manufactured with polypropylene.

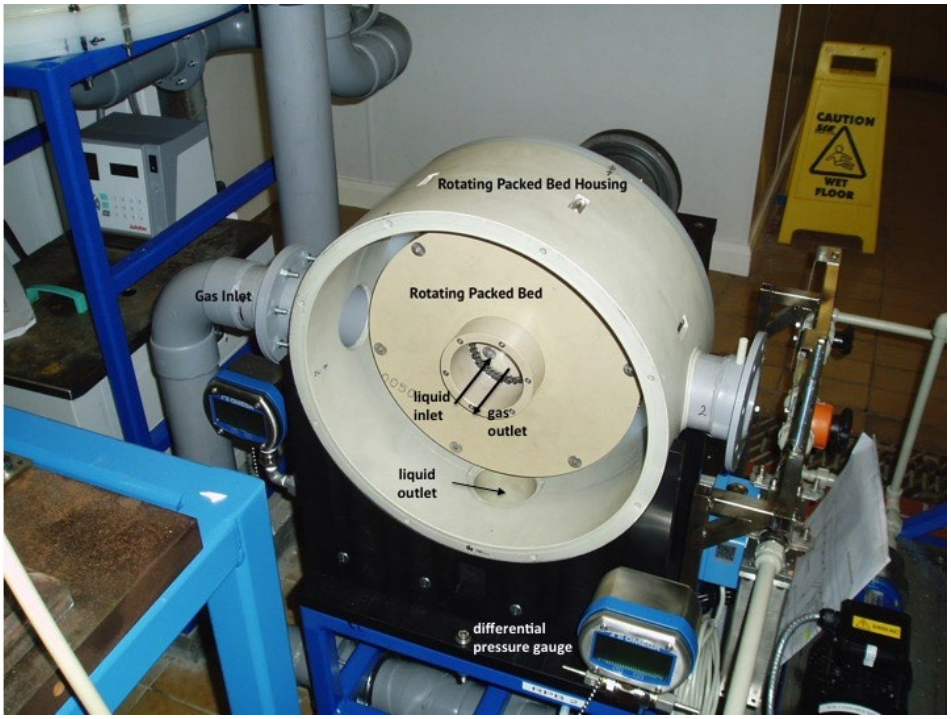

Figure 3.3: An inside view of the pilot-scale RPB rig.

The inner and outer diameter of the RPB rotor itself was 80mm and 300mm respectively as shown in Figure 3.4. The radial packed depth was 110mm, equivalent to the packed height of a conventional absorber column. The length of the RPB along the axis of rotation was 20 mm, considered equivalent to the diameter of a conventional packed column. The support frame was constructed using mild steel and was painted to protect it against corrosion from contacting the MEA solution. The frame was attached to a concrete base to provide a rigid support during rotor operation. The RPB support base held the RPB casing and the electric motor in place ensuring that the electric motor, drive shaft and rotor were properly aligned.

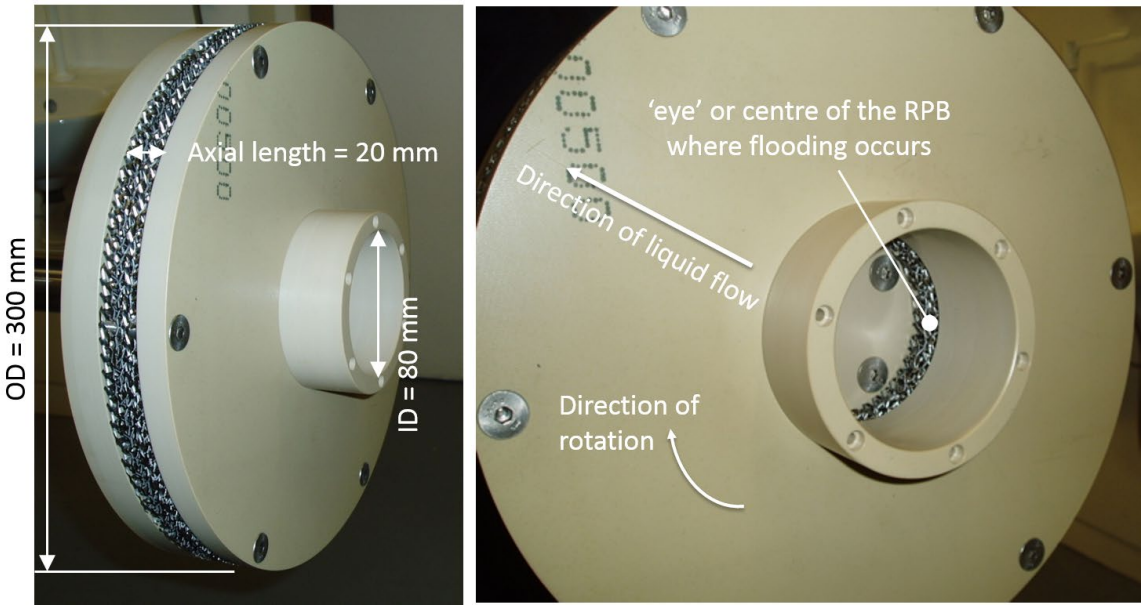

Figure 3.4: RPB rotor showing the inner and outer diameter.

The RPB shaft was driven by a 1.1 kW synchronous electric motor (ABB M3BP 80MC2) with a maximum speed of 3000 rpm. A frequency inverter (ABB ACS150-03E-03A3-4) controlled the motor speed. The RPB was driven through a 2:1 pulley and timing belt so that the maximum speed of the RPB was 3000 rpm. The motor was used to drive a rotor through a 2:1 pulley and timing belt system such that system was able to achieve a maximum speed of 1500 rpm. However, the maximum rotational speed used for the experimental runs was 1150 rpm due to mechanical and safety considerations at higher rotational speeds.

A flag mounted on the motor shaft and a stationary proximity sensor measured the speed of the motor. The motor was supported on two bearings and power consumption of the motor was measured using a torque arm attached to the base of the motor. Weights attached to the torque arm balanced the torque generated by the motor under load. The RPB packing as shown in

Figure 3.5a was made from stainless steel expanded mesh grade 707 supplied by the Expanded Metal Company. The voidage and surface area of the packing selected in this

work were 0.801 and 663 m^2/m^3 respectively balancing costs and the pressure drop requirements.

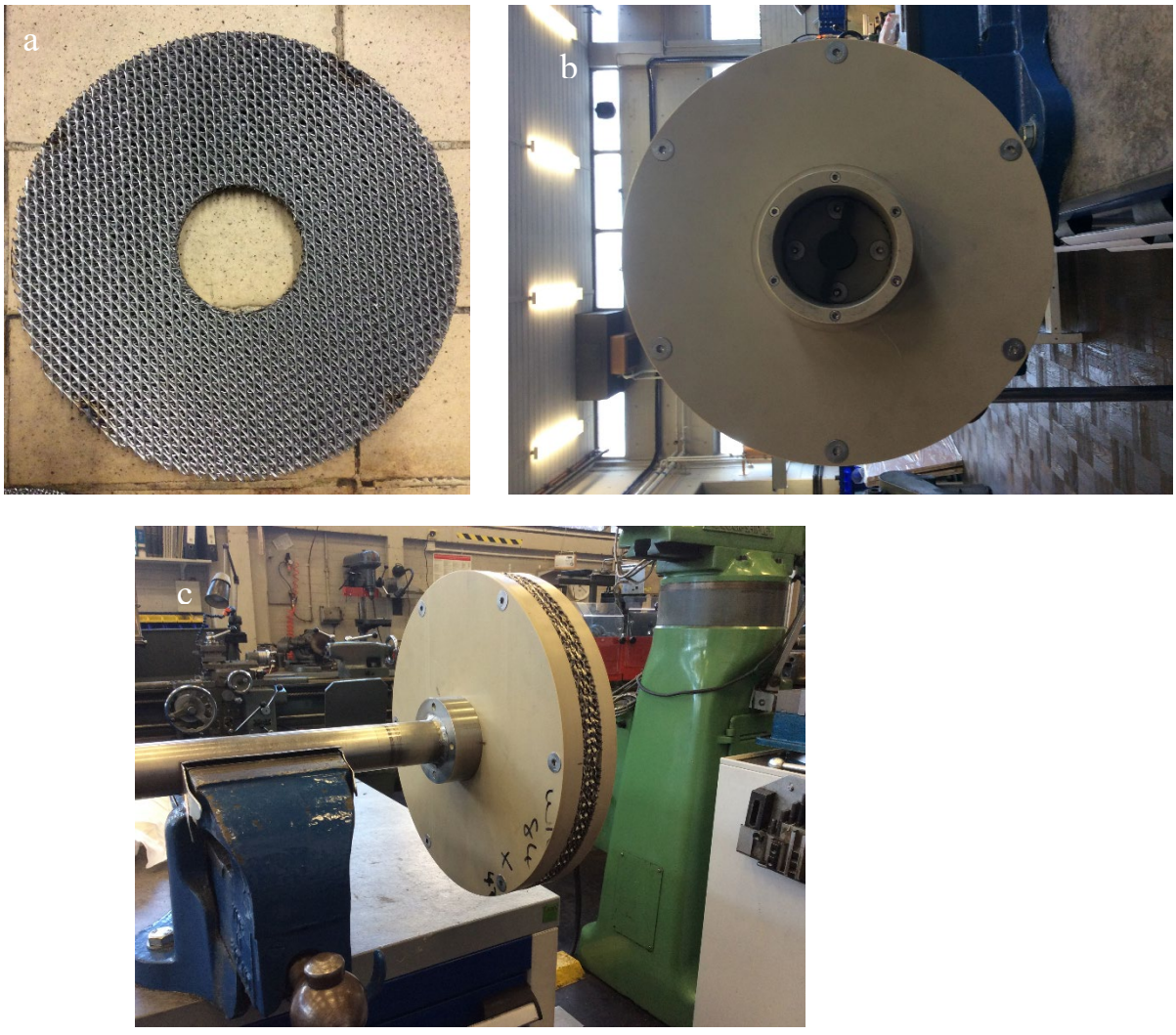

Figure 3.5:(a) Expamet packing used in the RPB (b) front view of the rotor (c) side view of the rotor with packing inside.

Selecting packing with higher voidage and surface area were much more expensive due to the difficulty of machine cutting. Agarwal *et al.* (2010) recommended that the packing voidage and specific surface area should be selected to balance costs, mass transfer efficiency and pressure drop. They recommended voidage values between 0.80 to 0.9 and specific surface areas above 600 m^2/m^3. Two discs made of PEEK attached to a stainless-steel drive shaft supported the packing for the counter-current and co-current RPB as

shown in Figure 3.5b and Figure 3.5c. For the cross-flow RPB, the packing construction was different to the other two configurations. The stainless steel expament (expanded mesh grade 707supplied by Expanded Metal Company) sheets were stacked together and sealed between the front and back cross plate covers made of stainless steel as shown in Figure 3.6a. The sheets were welded together and attached to the rotor. The total packing diameter was 20 mm as shown in Figure 3.6b.

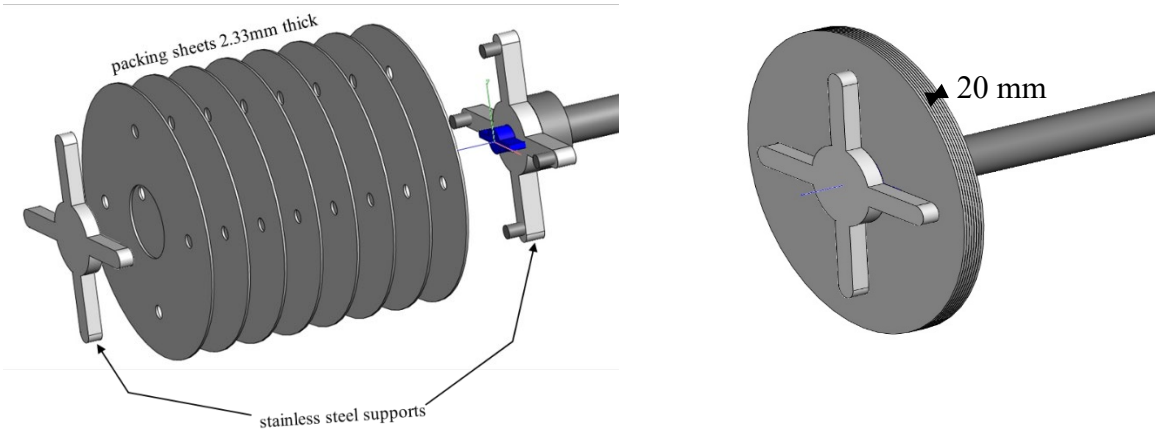

Figure 3.6: (a) Exploded view of cross-flow RPB packing (b) The cross-flow RPB rotor

The MEA solution was distributed onto the inner surface of the packing using a liquid distributor. Initially, a 4-arm distributor shown in Figure 3.7a was utilized for irrigating the bed.

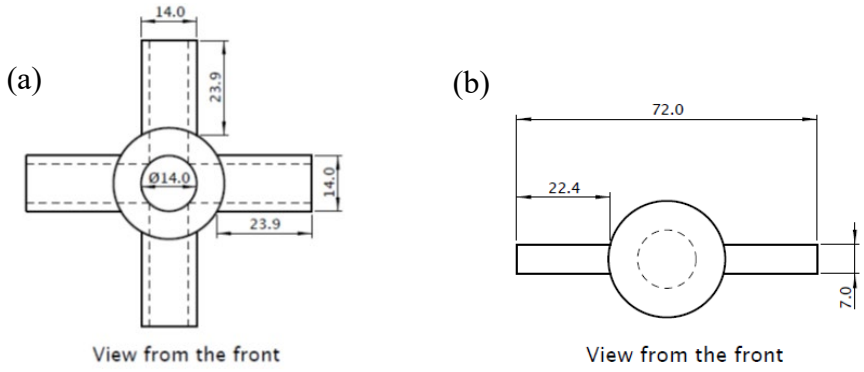

Figure 3.7: RPB liquid distributors (a) 4-arm distributor and (b) 2-arm distributor.

However, due to the design of the distributor, there was uneven distribution of the MEA solution within the RPB and a there were problems of leakage due to the MEA solution missing the packing and flowing into the front of the RPB. The distributor was changed to a two-arm design as shown in Figure 3.7b and smaller holes drilled into it. The two-arm liquid distributor was 3D printed and had three 2 mm holes drilled into the distributor arms of measuring 29.5mm in length.

3.1.2 The solvent feed system

The MEA solution was stored in a 300L prolypropylene solvent tank from where it was fed to the RPB. The solvent was fed into the RPB through 16mm outer diameter (OD) polypropylene pipe and was pumped using stainless steel magnetically coupled gear pump (Micheal Smith Engineers Ltd Liquidflow Series 4). The MEA solvent was recycled via a connected 3-way valve (Georg Fisher 543) to ensure thorough mixing of the solution and a homogeneous temperature of the solvent prior to being fed to the RPB. The required solution strength was prepared by pumping in the required amount of fresh MEA solvent (Dow Chemical >99.5% purity) from solvent drums (210 kg) and adding deionized water to make up the solution to the required strength. A drum pump (Crest Pumps model number CBP-TRP0900SEL) was used to transfer the solvent and water to the feed tank. The required mass to make up the solutions was measured using an electronic scale (Kern EOS). The solvent was heated to 40˚C using water circulated from a Julabo SE-26 circulating water bath connected to a heating coil that was submerged in the solvent with an external temperature probe connected to the solvent feed tank that automatically controlled the temperature. The solvent was fed to the rear of the RPB through the centre of the hollow stainless-steel shaft that was used to drive the RPB.

The mass flow of the solvent was measured using a Coriolis meter (Bronkhorst Rheonik RHM06, temperature range -196 to 400C, error: 0.1% of rate) connected to a laptop PC and monitored using the Bronkhorst FlowView program. The temperature of the solvent feed to the RPB and the solvent leaving the RPB were measured using a platinum resistance thermometer (Pico Technology SE019) monitored continuously using the picolog data logging software on a PC. The liquid flow rates through the liquid pump (0.37kW 230/1/50 frequency inverter (SMVector) were also controlled using the

Bronkhorst FlowView program. The temperature of the liquid flow was measured before entering into the RPB and after leaving the rotor before entering into the sump. The liquid leaving the RPB flowed into a sump where it was pumped using a sump pump out into a receiving tank. The liquid leaving the RPB was sampled so that the CO_2 loading could be determined.

3.1.3 The gas feed system

To provide simulated flue gas, air supply (pressure of 5.93 bar) was mixed with CO_2 (BOC Industrial Grade CO_2) supplied from a cylinder (BOC VK size, gauge pressure-50bar). The inlet CO_2 feed was supplied at 0.5 bar controlled by a BOC CO_2 pressure regulator and both the air and CO_2 were fed through thermal gas mass flow controllers (Bronkhorst model D-6383 (air) and Bronkhorst model D-6371(CO_2)). The inlet air and CO_2 flowrates were monitored on a PC using FlowView controlled by the FlowDDE communication software via a Bronkhorst high-tech unit connected to an actuated control valve (IMI Buschjost). After leaving the flowmeters, the air and CO_2 were mixed in the polypropylene piping connected to the humidifier. The humidifier was a 400 L capacity tank constructed with polypropylene filled to a depth of 700 mm with water. The water in the humidifier was heated to 40 ºC using hot water circulated through a stainless-steel coil from a Julabo F-34 water bath. The feed gas was then bubbled through porous polypropylene plate sitting close to the bottom of the humidifier.

An in-line temperature probe connected to the water bath heating up the humidifier was put in the gas pipework connecting the humidifier to the RPB. This was to ensure the temperature of the feed gas entering the RPB was maintained at 40˚C. The temperature, humidity and CO_2 content of the gas was measured at the RPB inlet and outlet using a GEM Scientific G100 gas analyser. The pressure drop between the gas inlet and gas outlet was measured using a differential pressure gauge (Omega Engineering DPG409).

3.1.4 The data collection system

The data acquisition system consisted of a laptop PC, a Pico logger data unit (4 active channels at about 2 readings per channel per second), pressure gauges and temperature probes. Air and liquid flow rates were monitored using Bronckhorst FlowView software

which was controlled using the Bronckhorst FlowDDE. Platinum resistance thermometers (PRTs) connected to a PT-104 data logger were used to collect inlet and outlet air and liquid temperature data. This was monitored on the PC with the Pico logger software supplied by Pico Technology. External probes from the water bath were connected to the amine tank and was used to ensure the amine temperature was maintained at 40^{o}C. Two Omega DPG409 pressure gauge (high accuracy- 0.08%) were used to measure the differential pressure between gas outlet and gas outlet as well as the liquid pressure at the sump of the RPB respectively. The change in CO_2 concentration from the inlet and outlet air feed was measured using a GEM Scientific G100 gas analyser.

3.2 Operation of the experimental facility

3.2.1 Experimental procedure

The experimental study was carried out in two main parts. The first part involved pre-loading the solvent to a lean loading between 0.1-0.15 mol CO_2/mol MEA to simulate the lean loading range used in industry obtained after solvent regeneration. The required solution strengths were prepared by pumping pure MEA solution (purity >99.5% Dow chemicals) from 210 kg drums into the amine feed tank and adding the required mass of distilled water using a barrel pump (Crest). The required pre-loading was achieved by feeding a dry air and CO_2 stream at 10 L s^{-1} and 20˚C through the humidifier to be heated up to 40 ˚C. The gas mixture was fed to the RPB in a pre-loading experimental run. The air stream contained 5 mol% CO_2 with air and CO_2 as shown in Table 3.1 and was contacted with the MEA solution at a liquid flow rate of 80 kg/hr. The inlet and outlet concentrations of CO_2 in the air were measured, taking readings three times using the gas analyser. The experiment was run continuously, feeding the entire contents of the amine tank through the RPB and then pumping the solvent back into the amine feed tank until the desired loading target was obtained.

The volume fraction of CO_2 in the inlet and outlet gas was measured using the G100 CO_2 analyser and liquid samples from the outlet were stored to be analysed within 48 hours. The RPB was run at each experimental variable for 5-7 minutes to reach steady state before gas and liquid samples are taken as well as data collected for other operating

parameters. Each CO_2 absorption experimental run was completed in approximately 2 hours.

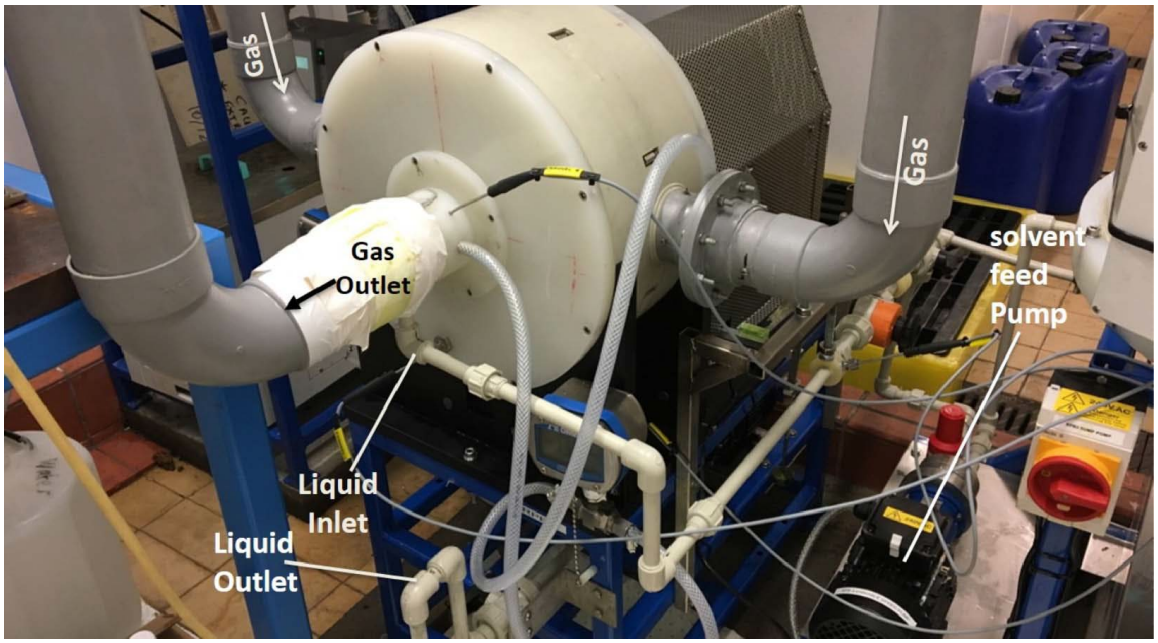

Figure 3.8: Liquid and gas flow path for the RPB (counter-current setup).

After pre-loading the MEA feedstock to the required lean loading, the CO_2 absorption experiments were then carried out using a gas feed stream with 12 mol% CO_2. This gas feed composition of air/CO_2 mixture was achieved by keeping the air and CO_2 mass flow rates at 8.8L/s and 0.8L/s respectively. This corresponded to an inlet CO_2 concentration of 12 mol% CO_2 reading on the CO_2 analyser. The change in the concentration of CO_2 between the inlet and outlet gas stream was measured using the Gem Scientific G100 analyser (with a measurement range of 0 to 100% and a resolution of 0.01%).

The inlet and outlet temperatures for both the liquid and gas feed was measured using a PT-104 Platinum Resistance Data Logger (Pico Technology) which was connected to platinum resistance thermometers (PRTs) positioned at specific entry and exit points in the rig. Sensors were linked to data logging software that displayed the temperature of each measured variable on a connected computer screen. The pressure drop readings across the RPB were taken as the differential pressure drop readings between the gas inlet

and outlet and was measured using Omega DPG409 pressure gauge. The pressure drop readings across the RPB were taken as the differential pressure drop readings between the gas inlet and outlet and was measured using the pressure gauge.

Table 3.1: Operating values for pre-loading experiments

Variable	Value	Unit
CO_2 flowrate	0.32	L/s
Air flowrate	9.5	L/s
Amine flowrate	80	kg/hr
Rotational speed	1000	rpm

The lean loading range (0.1-0.15 mol CO_2/mol MEA) was selected to be similar to the industrial CO_2 scrubbing, because MEA is usually cycled back and forth between the absorber and the stripper several times for CO_2 capture (Wang *et al.*, 2015). The preliminary solution concentrations tested were 30 wt%, 50 wt% and 90 wt% MEA solutions for the experimental validation runs on the RPB. Subsequently, experiments were carried out using 30 wt%, 50wt% and 70 wt% solutions. The concentrations selected were the most commonly studied MEA concentrations for CO_2 capture experiments. The MEA flow rate was varied for the different MEA solutions to give constant MEA:CO_2 molar ratios for the different MEA concentrations as shown in .

The L/G ratios for the 30 wt% MEA solution were 2.8, 3.3 and 3.7, 1.8, 2.1 and 2.4 for the 50 wt% MEA solution and 1.3, 1.5 and 1.7 for the 70 wt% MEA solution. The MEA flow rate were varied at the different MEA solvent concentrations to give constant MEA-CO_2 molar ratios. They were also selected to fit within the physical limitations of the flow rates that could be used on the RPB. During the test of each of the experimental parameter, the outlet CO_2 readings were taken after about 5 minutes (300s) to reach steady state before changing an operating variable. The inlet and outlet CO_2 concentration were recorded and liquid samples (5 – 10 ml) were taken from the front

and sump of the RPB. Liquid samples collected from the sump for loading analysis and additional liquid sample was taken at the periphery of the rotor through the front of the RPB. This was achieved by putting in place a stainless-steel bore pipe with a connected plastic tubing through the RPB front with the tip directly under the edge of the rotor.

Table 3.2.

The L/G ratios for the 30 wt% MEA solution were 2.8, 3.3 and 3.7, 1.8, 2.1 and 2.4 for the 50 wt% MEA solution and 1.3, 1.5 and 1.7 for the 70 wt% MEA solution. The MEA flow rate were varied at the different MEA solvent concentrations to give constant MEA-CO_2 molar ratios. They were also selected to fit within the physical limitations of the flow rates that could be used on the RPB. During the test of each of the experimental parameter, the outlet CO_2 readings were taken after about 5 minutes (300s) to reach steady state before changing an operating variable. The inlet and outlet CO_2 concentration were recorded and liquid samples (5 – 10 ml) were taken from the front and sump of the RPB. Liquid samples collected from the sump for loading analysis and additional liquid sample was taken at the periphery of the rotor through the front of the RPB. This was achieved by putting in place a stainless-steel bore pipe with a connected plastic tubing through the RPB front with the tip directly under the edge of the rotor.

Table 3.2: Amine flowrates and liquid-gas (L/G) ratios tested for counter-current configuration

Solvent concentration (wt%)	Amine Flowrate	Unit	L/G ratio (mass)	Corresponding molar ratio
30	118.8	kg/hr	2.7	3.8
	138.8	kg/hr	3.2	4.0
	154.8	kg/hr	3.6	4.4
50	79.0	kg/hr	1.8	3.8
	92.2	kg/hr	2.1	4.0
	105.4	kg/hr	2.4	4.4
70	56.4	kg/hr	1.3	3.8
	65.9	kg/hr	1.5	4.0
	75.3	kg/hr	1.7	4.4

It was positioned such that the liquid coming through the rotor went directly into the bore and was collected by extracting with a syringe through a plastic tubing connected to allow the collected fluid from the bore flow out of the RPB. However, due to the slow build-up of solvent at this location, samples tended to be no greater than 2 ml. Various amine flowrates were considered and tested under each individual rotational speed of 300 rpm, 600 rpm, 850 rpm and 1150 rpm for the three RPB configurations. The rotational speed of 1150 rpm was selected as the maximum feasible speed due to safety reasons.

3.2.2 Sampling and data collection

Liquid and gas sampling were carried out for each CO_2 absorption experimental run and analysed. Inlet and outlet gas samples were taken inline using a CO_2 analyser to determine the CO_2 concentration. The CO_2 analyser was allowed to run for 2-3 minutes at both the inlet and outlet sampling points for each experimental condition to reach a steady reading. The end of the CO_2 analyser was fitted with a filter to ensure that no

liquid was introduced into the analyser and that only dry samples (without MEA vapour) were collected while sampling.

A calibration curve was done for the CO_2 analyser by calibrating it against 5 mol% CO_2 and 10 mol% CO_2 standard bottles supplied by BOC. The analyser was run until the gas readings for each CO_2 gas composition stabilized and the results recorded in triplicates. The calibration curves for each gas composition are shown in Figure 3.9 and Figure 3.10 and it can be seen that the response time of the analyser to reach the expected mol% was 25 secs for both calibration curves. The result uncertainty was found to be 0.15%. In addition, liquid samples (5-10ml) were taken from the sump outlet of the RPB for liquid loading analysis, stored in sealed plastic vials, and analysed within 48 hours. For each experimental run at different solvent strengths, the lean MEA solution sample was taken prior to experimental runs for liquid pre-loading analysis and water content analysis. The experimental data collected during each experimental run include:

1. The liquid flow rate of MEA solution.
2. The flow rate of the air/CO_2 mixture.
3. The temperature of the liquid flowing into the RPB and temperature of the liquid at the front of the RPB.
4. Temperature of the liquid flowing out from the base of the sump.
5. The rotational speed of the RPB.

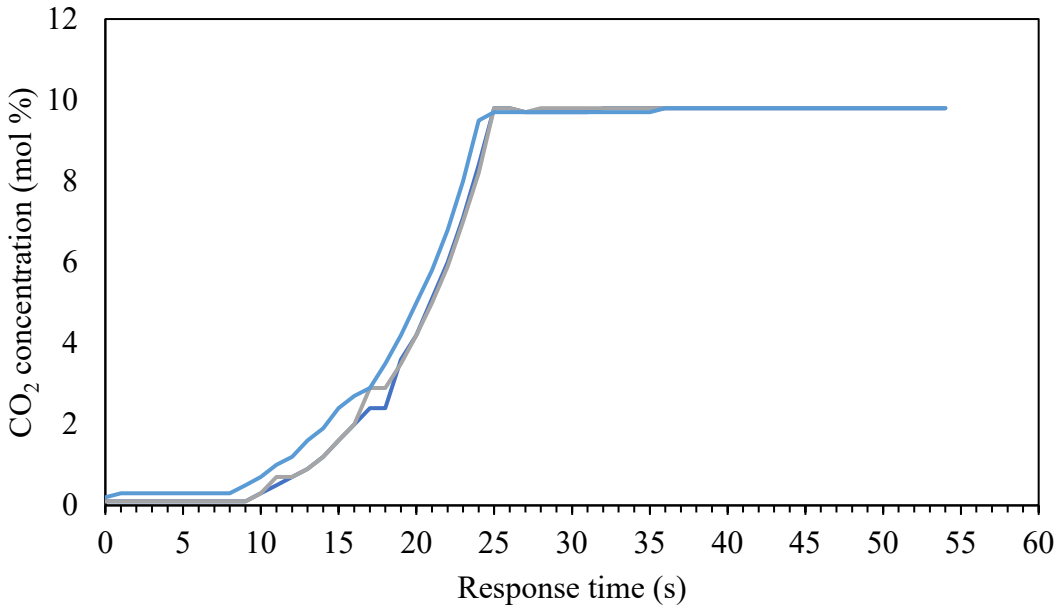

Figure 3.9: CO_2 analyser calibration curve using 10 mol% CO_2.

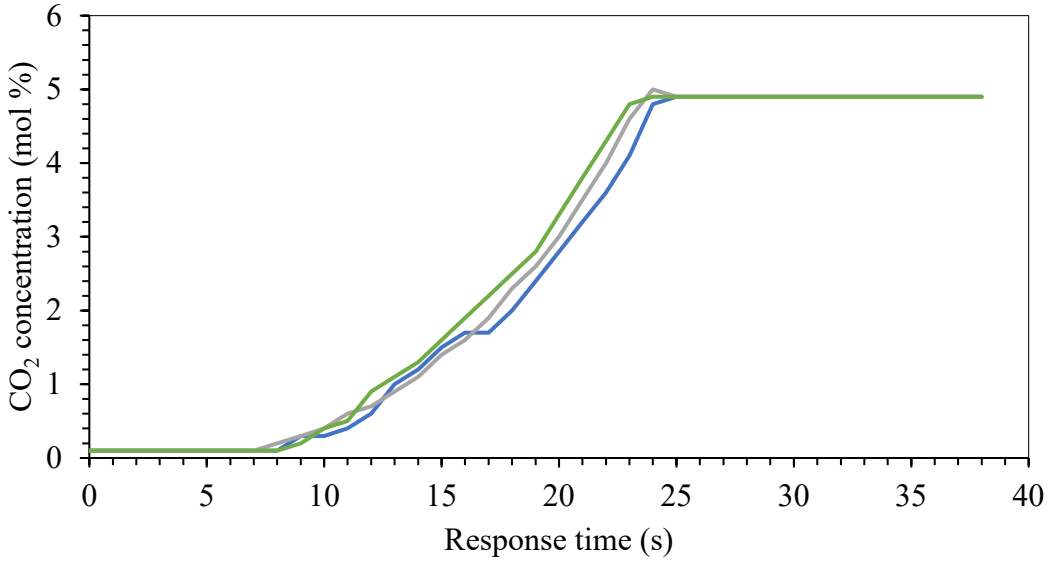

Figure 3.10: CO_2 analyser calibration curve using 5 mol% CO_2.

3.2.3 Liquid loading analysis

The CO_2 loading analysis of the liquid samples was determined by an acid-base titration method using a Metrohm 916 Ti-Touch autotitrator fitted with a LL Unitrode Pt1000 electrode and two 800 Dosino 20ml burette. The total alkalinity method as it is

commonly called is a direct method of determining CO_2 loading and a quick, reliable and cheap method to determine CO_2 loading (Masohan *et al.*, 2009). To carry out loading analysis of the lean and rich MEA solutions, between 1g to 4g of the sample (depending on expected concentration) was diluted with water to 100 ml. The required dilution depended on the expected loading, with a lower mass (1-2 g) used when a high loading is expected. The samples are titrated against a 1 M HCl solution to an endpoint of pH 7. The volume of HCl titrated was recorded before the titration was continued to an endpoint of pH 4. The following equation is used to calculate the alkalinity:

$$Alkalinity\ (mol\ L^{-1}) = \frac{Volume\ HCl\ at\ pH\ 4\ endpoint}{Volume\ of\ sample} \qquad (3.1)$$

The CO_2 loading is calculated by:

$$CO_2\ loading\ (mol\ L^{-1}) = \frac{Volume\ HCl\ at\ pH\ 4\ EP - Volume\ of\ HCl\ at\ pH\ 7\ EP}{Volume\ of\ sample} \qquad (3.2)$$

To convert the values to the mass concentration (relative to CO_2), the CO_2 loading in mol L^{-1} is multiplied by the molecular mass of CO_2. To express the CO_2 loading in moles of CO_2 per mole of alkalinity (α), the CO_2 loading in mol L^{-1} is divided by the alkalinity. The loading calculations was done automatically by the auto-titrator. This method was suitable for the large number of samples required to be analysed.

In addition, samples were analysed for water content determination by the Karl-Fisher method. The water titration determination was conducted using an automatic titrator (Metrohm 915 KF) using Hydranal-dry methanol (Sigma Aldrich) and Hydranal-composite 5 (Sigma Aldrich). The water titration determination was carried out three times to determine the exact MEA solution strength and ensure it was within the expected value.

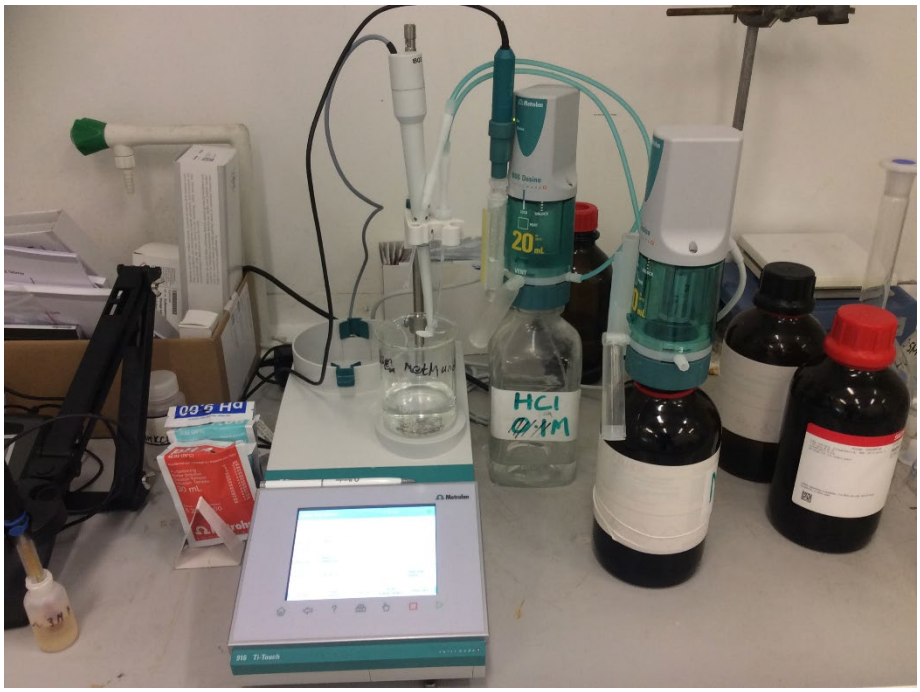

Figure 3.11: Metrohm auto-titrator.

3.3 Experimental data analysis

3.3.1 Calculation of height of transfer units

According to Jassim (2002), the height of the transfer unit (HTU) is used to express the efficiency of the RPB. The total height of a packed bed is found from the following equation below:

$$H = HTU * NTU \qquad (3.3)$$

Where *H* is total packed bed height and NTU is the number of transfer unit. The total height of the packed bed is then substituted with the radial depth in RPB (given as r_o-$r_{i,}$). Therefore the height of transfer units (HTU) is then expressed as:

$$HTU = \frac{r_o - r_i}{NTU} \qquad (3.4)$$

Where r_o and r_i are the outside and inside radii of the RPB respectively. The height of transfer unit (HTU) for the absorption runs here refers to the HTU_{OG} (overall gas phase). A lower HTU means that a smaller volume of absorber is required (Cheng and Tan, 2011).

3.3.2 Mass transfer

The overall volumetric gas mass transfer coefficients ($K_G a$) were based on gas phase CO_2 concentrations as they were more accurately measured at this stage of the experiments and the accuracy were within the range of 1-10% and it was also easier to employ overall gas mass transfer calculations (Jassim, 2002).

The difficulty of separation is usually expressed in terms of the number of transfer units (NTU). This is expressed based on the change in gas concentration and is defined by:

$$NTU_{OG} = \int_{y_1}^{y_2} \frac{dy}{y-y^*} = \ln\left(\frac{y_{CO_{2,in}}}{y_{CO_{2,out}}}\right) \qquad (3.5)$$

The equation assumes that the rate of reaction in the liquid phase is large enough to maintain zero CO_2 concentration in the liquid phase. It is assumed that the equilibrium partial pressure of CO_2 is negligible (y* =0) (Jassim *et al.*, 2007). This is because the CO_2 loading (mol/mol MEA) is low relative to y_{CO_2} and because of the fast chemical reaction between CO_2 and the concentrated amine solutions (Jassim *et al.*, 2007).

Kelleher and Fair (1996) gave the design of the RPB in terms of the area of transfer unit (ATU) as:

$$\pi(r_o^2 - r_i^2) = ATU_{OG} NTU_{OG} = \frac{Q_G}{K_G a_e Z} NTU_{OG} \qquad (3.6)$$

If equation 3.6 is rearranged, the overall gas-phase mass transfer coefficient is then given as:

$$K_G a_e = \frac{Q_G}{\pi(r_o^2 - r_i^2)Z} NTU_{OG} \qquad (3.7)$$

To evaluate the performance of the RPB for CO_2 absorption, the $K_G a$ values were measured at different operating variables that include the rotational speed, the gas-liquid ratio and solvent concentration. All the operating conditions for the study and the data were reproduced within a deviation of less than 5%.

3.3.3 CO_2 capture efficiency

According to Zhao *et al.* (2016), the CO_2 capture efficiency is generally considered one of the key parameters for evaluating CO_2 capture with RPBs. The important operating parameters to evaluating the RPB performance in terms of efficiency of CO_2 removal are rotational speed, the solvent concentration, CO_2 concentration, the gas-liquid flow rates and the reaction temperature.

The CO_2 removal efficiency is given as:

$$(\%)\ CO_2 \text{ removal efficiency} = \left(\frac{y_{CO_{2,in}} - y_{CO_{2,out}}}{y_{CO_{2,in}}}\right) X\ 100 \qquad (3.8)$$

In the equation above, $y_{CO_{2,in}}$ and $y_{CO_{2,out}}$ are the CO_2 concentrations in the inlet and outlet gas feed.

Although the concentration of solution to be prepared were to be 30 wt%, 50 wt% and 70 wt% for each experiment, the concentrations could vary slightly due to errors from the measurements of the large masses required for the experiment. As a result, a water content determination was carried out on some samples collected to obtain the accurate percentage mass of MEA in the solution. These values were then used in the calculation of the mass balance across the RPB for each experimental run.

3.3.1 Power consumption

The net force that held the torque arm on the motor in a horizontal position when the motor is under load driving the RPB was converted into power consumption using the equation below:

$$P = \omega_M LF \quad (3.9)$$

Where ω_M being the angular speed, L the length of the torque arm and F, the net force calculated from balancing attached weights to the electric motor.

3.4 Error analysis

In the course of the experimental runs, there are several possible sources of uncertainty that should be accounted for. The uncertainties were derived from the measuring equipment such as the pressure gauge (±0.1 mm Hg,), the water baths ((±0.1 C) temperature probes ((±0.1 C), CO_2 analyser ((±0.1 mol% C), the weighing scale (±0.1 g) so on. The HTU, $K_G a$, and CO_2 capture efficiency are derived values and therefore the possible contributing sources of errors should be evaluated. For estimating the errors of the $K_G a$ and HTU values, the following are the possible sources of error:

1. The uncertainties caused by weighing and preparation of MEA solutions.
2. The uncertainties due to the liquid and gas temperature measurements.
3. The uncertainties due to the liquid and gas flow rate measurements.
4. The uncertainties due to the CO_2 analyser measurements.
5. The uncertainty caused by the size measurements of the RPB size.

The reported values of the three $K_G a$ and HTU are broken down to analyse the effect of variables and can be written as:

$$D_a = f(T_{gas} T_{liquid,} q_{gas} q_{liquid} w_{MEA)})$$

For estimating the CO_2 efficiency, the sources of errors are:

1. The uncertainties caused by weighing and preparation of MEA solutions.
2. The uncertainties due to the CO_2 analyser measurements.

The combined standard uncertainty of this work have been evaluated by propagation law of uncertainties method (ISO GUM) (Kristiansen, 2003). The reported values can then be broken down to analyse the effect of variables and can be written as:

$$\%\, CO_2 = f(\%mol\, CO_2, w_{MEA)})$$

where the variables include all the influence factors such experimental temperature of gas and liquid, weight fraction of MEA.

The standard deviation is usually the recommended error to focus on and the size asked for is the combined standard uncertainty that is designated by $u_c^2(y)$ .The mathematical formulation using the variance is obtained by:

$$U_c^2 = \sum_{i=1}^{N} \left\{ \frac{\partial D}{\partial x_i} \right\}^2 u_i^2 \ (x_i)$$

Each of the variables are evaluated to provide an approximate estimate of the uncertainties and eventually the combined standard uncertainty.

Chapter 4. CO_2 absorption studies in a pilot-scale RPB with aqueous MEA solutions and counter-current gas-flow

4.1 Introduction

Experimental work was carried out on a counter-current RPB to investigate the performance in terms of overall gas mass transfer (K_Ga,), CO_2 capture efficiency and HTU. In addition, pressure drop and power measurements were taken. Firstly, CO_2 absorption experiment were carried out to validate the new RPB using 30 wt% and 90 wt% MEA solutions. Subsequently, a new set of experimental runs were carried out with 30 wt%, 50 wt% and 70 wt% MEA solutions at different concentrations, mass liquid-gas (L/G) ratios and rotational speeds. Synthetic flue gas mixture (67 vol% N_2, 18 vol% O_2 and 12 vol% CO_2) was used closely simulate industrial conditions. A novelty of this study was that the synthetic flue gas was saturated in a humidifier at 40˚C as would be the case with flue gas feed from a power plant. Prior to this work, other investigations on CO_2 capture using a RPB reported in the literature only used dry gases. This was significant because a dry gas will cause water to evaporate from the solvent affecting the rate of CO_2 absorption. Moreover, the number of moles of MEA reacting with the CO_2 for each of the MEA concentration stayed constant.

4.2 Experimental validation of the new pilot rig

4.2.1 CO_2 absorption runs

To validate the new RPB, preliminary CO_2 absorption experiments were carried out using 30 wt% and 90 wt% MEA solutions. Initial experimental test runs were carried out at rotational speeds between 600-1450 rpm. The lower speed of 600 rpm was selected due to the reported intensification effect in the RPB becoming observable at this rotational speed (Jassim, 2002). However, as a result of severe vibrations experienced at 1450 rpm that caused damages to the bearings of the motor and loud vibrations, subsequent rotational speeds were limited to an upper limit of 1150 rpm. Due to the speed range selected, the type of flow expected within the RPB was droplet flow resulting in less maldistribution of liquid occurring in the RPB and better mass transfer (Jassim *et al.*, 2007).

For the validation experiment, the focus was to compare $K_G a$ performance with other similar RPB work reported in literature. This was to confirm the new rig was giving expected results and identify any problems that need troubleshooting. Jassim (2007) carried out a comparable RPB mass transfer study using aqueous MEA solutions with similar concentration range and RPB dimensions. He carried out his study using a RPB with outer diameter and inner diameter 398 mm and 156 mm respectively and axial depth 25 mm. He also used MEA concentrations of 30 wt% and 100 wt%. The major differences between his work and this study was that the gas phase in his work was not saturated and the liquid-gas (L/G) mass ratios used were very high, around 33 while the industrially used range is usually between 3-5(Feron, 2016). The results of the overall gas phase mass transfer coefficient ($K_G a$) for CO_2 absorption for 30 wt% and 90 wt% MEA as a function of rotational speed and liquid/gas (L/G) mass flow ratio are shown in Figure 4.1. Jassim *et al.* (2007) reported $K_G a$ value of 1.05 s^{-1} for the 30 wt% MEA at 600 rpm while it was 2.2 s^{-1} for this work. For the 90 wt%, his result was 6.09 s^{-1} while it was 5.6 s^{-1} for this work.

A clear trend of the $K_G a$ results increasing with the MEA solution concentration can be seen as the $K_G a$ values more than double as the concentration increases from 30 wt% MEA to 90 wt% MEA. Increasing the MEA solution concentration led to increased reactivity due to the amount of moles of MEA in the solution increasing thereby raising the molar ratio of MEA/CO_2 which results in better CO_2 absorption (Kasikamphaiboon *et al.*, 2013). The reaction of MEA with CO_2 is a strong function of the solution concentration as it is a pseudo-first order reaction with respect to MEA concentration (Vaidya and Kenig, 2007b). It can also be seen that the L/G ratio has no effect on $K_G a$ for 30 wt% amine solutions but a noticeable effect for the 90 wt% solutions. This is explained by the observation that increasing the feed flow rate of the 30 wt% solution does not lead to significant increase in the MEA/ CO_2 being fed to the RPB. In comparison, a slight increase in the flow rate of the 90 wt% MEA resulted in a noticeable effect on the reaction kinetics due to the increased MEA moles present for reaction.

The increase in rotational speed seemed to have little effect on $K_G a$ for the 30wt% as there was only slight increase in the $K_G a$ values from 300 rpm-600 rpm and no

observable improvement past 850 rpm. This will suggest that increasing the rotational speed beyond 600 rpm for the 30 wt% MEA solution did not provide any significant advantages in mass transfer enhancement because the reaction kinetics was not fast enough for it to harness the advantages of the intensification. This is supported by Sheng *et al.* (2016) who found in their work that increasing the rotational speed of their rig beyond 800 rpm has little effect on K_Ga values for low concentration MEA solutions. For the 90 wt%, the result also seemed to be the same as the rotational speed only slightly increased the K_Ga results, although the K_Ga improved with higher L/G ratios. Increasing the rotational speed usually results in smaller liquid droplets and thinner films in the RPB and thereby improve mas transfer. However, the result observed could also be because the upper limit of the effective wetted surface area of the packing had been reached between 600-800 rpm and therefore further increase in the rotational speed did not result in any improvement of the surface area for mass transfer. This may be important for the 30 wt% MEA solution which has a lower viscosity in comparison to the 90 wt% solution

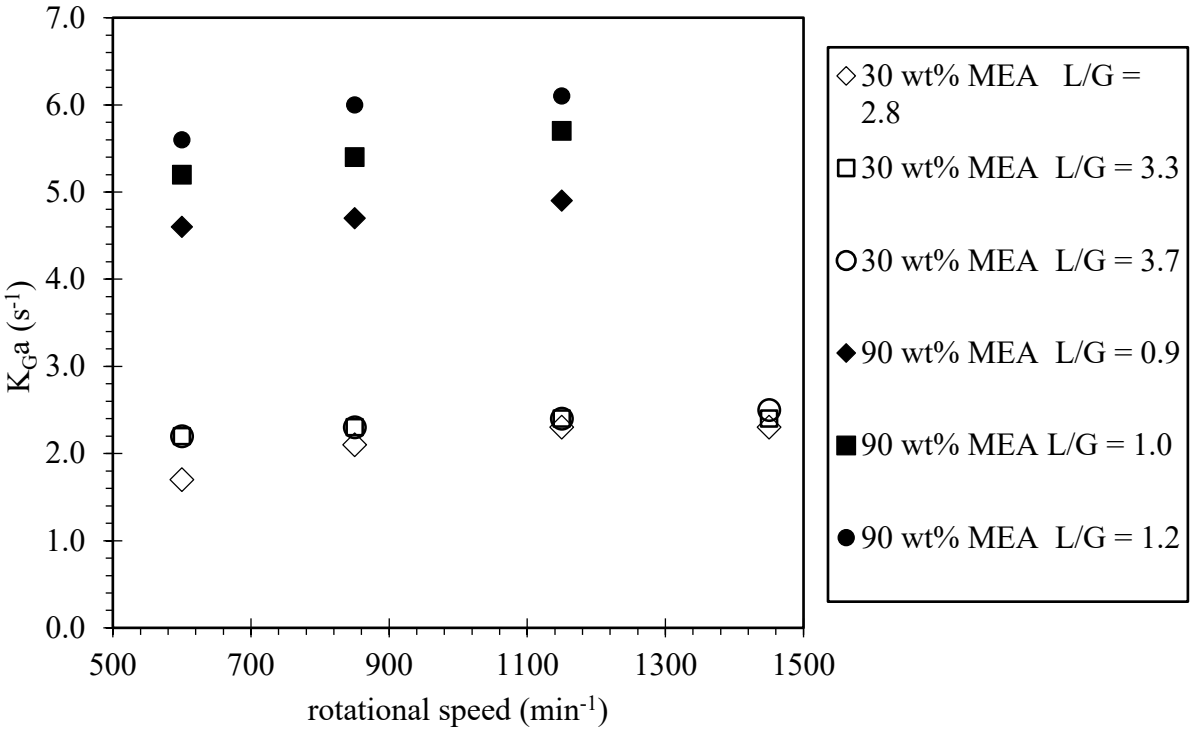

Figure 4.1: Overall gas-phase mass transfer coefficient for CO_2 absorption into MEA in this work.

Sheng *et al.* (2016) suggested that the limited improvement in mass transfer with increasing rotational speed could be because increasing the speed did not offer any further advantages in terms of the liquid distribution and resulted in the reduction of the liquid retention time within the packing which becomes a disadvantage for CO_2 absorption. This would seem to contradict the suggestion by Agarwal *et al.* (2010) that the RPB be run at as high a rotational speed as possible to get the maximum benefits of the high gravity fields in the RPB.

The measured values of K_Ga in the absorption runs were also in agreement with the results obtained by Jassim *et al.* (2007). Their work is comparable to this work in terms of the solution strengths and the lean amine loading (0.1 mol CO_2/mol MEA). The K_Ga values for the 30 wt% solutions obtained in this work were slightly lower than those obtained in their work because their 30 wt% MEA solution was preloaded to 0.33 mol CO_2/mol MEA. The experimental K_Ga values measured by Jassim in his work for the 75 wt% MEA solution are similar to the values for 90 wt% MEA in this work. The discrepancy observed can be attributed to the higher L/G ratios used for the tests he carried out which will affect the results significantly. They used very large L/G ratios (16 and 33) that would never be used in practice in the industry because of the implications for the regeneration cost of such large liquid flows.

The power consumption calculations were also made for the experiments from data collected from the torque arm measurements. It was found that the force required to maintain the torque arm in a horizontal position was constant with increasing liquid flow rate suggesting that the force required to overcome the friction from the seals installed on the drive shaft to prevent gas leaks and bypassing of the rotor was dominant. The measured torque was 0.86 Nm ± 0.25 Nm and the power consumption was found to increase from 108 -261W as the rotational speed increased from 600-1450 rpm. The results indicate that the torque arm needs to be longer so that changes in power consumption with liquid flow rate can be measured.

4.2.2 Troubleshooting and modifications to the rig

Initial runs with water and air on the new RPB quickly revealed that water was spraying from the tip of the RPB and entering the gas inlet pipework collecting in a low point and caused slugging flow in the gas inlet. This was fixed by changing the orientation of the gas inlet such that the gas feed flowed vertically downwards into the rotor case in the opposite direction to that shown in Figure 4.2. Knitmesh pads were placed in the gas inlet to prevent liquid entering the gas pipework.

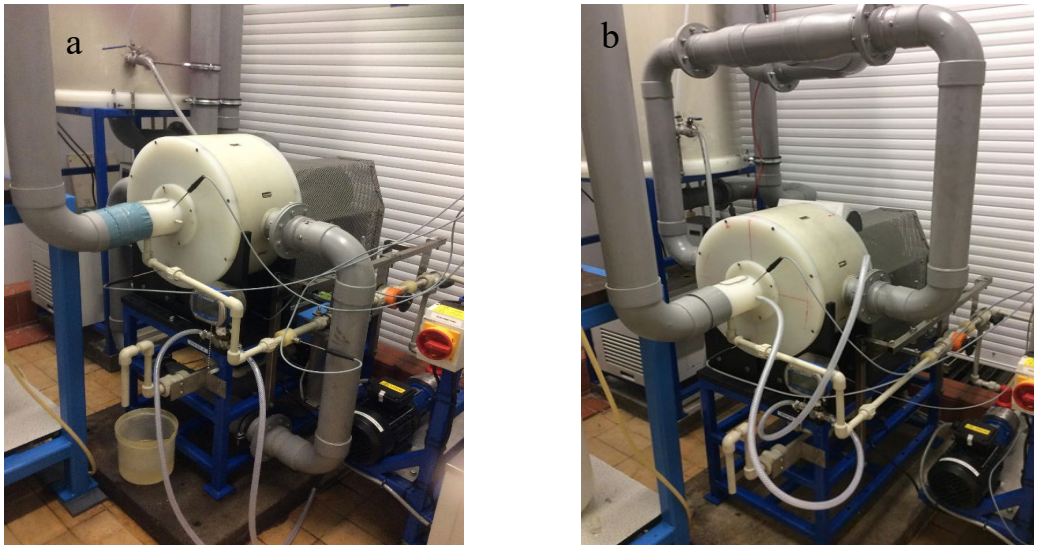

Figure 4.2: Modification of gas pipework. (a) Gas pipe inlet before modifications (b) gas pipework after modifications.

Furthermore, preliminary experiments with MEA solutions showed some anomalies in the gas inlet and outlet temperatures. The inlet gas and liquid temperatures were set for 40 ˚C ±0.1˚C and Figure 4.3 and Figure 4.4 show that there was a significant temperature rise of 40ºC for both gas outlet and liquid outlet for the 90 wt% MEA while this was not so for the 30 wt% solution. This could be because the 90 wt% MEA was a very viscous solution and the heat bulge was generated due to its high reactivity. This temperature rise was unexpected and investigated by measuring the flow rates of gas bypassing the seal on the RPB front using a hot wire anemometer.

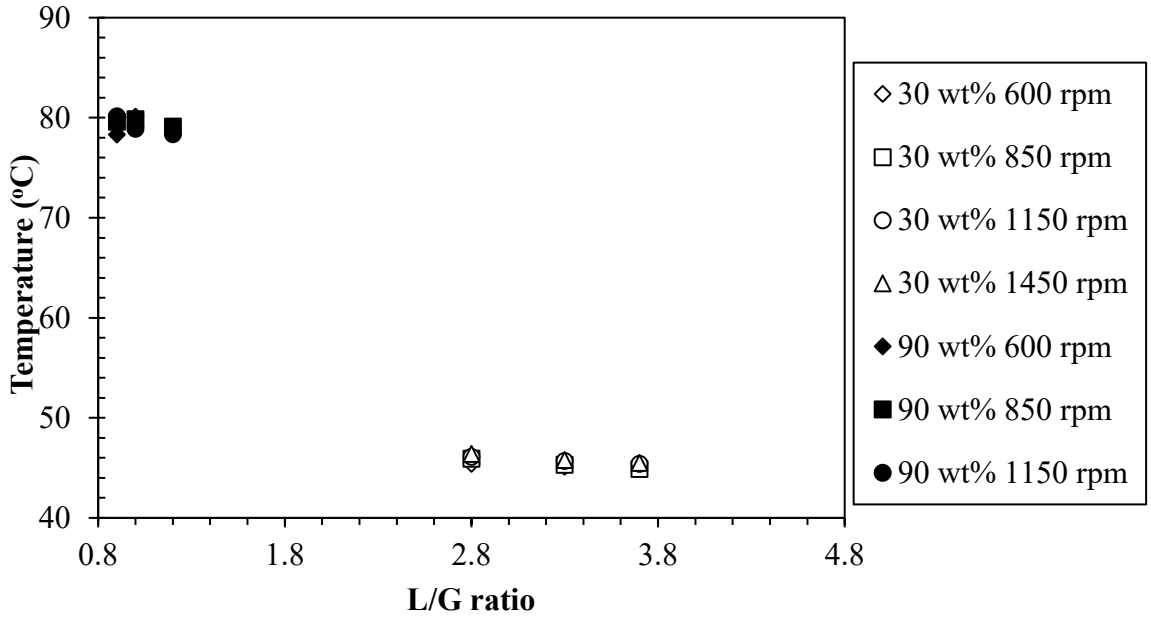

Figure 4.3: Gas outlet temperature for 30 wt% and 90 wt% MEA solutions for validation experimental run.

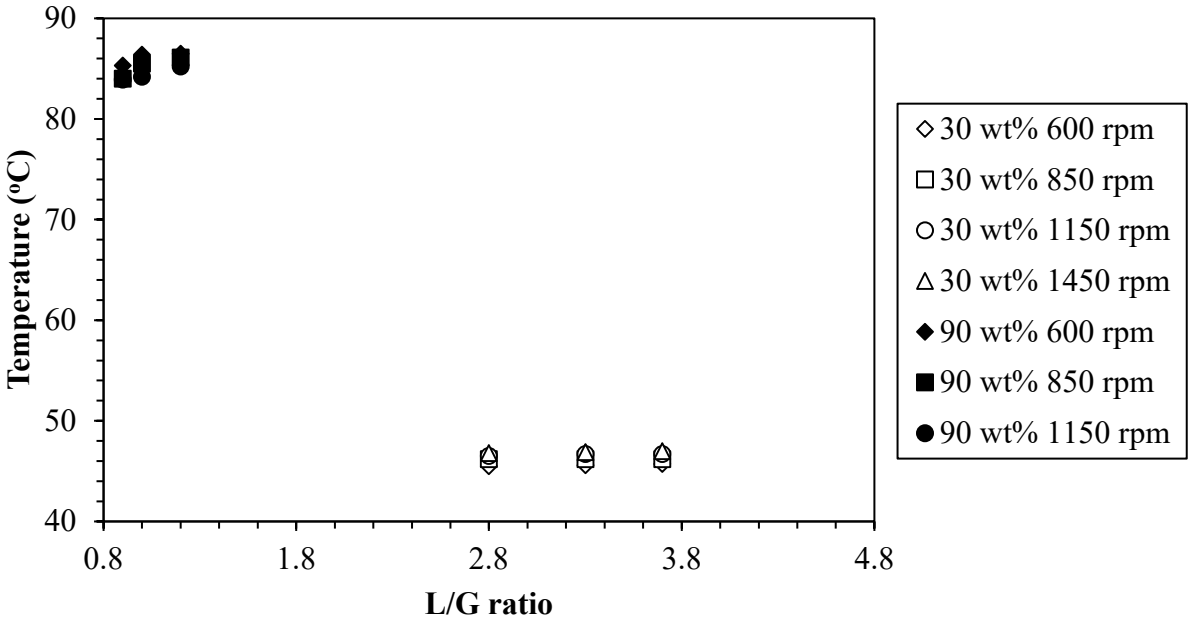

Figure 4.4: Liquid outlet temperature for 30 wt% and 90 wt% MEA solutions for validation experimental run.

It was found that up to 10% of inlet gas was leaking where the drive shaft entered the rotor case and up to 40% of the inlet gas was bypassing the rotor. To fix the problem, contact seals were installed on the drive shaft and between the gas outlet from the RPB and the rotor case. The front plate of the RPB casing was also machined to fit more tightly on the casing to eliminate gaps that caused liquid leakage during the validation experiments.

There was also significant wearing away of the bushes supporting the motor bearings when the rig was run continuously at 1450 rpm and the rotational speed range was limited to 1150 rpm for subsequent experiments. Furthermore, in addition to the sampling from the sump, an additional liquid sampling point was installed at the periphery of the rotor. This was achieved by putting in place a stainless-steel bore pipe through the RPB front with the tip directly under the edge of the rotor. It was positioned such that the liquid coming through the rotor collected directly into the bore and was collected by extracting with a syringe through a plastic tubing connected to allow the collected fluid from the bore flow out of the RPB.

4.3 Experimental absorption runs in the counter-current gas-flow configuration

4.3.1 Performance of the counter-current RPB in terms of HTU

Figure 4.5 shows the HTU results obtained for the different MEA concentrations as a function of the rotational speed, MEA concentration and L/G ratios. It can be observed that the HTU results trend shows a decrease in HTU values as the rotational speed increased and decreased as the MEA concentration increased. These findings are in agreement with what was observed by Rahimi and Mosleh (2015) in their work. However, a closer look at the results indicate noticeable reduction in the HTU results as rotational speed increased from 300 rpm to 850 rpm, but little change was observed beyond 850 rpm. This could be because at higher rotation speeds, the gas-liquid surface renewal rate is accelerated leading to the formation of small liquid droplets and thinner films within the RPB that results to a larger gas-liquid contact surface. This would result in mass transfer intensification but also a reduction in the liquid retention time in the packing and thus weaken CO_2 absorption efficiency (Sheng *et al.*, 2016). This was likely

a more predominant factor at rotational speeds beyond 850 rpm in this study resulting to little effect past 850 rpm.

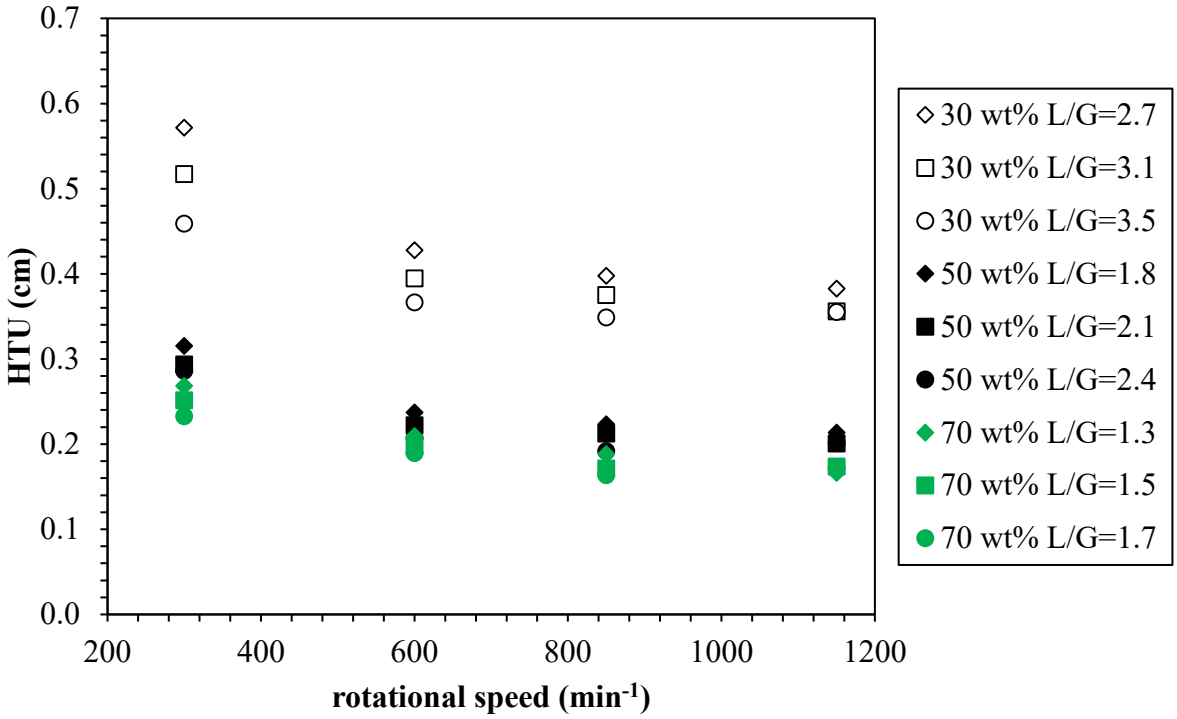

Figure 4.5**:** Effect of rotational speed on HTU at different L/G ratios, 12 vol % CO_2 in simulated flue gas and average lean/rich loading (mol CO_2/mol MEA).

The decrease in HTU with increasing MEA concentration can be explained by the fact that increasing the MEA concentration results in a better reaction rate between CO_2 and MEA (Sheng *et al.*, 2016). This is also in agreement with the work of Rahimi and Mosleh (2015) who found a similar dependence of HTU values on MEA concentration. The results in Figure 4.5 also indicate a considerable reduction in HTU results as MEA concentration increased from 30 wt% MEA to 50 wt% MEA but only a slight decrease in HTU values by increasing MEA concentration from 50 wt% to 70 wt%. This would suggest that using 70 wt% MEA concentrations did not yield any significant HTU advantages. This may be due to the enhancement provided by the RPB being most noticeable for lower MEA concentrations. The explanation for this is that higher concentration MEA solutions have better CO_2 absorption efficiency and the effect of

reduction in mass transfer resistances would more observable for the lower concentration MEA (Lin and Lin, 2013). For the effect of L/G ratio, the trend generally showed a reduction of HTU values with L/G ratios. For the effect of L/G ratio for the different MEA concentrations, it can be seen from Figure 4.5 that the effect of L/G ratio on HTU was higher for the 30 wt% MEA solution while there was little effect on 50 wt% and 70 wt% MEA. This can be explained by the fact that increasing the liquid volumetric flow rate leads to an increase in liquid holdup and gas−liquid contact area in the RPB. Consequently, this results in an increase in the mass-transfer efficiency. Moreover, using a higher liquid volumetric flow rate provides more absorption solution per unit of gas to absorb more CO_2. Both of these factors lead to a higher CO_2 removal efficiency and mass-transfer efficiency.

4.3.2 Evaluation of CO_2 capture efficiency results

Figure 4.6 shows CO_2 capture efficiency results at three different rotational speed, L/G ratio and MEA concentration for the counter-current RPB. The result trend shows that CO_2 capture efficiency increased with rotational speed and MEA concentration. It can be noticed that the CO_2 capture efficiency showed considerable improvement between 300rpm and 600 rpm but not much increase beyond 850 rpm. The 30 wt% MEA showed the lowest improvement past the rotational speed of 850 rpm. The 50 wt% and 90 wt % MEA solutions indicated little increase in CO_2 efficiency by increasing rotational speed to 1150 rpm. This indicated that the mass-transfer resistances were reduced with an increase in the rotating speed for the higher MEA concentration solutions. However, when the rotating speed was further increased, only a small effect on KGa was observed. This is in agreement with what was observed by Lin *et al.* (2003). This can be explained by the fact that the reduction of mass transfer resistance by increasing the rotating speed was compensated for by the short reduction time that was unfavourable for the CO_2 chemical absorption. This is even much important for the 30 wt% MEA solution that has a lower CO_2 absorption efficiency in comparison to 50 wt% and 90 wt% MEA solutions. This would mean increasing the rotational speed provides advantages for higher concentration MEA concentrations rather than for low concentration MEA solutions.

The higher MEA concentrations displayed better CO_2 capture efficiency performance with CO_2 efficiency increasing as MEA concentration increased from 30 wt% to 70 wt%. This is due to higher concentration amine solutions showing better CO_2 absorption resulting in better CO_2 capture efficiency results. The CO_2 capture efficiency increased with higher L/G ratios as can be seen in Figure 4.6. The enhanced CO_2 removal efficiency with respect to increased L/G ratio can be attributed to the higher reaction of the MEA with CO_2 when the liquid flow rate is increased. When the L/G ratio is increased, more CO_2 can be absorbed by the MEA solution leading to larger enhancement factor due to the increased MEA concentration with sufficient contact time allowed for absorption despite the increasing the liquid flow (Tan and Chen, 2006).

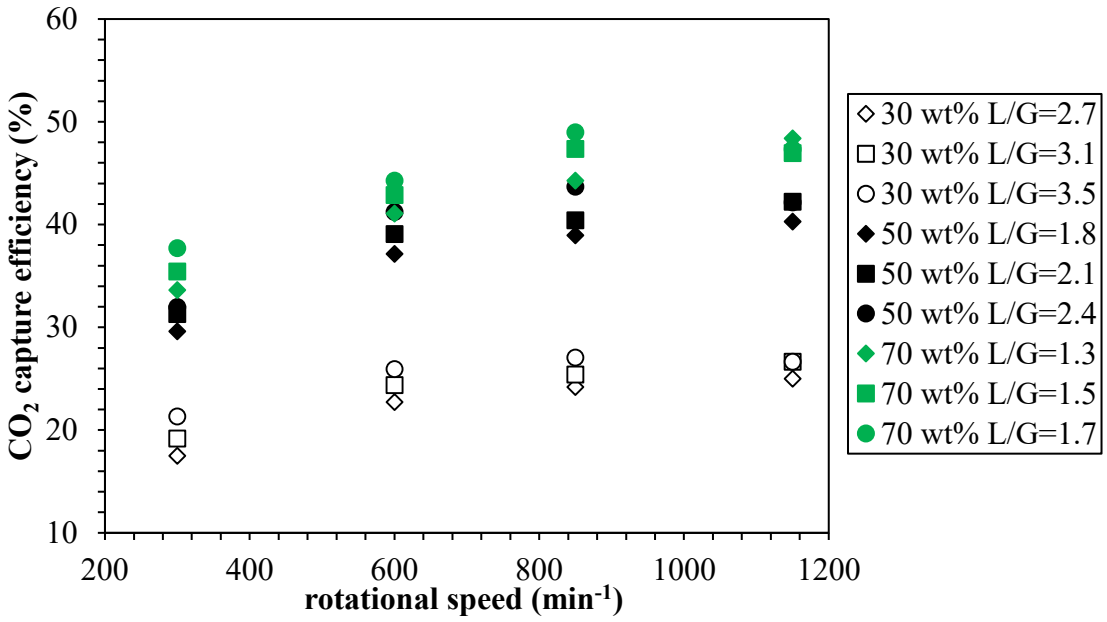

Figure 4.6**:** Effect of rotational speed, L/G ratio and MEA concentration on CO_2 capture efficiency.

Figure 4.6 also shows that the rotating speed had a larger effect on K_Ga at lower MEA concentrations when the rotating speed was less than 1150 rpm. This is also explained by the higher concentration MEA having a better CO_2 absorption than the lower MEA concentrations. This means an increase in K_Ga resulting from an enhancement in the

absorption due to a reduction of mass transfer resistances at high rotating speeds was more pronounced at the 30 wt% MEA concentrations (Lin and Lin, 2013). The results obtained generally indicated that increasing rotating speed achieved a high CO_2 removal efficiency.

4.3.3 Mass transfer characteristics of the counter-current RPB

The results for the overall gas phase mass transfer coefficient (K_Ga) as a function of rotational speed, L/G ratio and MEA concentration are shown in Figure 4.7. The trend showed that the KGa values generally increased with increasing rotational speed. This demonstrates that increasing the rotational speed reduces the mass-transfer resistances in the RPB and indicates mass transfer enhancement due to hyper-gravity fields in the RPB (Lin et al., 2003).

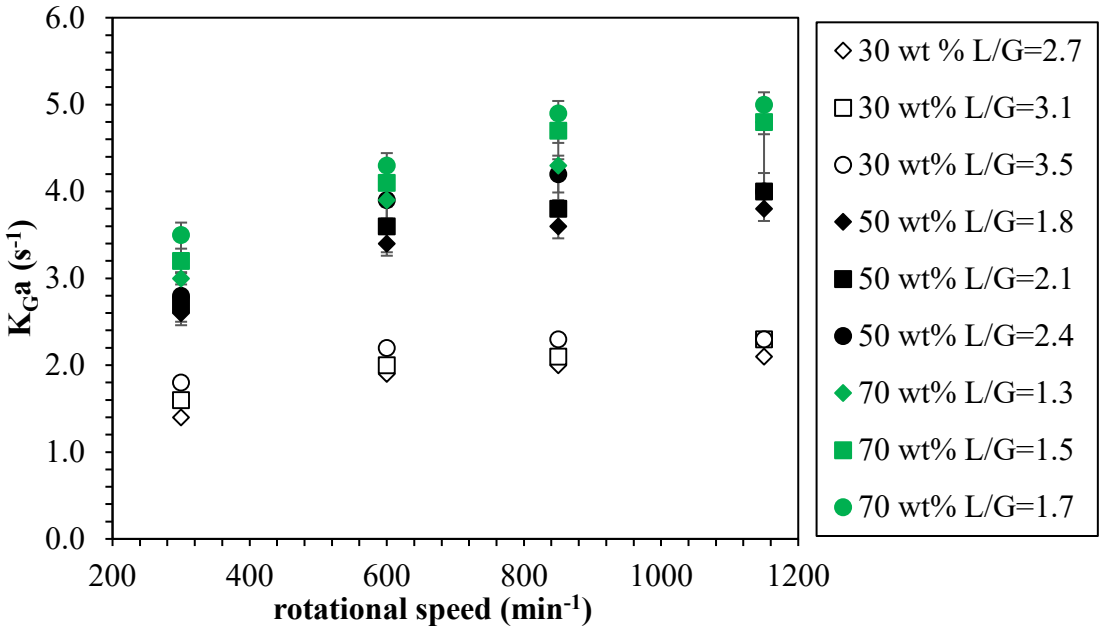

Figure 4.7: Effect of rotational speed, L/G ratio and MEA concentration on overall gas-phase mass transfer coefficient.

The higher centrifugal environment generated from increasing the rotational speed not only reduce mass transfer resistances but also increases the effective surface area for contact. At higher rotational speeds, there is better mixing achieved within the RPB leading to the formation of small liquid droplets and thinner films that increase the gas-

liquid contact surface and the rate of gas-liquid surface renewal (Rahimi and Mosleh, 2015). Sun *et al.* (2012) suggested that larger gas-liquid contact area and increased rate of the renewal of the gas-liquid interface lead to higher mixing efficiency due to the HIGEE environment in the RPB and ultimately result in increased $K_G a$. However, there were mixed results in terms of the effect of rotational speed on mass transfer enhancement for the different MEA concentrations. For example, there was only a slight increase in the $K_G a$ results for the 30 wt% MEA solutions beyond 600 rpm. For 30 wt% MEA, the $K_G a$ value increased from 2.2 s^{-1} to 2.3 s^{-1} as rotational speed increased from 600-1150 rpm while for the 70wt% MEA, it increased from 4.3 s^{-1} to 4.9 s^{-1} at a similar MEA/CO_2 molar ratio (4.4). For the 30 wt% MEA solution, almost doubling the rotational speed caused only a slight increase in $K_G a$ results and this can be explained by the mass transfer being mostly limited by the reaction in liquid phase (Wojtasik *et al.*, 2018). Therefore, the advantage of the intensification of the RPB could not be fully harnessed for the 30 wt% MEA solution.

Another possible explanation could be that the 30 wt% MEA solution showed a worse $K_G a$ performance with respect to rotational speed because it had the lowest CO_2 absorption coupled with less retention time in the RPB. Therefore, the increase in rotational speed became a disadvantage rather than an advantage. This agrees very well with the findings of Ma and Chen (2016). They found that when using concentrated alkanolamines for CO_2 capture, the reduction in $K_G a$ values was less significant for high amine concentration than for lower concentration amines as rotational speed was increased. This is due to the increased rate of reaction of higher concentration amines that means that there is still effective reaction of CO_2 and MEA despite the shortened residence time that was not the case for low concentration MEA solutions. From the results obtained, it may be argued that contact time plays a more important role for mass transfer for lower concentration MEA solutions and it may be better to run the RPB at lower rotational speeds for low concentration MEA solutions. For the 50 wt% and 70 wt% MEA solution, it can be observed that that there was higher $K_G a$ values as the rotational speed increased. This may be due to better CO_2 absorption by higher MEA solution concentration.

In general, when considering the $K_G a$ results, it is should be highlighted that although they generally improved with respect to rotational speed, this dropped off beyond 600 rpm. This could possibly be due to the reduction in the retention time within the RPB packing resulting in less time for the gas and liquid phase to react. This explanation was also provided by Lin *et al.* (2003) in their work when they found that $K_G a$ values increased with rotational speed up to 1000 rpm when capturing CO_2 using NaOH in the RPB, but their results dropped considerably above 1000 rpm. They suggested that this could be due to the reduction in retention time that was unfavourable to chemical absorption and therefore compensating for the reduction in the mass-transfer resistances that was obtainable at higher rotational speeds.

The residence time in the RPB has also been reported to approach a constant value when the rotational speed is sufficiently high, usually in the range 800-1000 rpm (Guo *et al.*, 2000). The result trend of this work was also in agreement with that carried out by Sheng *et al.* (2016) whose findings showed that increasing the rotation speed beyond 800 rpm had very little effect on $K_G a$. Their explanation was also that it could be due to reduction of the liquid retention time in the packing that negatively affects the CO_2 absorption. They also argued that this became much more significant beyond 800 rpm resulting in a little increase in $K_G a$ values that has also been observed in this study.

With respect to the effect of MEA solution concentration, the most noticeable trend was that $K_G a$ showed dependence on the MEA solution concentration as it more than doubled from 30 wt% MEA to 70 wt% MEA. This is likely due to the increase in the rate of reaction between CO_2 and MEA as the MEA concentration increases thereby resulting in an increase in $K_G a$. This can be further explained by the fact that at a given gas and liquid flow rate, mass transfer will increase with increasing MEA concentration due to the higher amounts of hydroxide ions per unit volume available for reacting with the CO_2 when MEA concentration is increased (Rahimi and Mosleh, 2015). Moreover, in a mass transfer process enhanced by chemical reaction within a RPB, the two main factors that influence the mass transfer coefficient are the rate of renewal of the liquid film and the reaction rate (Qian *et al.*, 2010). Therefore, increasing the rate of liquid film renewal and the reaction rate will result in an increase of the mass transfer coefficient.

Furthermore, in a chemical reaction with a high rate of reaction such as MEA solutions at high concentration, a stable gas-liquid concentration gradient will be formed even in an extremely thin liquid film. This is such that the liquid film renewal no longer plays an important role in the intensification of the mass transfer process. The mass transfer coefficient then becomes a function of just the rate of chemical reaction in such a condition (Qian *et al.*, 2010).

Figure 4.7 shows that $K_G a$ results improved with increase in L/G ratio at the different MEA concentration. This is because at higher liquid flow rates, there is more solution provided to absorb more CO_2 which results to higher mas transfer efficiency. As the gas flow rate remained constant, the increase in the liquid flow rate led to an increase in liquid hold-up and gas-liquid contact area in the RPB that resulted better mass-transfer efficiency (Sheng *et al.*, 2016). Another possible explanation is that increasing the liquid flow rate leads to growth in the gas-liquid interfacial area that include films on the surface of the packing and droplets within the bed porosity (Rahimi and Mosleh, 2015). Moreover, the increase in the spread of more liquid films on the packing and liquid droplets flying into voidage of the bed packing provides a larger gas-liquid interfacial area for mass transfer (Chiang *et al.*, 2009).

It can be observed that the effect of L/G ratio also varied among the different MEA solutions. The 30 wt% MEA solutions showed only a slight increase in $K_G a$ as a function of L/G ratio while 50 wt% MEA solutions showed very little improvement with respect to increase in L/G ratio. The 70 wt% MEA showed the best improvements in $K_G a$ results with respect to increase in the L/G ratio and this can be explained by its high CO_2 absorption due to increased reaction rate. The power consumption for the counter-current RPB was investigated and the force required to maintain the torque arm in a horizontal position was found to be constant with increasing liquid flow rate suggesting that the force required to overcome the friction from the seals is dominant. The measured torque was 0.86 Nm ± 0.25 Nm. The power consumption was found to increase from 54 -207 W as the rotational speed increased from 300-1150 rpm. The results indicate the torque arm needs to be longer so that changes in power consumption with liquid flow rate can be measured.

4.3.4 Pressure drop measurement in the counter-current RPB

The pressure drop ΔP, was measured across the gas inlet and gas outlet and so the pressure drop measured in this work was the total pressure because of both frictional and centrifugal forces within the RPB.

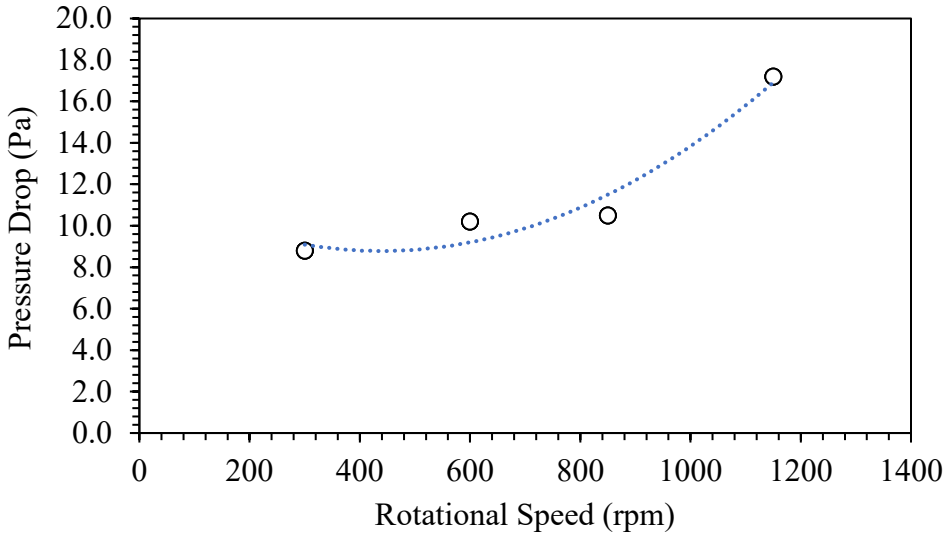

Figure 4.8: The effect of rotational speed on gas pressure drop for 70 wt% MEA solution.

Figure 4.8 shows the result obtained for the pressure drop across the rig when running with the 70 wt% MEA. It is apparent that the pressure drop across the RPB increases with the rotational speed. This can be explained by the increased vigorous collision of the gas and liquid occurring in the RPB as the rotational speed was increased.

4.3.5 Analysis of the outlet liquid and gas temperature results

The inlet liquid temperature for all the experimental runs was set to 40 ºC. This temperature was used as industrial flue gas is cooled to this temperature before being fed into the absorber (Feron, 2016). It can be seen from Figure 4.9 that the most noticeable trend was that the outlet liquid temperature increased with MEA concentration. At the different MEA concentrations used, there was little effect of the L/G ratio on the outlet liquid temperature. For the 30 wt% MEA, there was no observable effect of rotating speed on the outlet liquid temperatures.

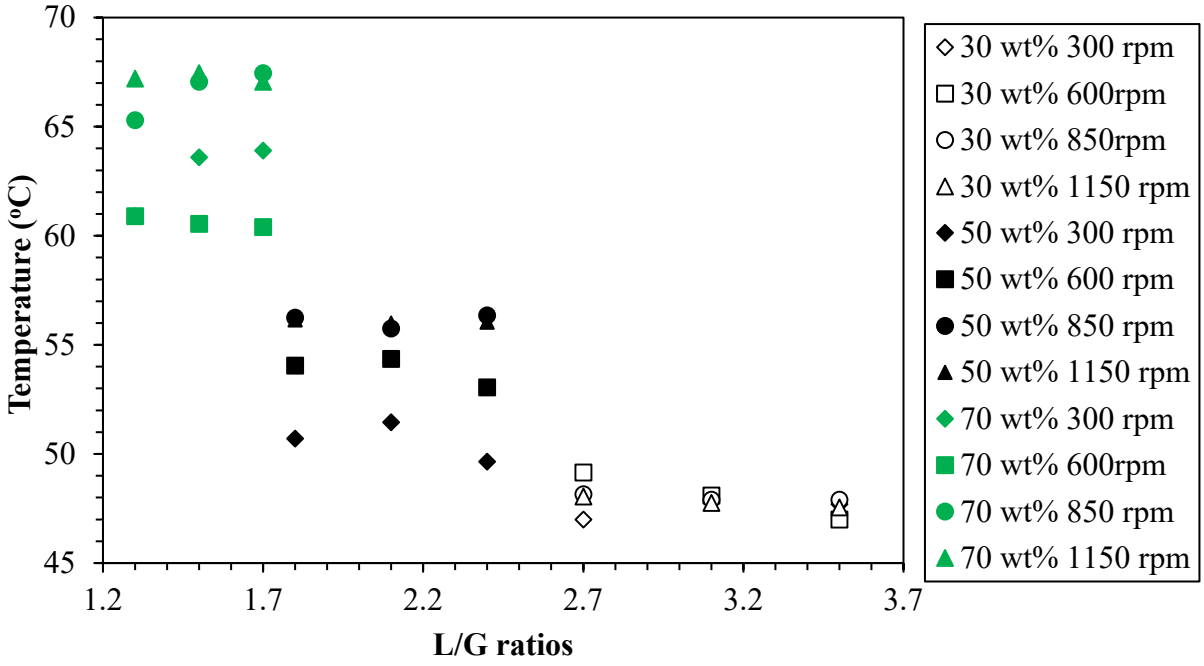

Figure 4.9: Liquid outlet temperature profile at different MEA concentrations and L/G ratio (30 wt%, 50 wt% and 70 wt%).

However, at 50 wt%, the highest outlet liquid temperatures were at the higher rotor speeds (between 850 and 1150 rpm) while the lower outlet liquid temperature was at 300 rpm, the lowest rotational speed. This can be attributed to the increased effective mixing and contact between the gas and liquid as the rotational speed increases increasing the reaction rate. The results obtained indicate that the solvent strength has the biggest effects on the outlet liquid temperature. This is due to the reaction of MEA and CO_2 being a very exothermic reaction (Lv *et al.*, 2015). As the solution concentration of the solvent was increased, the moles of MEA available for reaction with CO_2 also increased resulting in a faster reaction and increased temperature. The temperature results for the gas outlet were more scattered as shown in Figure 4.10.

However, it can be seen that the lowest outlet gas temperatures for each MEA concentration were at 300 rpm and the outlet gas temperatures were highest at 1150 rpm. There also seemed to be a decrease of the outlet gas temperature with increase in L/G ratio at 1150 rpm and 600 rpm. As the gas phase composition (12 vol% CO_2) was

constant for all the experiments, the trend was that the outlet gas temperature was strongly influenced by the concentration of the MEA solution for the reaction. The highest outlet gas temperatures can be seen to be at the highest MEA concentration and vice versa.

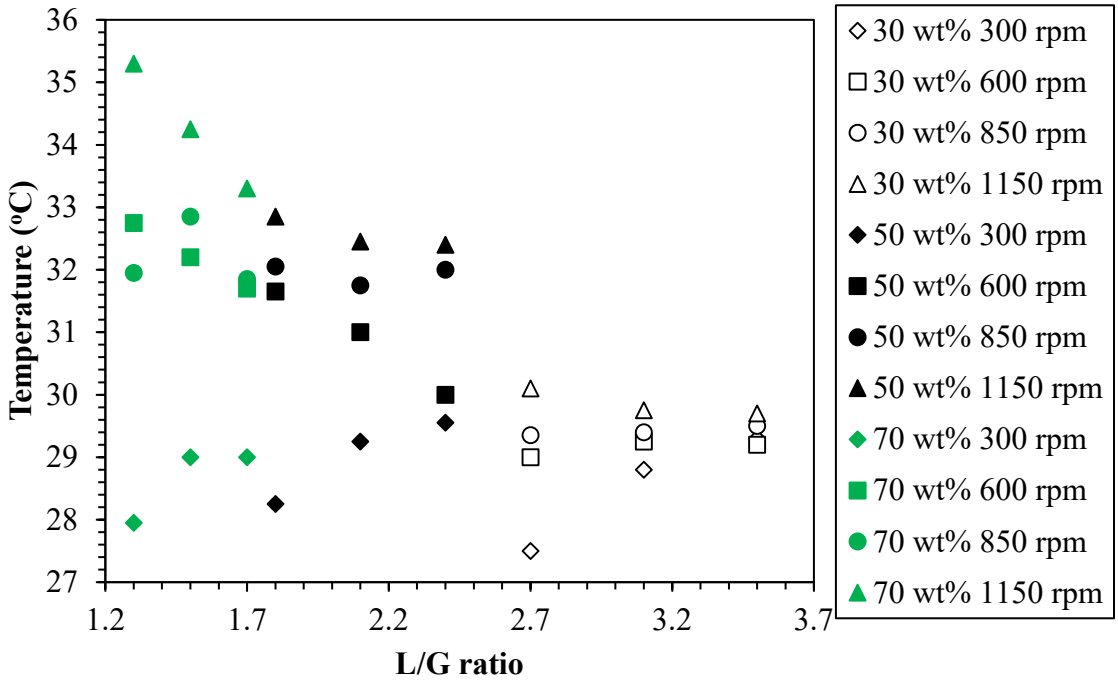

Figure 4.10: Gas outlet temperature profile at different MEA concentration and L/G ratio.

For the liquid loading analysis, samples from the sump collection point and from the periphery of the rotor (just after the liquid comes out from the rotor) were analysed and the CO_2 loading obtained through titration. Table 4.1 shows the rich CO_2 loading at the front and the sump. It can be seen that the loading increases at the different rotational speeds between the periphery and the sump except for 1150 rpm. The increase in CO_2 loading indicates that more CO_2 was captured by the MEA solution within the RPB casing before exiting the RPB. According to Luo *et al.* (2012a), the RPB could be divided into three major mass transfer zones. These are the end zone (the part of the packing closest to the inner edge of the rotor), the bulk zone (the remaining zone of the rotor) and the cavity zone (the zone between the outer edge of the rotor and the inner edge of the RPB casing). This was also indicated by Gao *et al.* (2016) who described it as the zone

that was between the outer edge of the rotor and the external RPB shell. In their mathematical model explaining the behaviour of liquid droplets in this zone, they suggested that the size of the droplets in this cavity zone were very similar to the droplets at the outer edge of the packing and unlike the droplets within the packing, these droplets are faster, smaller and unaffected by centrifugal force. It can be seen from Table 4.1, 4.3 and 4.4 that there was trend for the CO_2 loading from the outer edge of the rotor (front) to be lower than that from the liquid outlet (sump). This was attributed by Yang *et al.* (2011) to be due to the contribution of this cavity zone (ø) to the gas-liquid mass transfer which they estimated using the equation:

$$ø = \frac{C_o - C_1}{C_o} \; X \; 100\% \qquad (4.1)$$

where C_o is the liquid outlet CO_2 loading, and C_1 is the CO_2 loading from the outer edge of the packing. In their work, the value of ø ranged from 13-17%. Sun *et al.* (2012) indicated that the total mass transfer within the RPB was the sum of the mass transfer within the packing, mass transfer within the hollow region of the RPB as well as the space between the rotor and the RPB casing (cavity). Although, this work does not set out to measure the amount of mass transfer taking place in this cavity zone, the loading results obtained from the rotor periphery and the liquid outlet could be evidence in support of the additional mass transfer occurring in the cavity zone. Experimental studies on the $K_G a$ values in the RPB have tended to assume that the mass transfer takes place only within the packing but there been stronger evidence in recent studies that this may not be the case. Examples of such studies include the recent work done by Sang *et al.* (2017) to visually investigate the liquid flow pattern and droplet formation in the cavity zone.

Table 4.1: Liquid loading analysis results at 30 wt% MEA

MEA (wt%)	Rotational speed (rpm)	L/G ratio	Average lean/rich loading on rotor periphery	Average lean/rich loading from sump
30	300	2.7	0.146	0.183
		3.1	0.152	0.169
		3.5	0.148	0.167
	600	2.7	0.183	0.197
		3.1	0.190	0.192
		3.5	0.167	0.166
	850	2.7	0.208	0.213
		3.1	0.191	0.205
		3.5	0.194	0.188
	1150	2.7	0.203	0.202
		3.1	0.201	0.198
		3.5	0.199	0.196

One of the interesting results Yang *et al.* (2011) found was that the contribution of the mass transfer rate of the cavity zone diminished with increasing rotational speed. It can be seen from Figure 4.11 that CO_2 loading from the outer edge of the rotor (front) for 30 wt% MEA at L/G ratio 2.7 is lower than that from the liquid outlet (sump). This is possibly due to further reaction taking place in the cavity zone of the RPB after the liquid has left the packing. The marked difference between the front and sump loadings at the two L/G ratios could be due to the surface of the packing not being effectively wetted at lower L/G ratio. However, as the rotational speed increased, the packing became effectively wetted and the increase in L/G ration did not have any noticeable effect on the liquid loading. It can also been seen that the difference in loading between the sump and front was decreased with the increase in rotational speed until it was very little at the higher end of the rotational speed which will seem to support the suggestion of Yang and co-workers (2011).

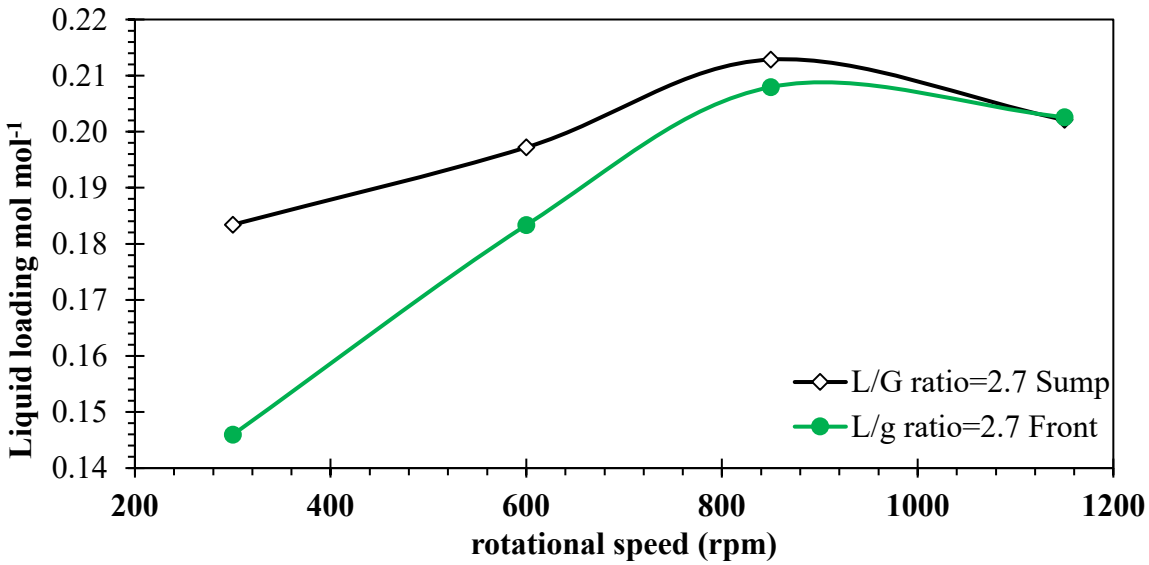

Figure 4.11: CO_2 loading at L/G=2.7 at 30 wt% MEA as a function of rotating speed.

Table 4.2: Liquid loading analysis results at 50 wt% MEA

MEA (wt%)	Rotational speed (rpm)	L/G ratio	Average lean/rich loading on rotor periphery	Average lean/rich loading from sump
50	300	1.8	0.121	0.133
		2.1	0.129	0.116
		2.4	0.121	0.122
	600	1.8	0.170	0.133
		2.1	0.165	0.131
		2.4	0.140	0.121
	50	1.8	0.161	0.148
		2.1	0.161	0.135
		2.4	0.143	0.130
	1150	1.8	0.176	0.140
		2.1	0.154	0.140
		2.4	0.141	0.140

Table 4.3: Liquid loading analysis results at 70 wt% MEA.

MEA (wt%)	Rotational speed (rpm)	L/G ratio	Average lean/rich loading on rotor periphery	Average lean/rich loading from sump
70	300	1.3	0.210	0.117
		1.5	0.214	0.124
		1.7	0.211	0.127
	600	1.3	0.176	0.153
		1.5	0.149	0.135
		1.7	0.153	0.137
	50	1.3	0.184	0.134
		1.5	0.199	0.136
		1.7	0.170	0.127
	1150	1.3	0.210	0.149
		1.5	0.222	0.132
		1.7	0.188	0.139

4.4 Summary

Experimental validation of the new pilot-scale RPB rig was carried out by measuring the rate of CO_2 absorption using 30 wt% and 90 wt% amine solutions. The overall gas phase mass transfer coefficient was calculated by measuring the change in CO_2 concentration between the gas inlet and gas outlet and it was found to be in the range of 1.8 – 6.2 s^{-1}. In addition, the number of transfer units was found to be in the range 0.22-0.84 indicating that the height of a transfer unit in the RPB as in the range 0.50 – 0.13 m. It was found that the concentration of the amine solution had the biggest effect on the rate of CO_2 absorption followed by L/G ratio. For the absorption runs on the counter-current RPB, the rate of CO_2 absorption was measured in a RPB using 30, 50 and 70 wt% amine solutions as solvents. The change in CO_2 concentration between the gas inlet and gas outlet was used to calculate the number of transfer units and the overall gas phase mass transfer coefficient. The number of transfer units was found to be in the range 0.22-0.84 indicating that the height of a transfer unit in the rotating packed bed as in the range 0.50

– 0.13 cm. The measured overall mass transfer coefficients were in the range of 1.8 – 6.2 s^{-1}.

Chapter 5. Application of co-current flow RPB for CO_2 absorption studies with aqueous MEA solutions

5.1 Evaluation of HTU for the co-current RPB

5.1.1 Effect of rotational speed

Figure 5.1 shows the HTU results for the co-current RPB as a function of rotational speed. The RPB was operated between 300-1150 rpm using MEA solution at three different concentrations (30 wt%, 50 wt% and 70 wt%) and L/G ratios. The results showed that the HTU values decreased with increasing rotational speed for 30 wt% MEA solutions. For the 50 wt% and 70 wt% MEA solutions, the HTU values reduced as the rotational speed increased from 300-600 rpm but increased slightly increased past 600 rpm.

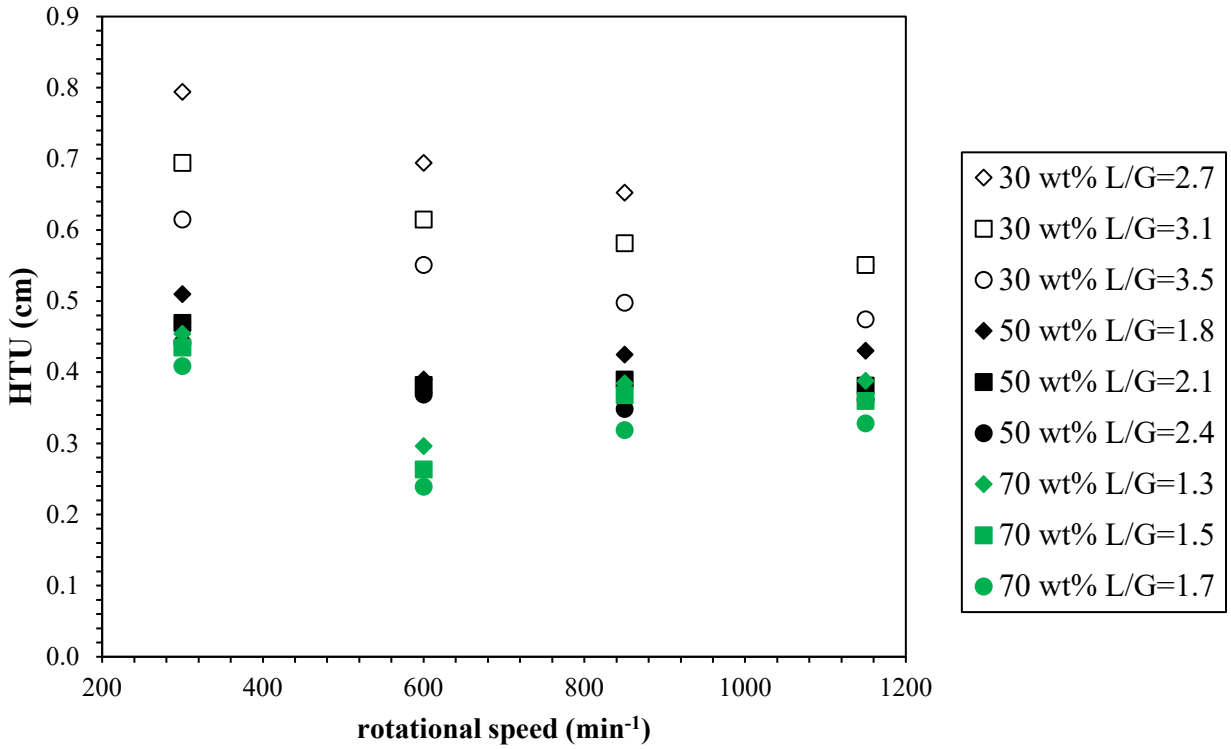

Figure 5.1: HTU values as function of rotational speed and L/G ratios.

The HTU results trend are quite interesting, as they did not follow the expected trend for the HTU values to decrease as the rotational speed increased. It is important to note that the fluid mechanics of the RPB is highly complex and not yet fully understood (Xie *et al.*, 2017). Therefore, the characteristics of the liquid flow and the mass transfer behaviour within the RPB is difficult, especially for the different gas-flow configurations. A possible explanation for the result trend observed is that contact time has greater effect on the mass transfer at higher rotational speeds in the co-current RPB. This could be more predominant in higher concentration MEA solutions due to their increased viscosity coupled with the short retention time in the RPB resulting in a lower mass transfer driving force in the RPB.

Co-current RPBs have been reported to have lower mass transfer driving force at the expense of a low pressure drop (Chu *et al.*, 2014). Cheng and Tan (2011) reported a similar result with their lowest HTU values at 600 rpm and highest HTU values at 1200 rpm in a CO_2 absorption experiment with mixed amine solutions (MEA and PZ) in a co-current RPB. They suggested that although the mass transfer resistances are reduced at higher rotating speeds, this could be offset by the decrease in gas-liquid time at high rotating speeds. The results as shown Figure 5.1 would seem to be in agreement with their suggestion. This is a very interesting result as it would have implications for the selection of MEA concentrations and selection of possible solvent mixtures for use in the co-current RPB. Moreover, this would suggest that increasing the rotational speed may not the best for the co-current RPB.

5.1.2 Effect of liquid flow rate

The most noticeable effect of increasing liquid-gas (L/G) ratio was for the 30 wt% MEA solutions. The increase in the L/G ratios led to a marked reduction in the HTU values for the 30 wt% MEA solutions while the effect of L/G ratios on the HTU values for the 50 wt% and 70 wt% MEA solutions were less noticeable. This was in agreement with the work of Jassim (2002) who found that the effect of increasing liquid flowrate on enhancing the mass transfer was more apparent at 30 wt%. Jassim (2002) suggested that at higher MEA concentration, it would appear that the HTU was independent of the liquid flow rate.

5.1.3 Effect of concentration

The results presented in Figure 5.1 also indicate that there was a clear drop in the HTU values observed as the MEA solution concentration increased, especially at the highest liquid-gas (L/G) ratios. The 70 wt% MEA solution yielded an HTU value of 0.24 cm at L/G ratio of 1.7 and 600 rpm. This is believed to be due to the increased absorption efficiency due to accelerated absorption chemistry (Jassim, 2002). Therefore, it is possible to obtain smaller HTU in a co-current RPB than in conventional packed columns using highly concentrated alkanolamine solutions (Ma and Chen, 2016).

5.2 Co-current RPB CO_2 capture efficiency with aqueous MEA solutions

5.2.1 Effect of rotational speed

The effects of the concentration of the aqueous monoethanolamine (MEA) solution (30 wt%, 50wt% and 70 wt%), the rotational speed and the liquid-gas (L/G) ratio on the CO_2 capture efficiency were investigated. Figure 5.2 presents the CO_2 capture efficiency results using MEA solutions ranging from 30 wt% to 70 wt% in a co-current RPB. It can be seen that for the 30 wt% solutions, the CO_2 capture efficiency improved along with the increase in rotational speed. However, contrary to expectations, the highest CO_2 capture efficiencies for the 50 wt% and 70 wt% MEA solutions were observed at 600 rpm. In addition, after reaching 850 rpm, the increase in CO_2 capture efficiency was little when compared with lower rotational speed. This can be explained that increasing the rotational speed in the range of 300 rpm to 850 rpm results in thinner liquid films and smaller drops as a result of higher centrifugal forces which reduces the mass transfer resistance. However, at higher rotational speed, there is reduced contact time between gas and liquid which negatively affects mass transfer and the CO_2 capture efficiency (Li *et al.*, 2016).

5.2.2 Effect of liquid flowrate

Increasing the liquid-gas (L/G) ratio had some effect on the CO_2 capture efficiency. The CO_2 capture efficiency increased as the L/G ratio increased although to varying degrees at the different solution concentrations. In general, it was observed that the capture efficiency increased with increasing L/G ratio. This is due to increase in the effectiveness

of the wetting of the packing that enlarges the contact surface between the gas and the liquid. This favours the gas-liquid mass transfer and CO_2 capture efficiency within the co-current RPB (Li *et al.*, 2016).

5.2.3 Effect of concentration

It is surprising to observe that there was no significant effect of solution concentration on the CO_2 capture efficiency. Although the CO_2 capture efficiency increased as the solution concentration was increased from 30 wt% to 50wt %, there was no marked difference in CO2 capture efficiency between 50 wt% and 70 wt% except at 600 rpm.

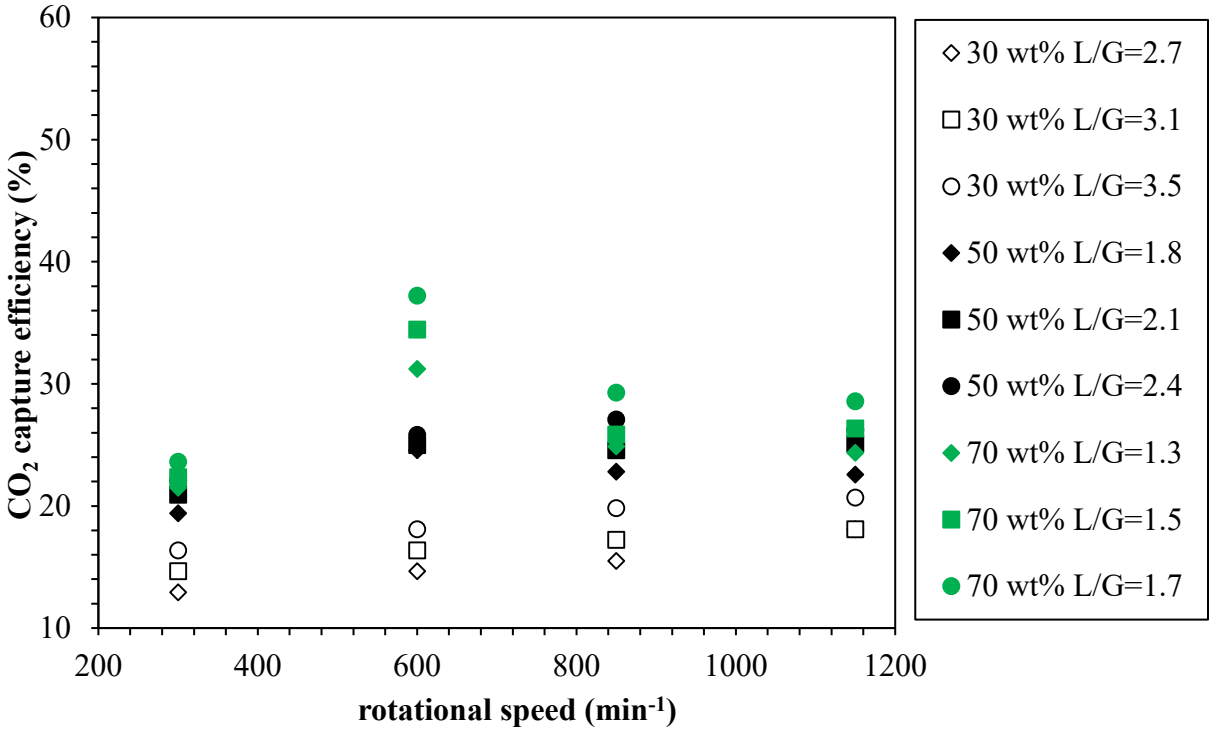

Figure 5.2: Effect of rotational speed and L/G ratio on the CO_2 capture efficiency.

5.3 Mass transfer intensification in the co-current RPB

5.3.1 Effect of rotational speed

Absorption experiments were performed under atmospheric pressure at three different monoethanolamine concentrations (30 wt%, 50 wt% and 70 wt%). Figure 5.3 shows the

mass transfer performance of the co-current rotating packed bed operated at four different rotational speeds (300, 600, 850 and 1150 rpm) at a lean amine temperature of 40ºC. Figure 5.3 presents the overall gas-side mass transfer coefficient ($K_G a$) results for the co-current rotating packed bed as a function of the aqueous monoethanolamine (MEA) concentration (ranging from 30 wt% to 70 wt%), rotational speed and liquid-gas (L/G) ratio. It can be seen that the overall gas-side mass transfer coefficient improved with increasing rotational speed for the 30 wt% MEA. However, the results for the 50 wt% and 70 wt% MEA solutions showed an unexpected trend. Their $K_G a$ values increased considerably when the rotational speed increased from 300 rpm to 600 rpm. The $K_G a$ values then dropped as the rotational speed increased further to 850 rpm after which there was no noticeable improvement in $K_G a$ values as the rotational speed increased to 1150 rpm.

The unusually high $K_G a$ values obtained at 600 rpm in comparison to 850 rpm and 1150 rpm for 50 wt% and 70wt% aqueous solutions were surprising as it was expected that the $K_G a$ values would increase with increasing rotational speed. Although Jassim (2002) suggests that the more efficient operation of the RPB is at higher rotor speeds as higher rotational speeds leads to reduction of the angular maldistribution of MEA solution in the RPB, the result obtained in the co-current RPB did not completely agree with this. The mass transfer results can be explained in terms of the hydrodynamics as the mass transfer within the RPB is significantly influenced by the characteristics of the liquid flow, the effective interfacial area and amount of liquid holdup (Xie *et al.*, 2017). It is important to note that in the co-current flow RPB, the gas and liquid flow along the same direction into the RPB packing. The expected increase in $K_G a$ values is because increasing rotational speed provides a higher centrifugal force that reduced mass transfer resistance by creating thinner liquid films and smaller droplets. Although the results obtained for the 50 wt% and 70 wt% MEA solutions were unexpected, the possible explanation for the sharp decrease in $K_G a$ values at the higher rotational speeds might be that there was a significant decrease in the residence time of the liquid and in the effective wetted area of the packing at the higher rotational speeds. The reduction in residence time would mean that the aqueous solution would decrease significantly the contact time between the liquid and gas phase. Increasing the rotational speed of the RPB will lead to shorter residence

time because of the acceleration of the liquid by centrifugal forces within the RPB (Jassim, 2002).

Moreover, the contact area for the absorption process would be greatly diminish if the wetted area of the packing reduced. This explanation is supported by the work of Li *et al.* (2016) on a co-current RPB where they found improvement in their overall gas-side mass transfer coefficient between 500 rpm and 900 rpm and significant reduction in the K_Ga values after 1100 rpm. They explained that in a co-current flow RPB, the gas and liquid flow along the same direction into the packing, and at higher rotational speed, the liquid stream tends to leave the packing more quickly than at lower rotational speed.

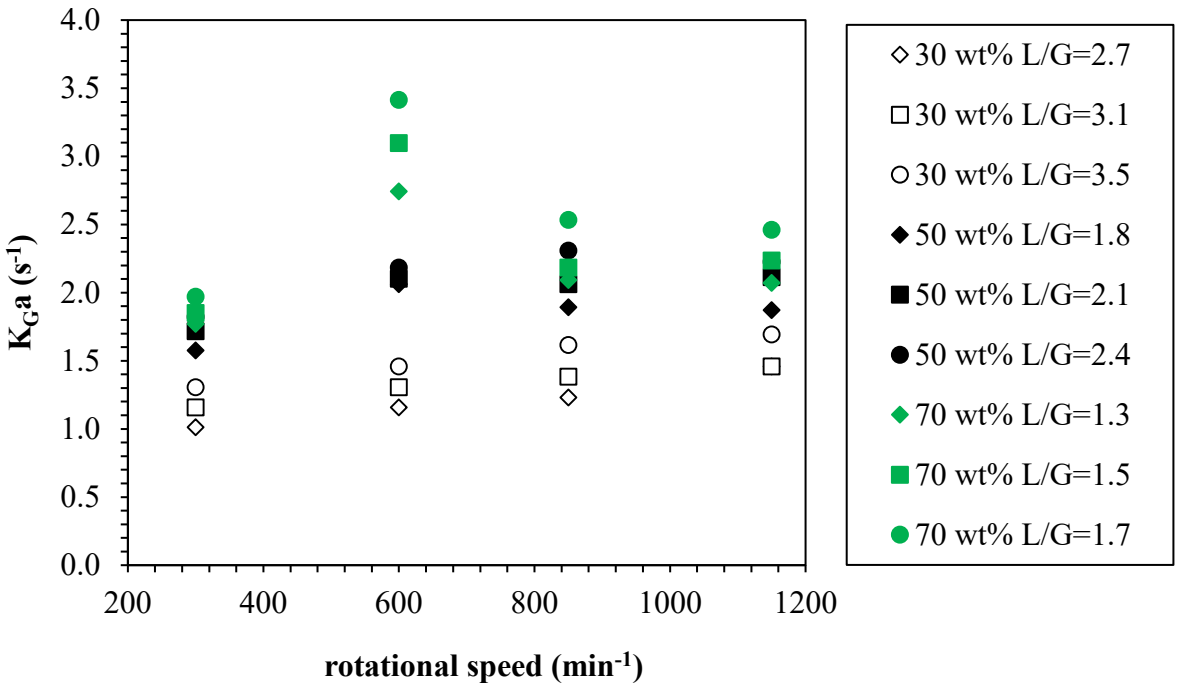

Figure 5.3: Effect of rotational speed, L/G ratio and MEA concentration on overall gas phase mass transfer coefficient.

This would mean that the packing was then underused coupled with shorter contact time will result in lower K_Ga values. This provides a possible explanation for the unexpected results observed at 600 rpm and the reduction in K_Ga values as the rotational speed is increased. In general, it was expected that the overall gas-side mass transfer coefficient

would increase with rotational speed due to the increase in rotational speed reducing the mass transfer resistance and thereby enhancing mass transfer (Ma and Chen, 2016).

5.3.2 Effect of liquid flowrate

The trend in the results generally show an improvement in the $K_G a$ values with increasing liquid-gas (L/G) ratios. This is not surprising because the increasing L/G ratio means more MEA solution is available to absorb more CO_2 and the liquid-side mass transfer resistance is reduced (Cheng and Tan, 2009). However, Jassim (2002) suggested that introducing liquid into the RPB at higher liquid flowrates results in shorter residence time because of higher liquid superficial velocities. This will be noticeable for lower concentration amines compared to higher concentration MEA solutions that have higher residence time due to their higher kinematic viscosity (Jassim, 2002). The most noticeable effect of L/G ratio on KGa values was for 70 wt% MEA solutions at 600 rpm as there was considerable increase in the $K_G a$ values as the L/G ratio increased. This could be explained to the decrease in residence time in the RPB as the rotational speed increases due to the high acceleration of the liquid (Guo *et al.*, 2000). Generally, the results also showed that although increasing the L/G ratios had some effect on the $K_G a$ values, this effect was not significant.

5.3.3 Effect of concentration

There is a clear indication that overall gas-side mass transfer coefficient values improved with increasing aqueous monoethanolamine (MEA) solution concentration. At 850 rpm, the average $K_G a$ values were 1.4 s^{-1} at 30 wt%, 1.9 s^{-1} at 50 wt% and 2.2 at 70 wt%. This can be attributed to the enhanced absorption kinetics as the total solubility of CO_2 and the driving force for forward reaction are proportional to the MEA concentration (Jassim *et al.*, 2007).

5.4 Co-current flow RPB pressure drop

Generally, the reported pressure drop in literature for rotating packed beds tends to be total pressure drop and is generally considered to be a sum of the centrifugal pressure difference and the frictional pressure drop in the rotor (Rao *et al.*, 2004). There are currently limited studies on gas pressure drop on co-current RPBs and no work was found

so far in literature investigating gas pressure drop for CO_2 capture using monoethanolamine (MEA) solutions with co-current rotating packed beds. A digital pressure gauge (Omega DPGM409 – 025HDWU accuracy-0.08%) connected across the gas inlet and outlet piping was used to measure the differential gas pressure across the packed bed. The differential pressure readings taken by the pressure gauge in millimetres water column (mmH_2O) and was converted to Pascal by multiplying the values obtained by 9.8066.

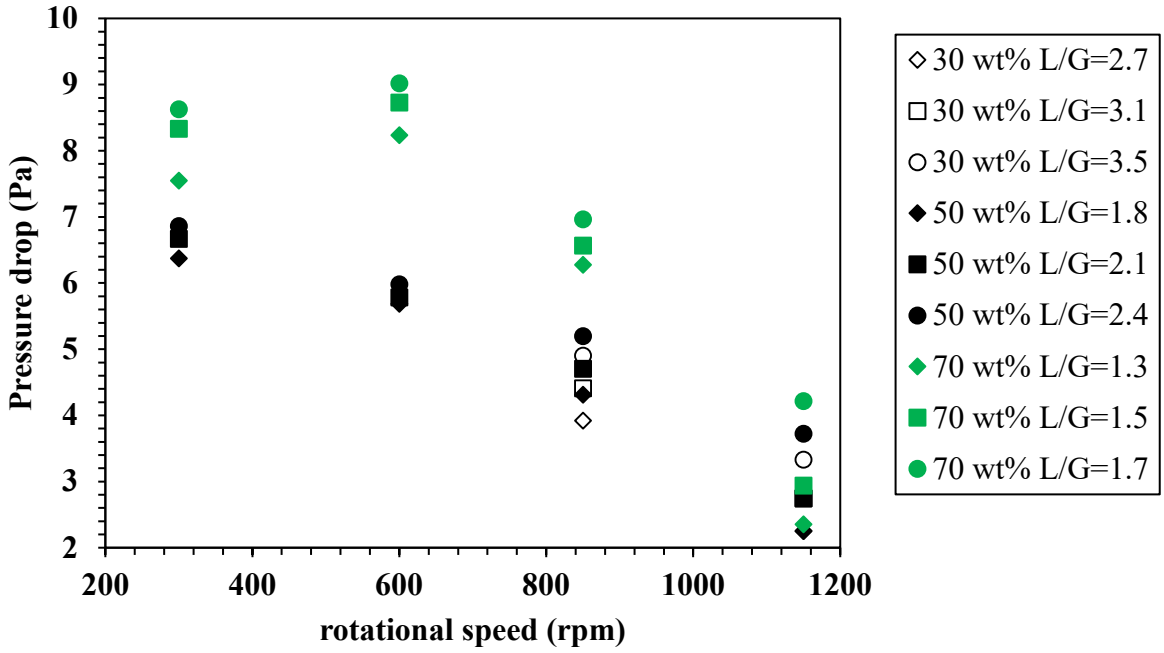

Figure 5.4: Total gas pressure drop as a function of rotational speed, MEA concentration and L/G ratio.

Figure 5.4 shows the pressure drop results for the co-current RPB at varying rotational speed, liquid-gas ratios and MEA concentrations. . The gas pressure drop results for 30 wt% MEA solutions are shown at two rotational speeds (850 rpm and 1150 rpm) only. The pressure gauges were unable to take any measurements at 300 rpm and 600 rpm. This was possibly due to the pressure gauges not being sensitive enough to register the readings at these conditions. The pressure drop results shown in Figure 5.4 indicate that as the rotational speed increased, the pressure drop values generally decreased. The only

exception was the pressure drop results for 70 wt% MEA solution. It was observed that the pressure drop values increased slightly as the rotational speed increased from 300rpm to 600 rpm.

Nevertheless, the pressure drop results obtained show a general trend that is in agreement with the findings of Li and Hao (2013). In their work, they found that the gas pressure drop in a co-current rotating packed decreased with increasing rotational speed. When the rotating packed is dry, the rotor speed has a somewhat linear relationship with the pressure drop, but the pressure drop then initially decreases with rotational speed once liquid is introduced into the rotating packed bed (Liu *et al.*, 1996). The results obtained in this work are in agreement with this as the pressure drop values decreased as the rotational speed increased from 300 rpm to 1150 rpm. Moreover, Liu *et al.* (1996) found that above 1200 rpm, the pressure drop generally remained constant. This would seem to suggest that at high rotational speed, the liquid holdup may become reduced and this enables gas to pass more easily. This could not be confirmed in this work, as the rotational speed was not increased beyond 1150 rpm due to mechanical and safety considerations.

It would appear that increase in the liquid flow rate had some effect on the pressure drop albeit a small one. The trend was that there was an increase in the gas pressure drop as the liquid flow rate increased. This results of this work contradict Li and Hao (2013) who suggested that the gas pressure drop decreased with increasing liquid flow rate. However, the gas pressure drop is expected to be strongly dependent on the gas flow rate and not the liquid flow rate (Liu *et al.*, 1996). This is also supported by Rao *et al.* (2004) who have suggested that the liquid flow should have no effect on total pressure drop if the gap between the inner periphery and the liquid distributor is negligible. There also is an indication that the solution concentration had an effect on the pressure drop results. It is apparent that the gas pressure drop increased as the MEA solution concentration increased from 30 wt% to 70 wt%.

5.5 Summary

The performance of a co-current RPB with respect to HTU, CO_2 absorption and mass transfer were investigated. The results showed that in terms of increasing rotational speed for better performance, the MEA concentration became an important factor as well as the residence time. Increasing L/G ratio generally improved CO_2 capture efficiency and mass transfer as it resulted in improved liquid distribution and larger interfacial area for CO_2 absorption. The MEA concentration had the biggest effect on the rate of CO_2 absorption due to improvement in reaction kinetics. The gas pressure drop measured in the co-current RPB was in the range of 2.4 Pa to 8.6 Pa and decreased with rotating speed. This demonstrated the advantage of the co-current with respect to pressure drop within the RPB.

Chapter 6. Assessment of cross-flow RPB for CO_2 absorption with aqueous MEA solutions

6.1 Cross-flow RPB HTU results

6.1.1 Effect of rotational speed

Figure 6.1 shows results of the height of transfer unit (HTU) as a function of the rotational speed with speed ranging from 300 rpm to 1150 rpm for the different MEA concentrations. It is expected that increasing the rotational speed would intensify the rate of mass transfer of CO_2 from the gas phase to the liquid phase (Lin and Chen, 2011c). This is because as the rotational speed increases, the resulting centrifugal acceleration could possibly provide thinner liquid films and tiny droplets (Lin *et al.*, 2008).

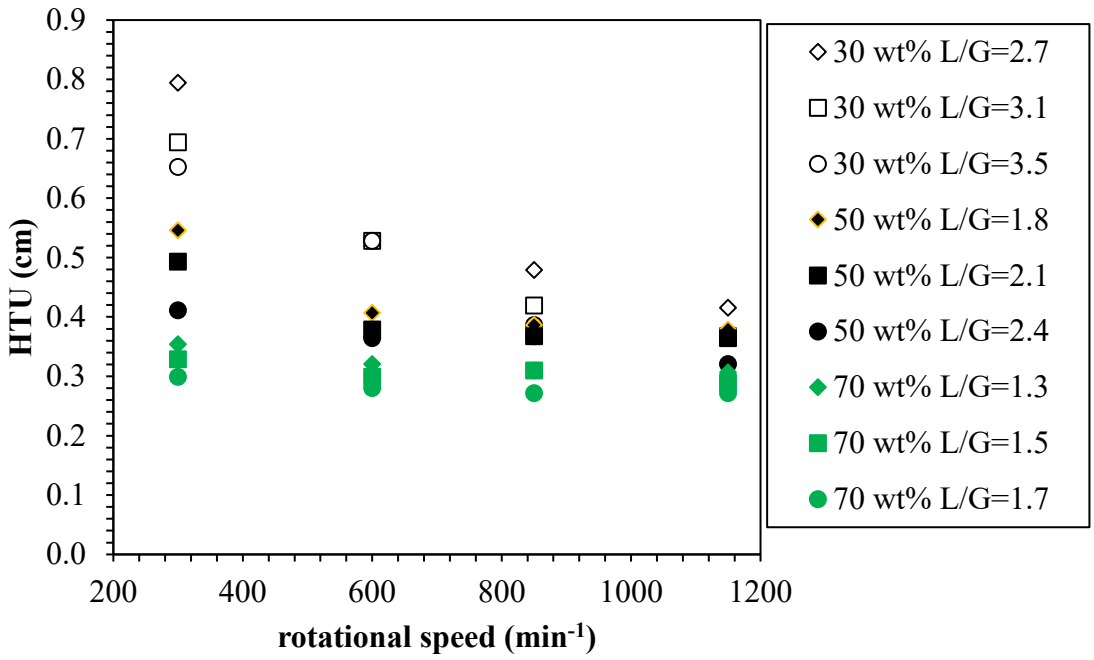

Figure 6.1: HTU values as function of rotational speed and L/G ratios.

It is apparent that the increase in rotational speed results in a reduction of the HTU values. This is in agreement with the work done by Lin and Chen (2011c) where they used MEA solution in CO_2 removal using a cross-flow RPB. The same phenomenon was also observed by Lin *et al.* (2008) in their work using NaOH solutions for CO_2 removal

in the cross-flow RPB. The effect of rotational speed on HTU values varied for the different MEA solution concentrations. The results show that the most noticeable effect of rotational speed was for aqueous 30 wt% solutions where the HTU values decreased from 0.79 to 0.36 cm. However, there was only a slight change in HTU values for the 50 and 70 wt% MEA solutions as rotational speed increased. The 70 wt% MEA solutions showed very little variation in HTU values as the rotational speed increase. This indicated that increasing the rotational speed did not yield any considerable advantage in HTU reduction for the 50 and 70 wt% aqueous MEA solutions compared to the 30 wt% MEA solutions. This would suggest that the rotational speed was not an important influence on the HTU values for MEA solutions of higher concentrations. This may be due to the effect of the rotational speed on the cross-flow contact of the liquid and gas. The accelerated mixing of the gas and liquid phase at higher rotational speeds may have slightly changed the cross-flow contact.

6.1.2 Effect of liquid flow rate

The HTU values decreased with increasing liquid flow rate as indicated by the liquid-gas ratios for the different MEA concentration at given rotational speeds. This is to be expected, as the increase in liquid flow rate would increase the amount of MEA going into the RPB. The results indicate that the increased L/G ratios may lead to the enhancement of the reaction rate and invariably the mass transfer. It is evident that the effect of increasing the liquid flow rate is predominant at 300 rpm compared to the higher rotational speeds. This may be due to the increased liquid flow rate wetting more of the surface area of the packing and enabling more contact surface for mass transfer. At lower rotational speeds such as 300 rpm, the surface of the packing tend not to be effectively wetted due to the predominant rivulet flow regime present in the RPB. As the rotational speed increases, the surface of the packing becomes more effectively wetted. It can be seen that at higher rotational speeds, the effects of L/G on the HTU values tends to diminish. This may be due to the reduction in residence time of the MEA solution in the RPB which negatively affects the enhancement of the CO_2 removal.

6.1.3 Effect of concentration

As can be seen from Figure 6.1, there was reduction in the HTU values as the MEA concentration increased. This is because increasing the MEA concentration will provide higher amounts of MEA per volume available for reacting with more CO_2 at a given rotational speed and L/G ratio. This was consistent with the findings of Lin *et al.* (2008) that showed that increasing the concentration of NaOH for CO_2 removal in a cross-flow RPB led to increase in K_Ga values and therefore lower HTU values.

6.2 CO_2 capture efficiency of the cross-flow RPB

6.2.1 Effect of rotational speed

Figure 6.2 summarizes the CO_2 capture efficiency values as a function of the rotational speed at three different MEA concentrations (30 wt%, 50 wt% and 70 wt%). It is evident that the CO_2 capture efficiency increases with the rotational speed as is to be expected on a cross-flow rotating packed bed (Lin *et al.*, 2006). Increasing the rotational speed provides potentially higher rate of mass transfer and increased gas-liquid interfacial area that is beneficial to CO_2 absorption (Lin *et al.*, 2010).

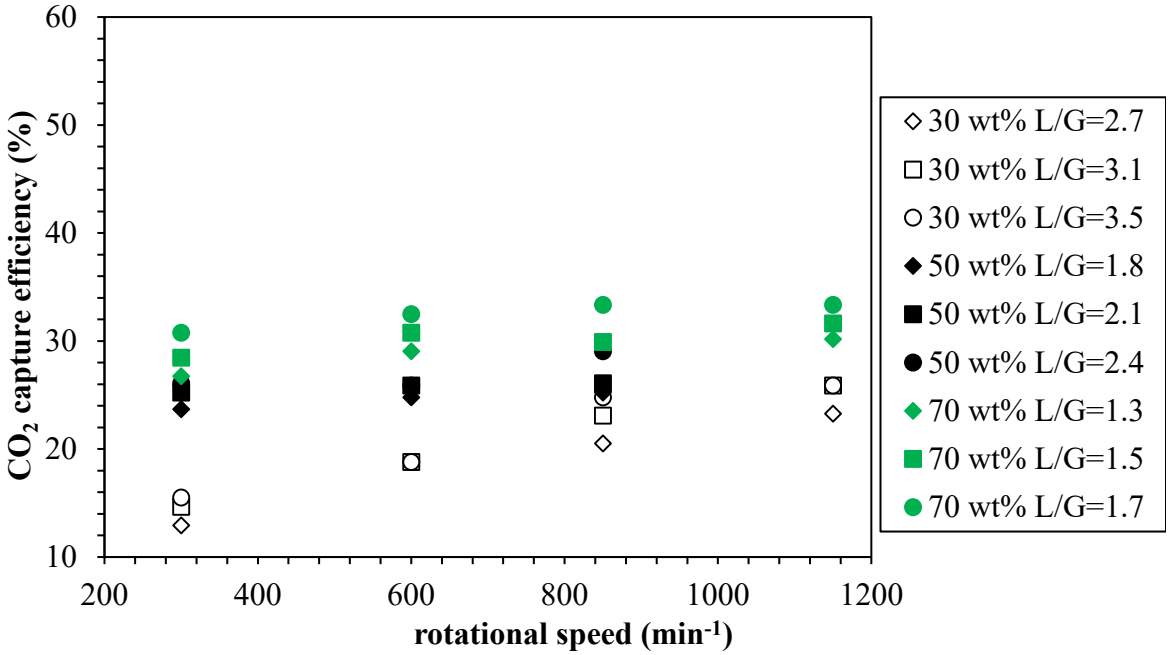

Figure 6.2: CO_2 capture efficiency as a function of rotational speed and L/G ratios.

However, it is also possible that increasing the rotational speed could result in reduced contact time between the gas and liquid and negatively impact CO_2 absorption. However, it can be seen based on the observed result that the CO_2 capture efficiency increased with increasing rotational speed for all the MEA concentrations tested. This will imply that the reduction of the contact time did not adversely affect the CO_2 absorption. However, it is also apparent that as the rotational speed is increased, the effect on the CO_2 capture efficiency is diminished. At the higher rotational speeds, there is little or no improvement in the CO_2 capture efficiency; this is seen when the rotational speed is increased above 850 rpm. This will seem to suggest that as the rotational speed increased, the effect of the reduction in contact time between the gas and liquid became more prominent.

The results presented in Figure 6.2 also indicate that the effect of rotational speed was most noticeable on the 30 wt% MEA solutions. This could be because of the increased effectiveness of the wetting of the packing with the 30 wt% MEA solutions as the rotational speed increases. This effect is likely significant for the 30 wt% MEA due to the lower mass transfer enhancement in comparison to the higher concentration MEA solutions. Therefore, coupled with the low MEA concentration, liquid maldistribution in the packing will significantly lower the CO_2 removal efficiency. The liquid maldistribution in the packing at the lower rotational speed for the higher MEA solutions (50 wt% and 70 wt% MEA) is possibly compensated for by the enhanced CO_2 absorption reaction.

6.2.2 Effect of liquid flow rate

The effect of liquid-gas (L/G) ratios on the CO_2 capture efficiency is also shown in Figure 6.2 as a function of rotational speed and MEA solution concentrations. The mass flow rate of the gas feed for the experimental runs were kept constant while the liquid flow rates were varied to give different L/G ratio. The general trend was that increasing the L/G ratio flow improved the CO_2 capture efficiency. However, the effect observed varied at the different MEA solution concentrations tested. The effect of increasing the liquid flow rate on CO_2 capture efficiency was most apparent for the 70 wt% MEA. This could be because it is a highly concentrated solution and increase in the liquid flow rate provides more amount of MEA in solution for CO_2 removal. For the 50 wt% MEA

solutions, the effect of increasing L/G ratio on the CO_2 removal was very minimal but an improvement was observed in the CO_2 capture efficiency. A possible explanation given by Lin *et al.* (2010) to explain this was that higher liquid flow rates may result to less contact time thus leading to lower enhancement in the CO_2 capture efficiency at higher liquid flow rates.

6.2.3 Effect of concentration

The effect of the MEA solution concentration on the CO_2 capture efficiency is shown in Figure 6.2. It can be seen that the CO_2 capture efficiency increased with increasing MEA solution concentration at fixed rotational speed. This was to be expected as increasing the concentration of the MEA solution would be favourable for CO_2 absorption. This is because it will result in a reduction in liquid-phase mass transfer resistance resulting in more MEA being utilized in absorbing CO_2. It was also observed that at the higher rotational speeds, the 30 wt% and 50 wt% MEA results become more comparable.

6.3 Mass transfer performance of CO_2 capture in the cross-flow RPB

6.3.1 Effect of rotational speed

The results for the overall gas mass transfer coefficient for the three concentrations studied in this work are shown in Figure 6.3. It is important to note that although the L/G ratios vary for the different aqueous MEA solution concentrations, the molar ratios remained constant for the three different MEA concentrations. It can be seen that K_Ga values increased as the rotational speed was increased from 300-600 rpm in the cross-flow RPB. Lin *et al.* (2008) suggested that this effect can be attributed to the centrifugal acceleration which potentially provided thinner liquid films and tiny droplets resulting in a better gas-liquid mass transfer. However, increasing the rotational speed above 600 rpm did not have a noticeable effect on the overall gas-side mass transfer coefficient (K_Ga) values. The increase in MEA concentration is thought to reduce mass transfer due to the viscosity increase that reduces the rate of diffusion of the reactive species (Jassim, 2002). Although higher concentration MEA have higher residence time in the RPB packing, the increased viscosity could have affected mass transfer negatively such that increasing the rotational speed did not lead to improvement in mass transfer. Another reason could be

due to the increased rotational speed of the rotor that reduces the effective contact of the gas phase with the liquid in the cross-flow configuration. One of the challenges with the cross-flow RPB is the technical difficulty in its design to get the liquid and gas to contact in a truly cross-flow contact.

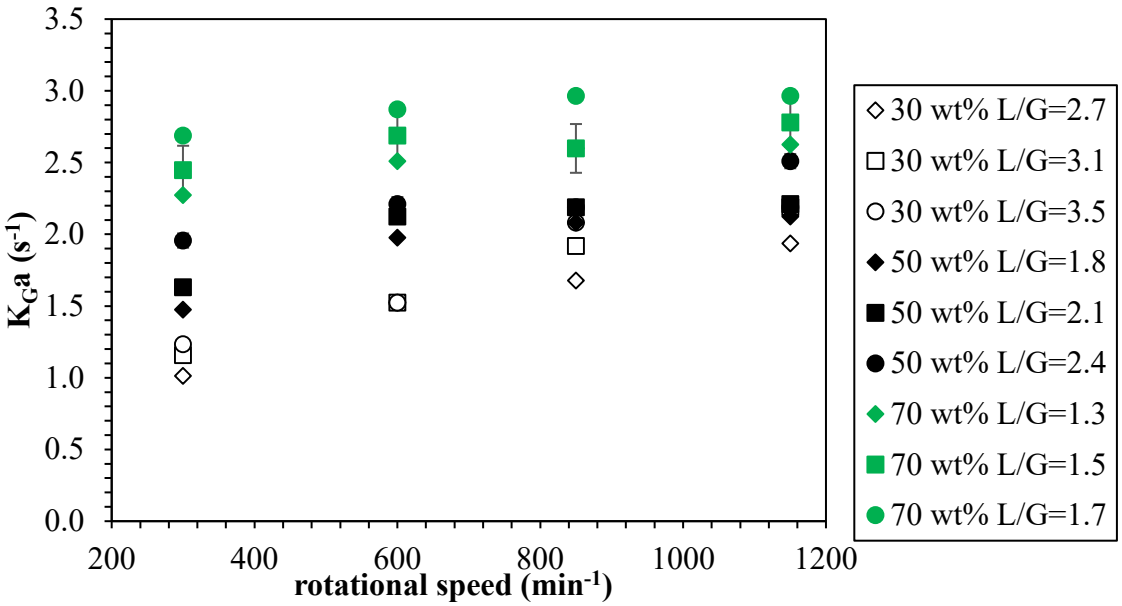

Figure 6.3: Effect of rotational speed, L/G ratio and MEA concentration on overall gas phase mass transfer coefficient.

This could possibly have influenced the mass transfer as the increasing rotational speed may have caused the liquid and gas to not contact in the expected cross-flow mode. The results also indicate that the effect of rotational speed on the K_Ga gradually declined as the rotational speed increased from 850 rpm to 1150 rpm.

6.3.2 Effect of liquid flow rate

Figure 6.3 indicates the effect of the increasing liquid-gas ratio by increasing liquid flow rate in the K_Ga values at fixed rotational speeds (ranging from 300 -1150 rpm) and different MEA concentrations. For the 30 wt% MEA, there was no noticeable improvement in the mass transfer performance with increase in the liquid flow rate. This could be due to the number of moles of MEA available for reaction that did not increase significantly for the 30 wt% MEA in comparison to the higher concentration MEA

solutions. However, it is apparent that the increase in liquid flow rate yielded an increase in $K_G a$ values at each of the rotational speeds and for each MEA concentration. This could be attributed to the fact that there was more MEA solution used to absorb the CO_2 at high liquid flow rates at any given MEA concentration. The liquid-phase mass transfer resistance is also lowered due to the intensive mixing of the liquid making it favourable for CO_2 absorption (Lin and Chen, 2008; Lin *et al.*, 2008).

6.3.3 Effect of concentration

The $K_G a$ values are also shown in Figure 6.3 as a function of the MEA concentration ranging from 30 wt% to 70 wt% at fixed rotational speed and varying liquid-gas ratios. Tt is clear that the $K_G a$ values increased with increasing MEA concentration at some rotational speeds and L/G ratios,. This is attributed to the fact that increasing the MEA concentration provides higher moles of MEA per volume of solution for reacting with more CO_2 at a given rotor speed and L/G ratio. It is apparent that the $K_G a$ values were strongly affected by the solution concentration.

6.4 Pressure drop through the cross-flow RPB

The cross-flow RPB has been suggested to reduce pressure drop in the counter-current RPB especially in gas-liquid mass transfer processes with high gas flow rates (Qi *et al.*, 2016). They suggest that despite the counter-current RPB having a better mass transfer performance than cross-flow RPBs, it is limited in dealing with gas streams of lower flow rate and may not be suitable for high gas flow rate requirements. The differential gas pressure readings were taken using a digital pressure gauge (Omega DPGM409 – 025HDWU accuracy-0.08%) connected across the gas inlet and outlet piping. The differential pressure readings taken by the pressure gauge in millimetres water column (mmH_2O) and was converted to Pascal by multiplying the values obtained by 9.8066.

The pressure drop results for the cross-flow RPB are shown in Figure 6.4. The pressure drop readings are shown as a function of rotational speed and liquid flow rate. The results show that the gas pressure drop increased as the rotational speed increased. This was in agreement with the findings of Qi *et al.* (2016) who found that the wet pressure drop of a

cross-current RPB increased with increasing rotational speed. They also found that this was regardless of the liquid flow rate; especially at a low gas flow rate.

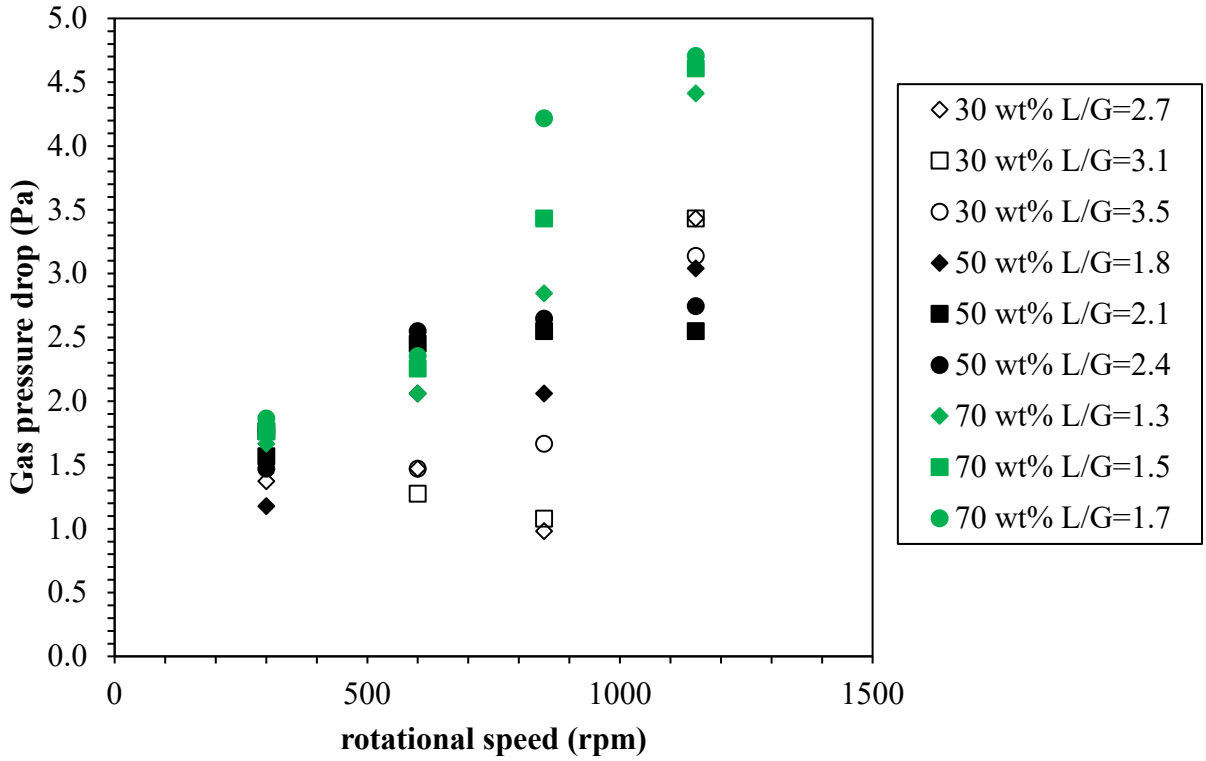

Figure 6.4: Total gas pressure drop as a function of rotational speed, MEA concentration and L/G ratio.

An anomaly in this trend was observed at 850 rpm where the gas pressure drop for the 30 wt% and 50 wt% MEA solutions decreased as the rotational speed was changed from 600 rpm to 850 rpm. The pressure drop results also show that the liquid flow rate had some effect on the pressure drop although these varied in the different MEA concentrations. The trend showed an increase in the gas pressure drop as the liquid flow rate increased.

6.4.1 Summary

The performance of a cross-flow RPB for capturing CO_2 from simulated saturated flue gas using aqueous MEA solutions has been studied. The performance of the cross-flow with respect to rotational speed showed that at higher rotational speeds, the mass transfer

and CO_2 capture efficiency could be influenced by a change in the cross-flow contact mode. In general, the advantages of increasing rotational speed to generate higher gravity fields (HIGEE) was harnessed in the cross-flow RPB.

Chapter 7. Industrial scale-up of the RPB for carbon capture from flue gas using aqueous MEA solutions

7.1 Evaluation of experimental studies of gas-flow configurations for CO_2 capture

So far, the performance of the three RPB configurations for CO_2 capture have been investigated with respect to HTU values, CO_2 capture efficiency and overall gas mass transfer coefficient. The effects of rotational speed, liquid-gas ratio (L/G) and MEA solution concentration on their performance considered. In this chapter, the performance of the three different RPBs are compared in detail in terms of these parameters.

7.1.1 Appraisal of HTU results

Figure 7.1, Figure 7.2 and Figure 7.3 present the HTU results for the 30 wt%, 50 wt% and 70 wt% MEA solutions respectively for the three RPB configurations.

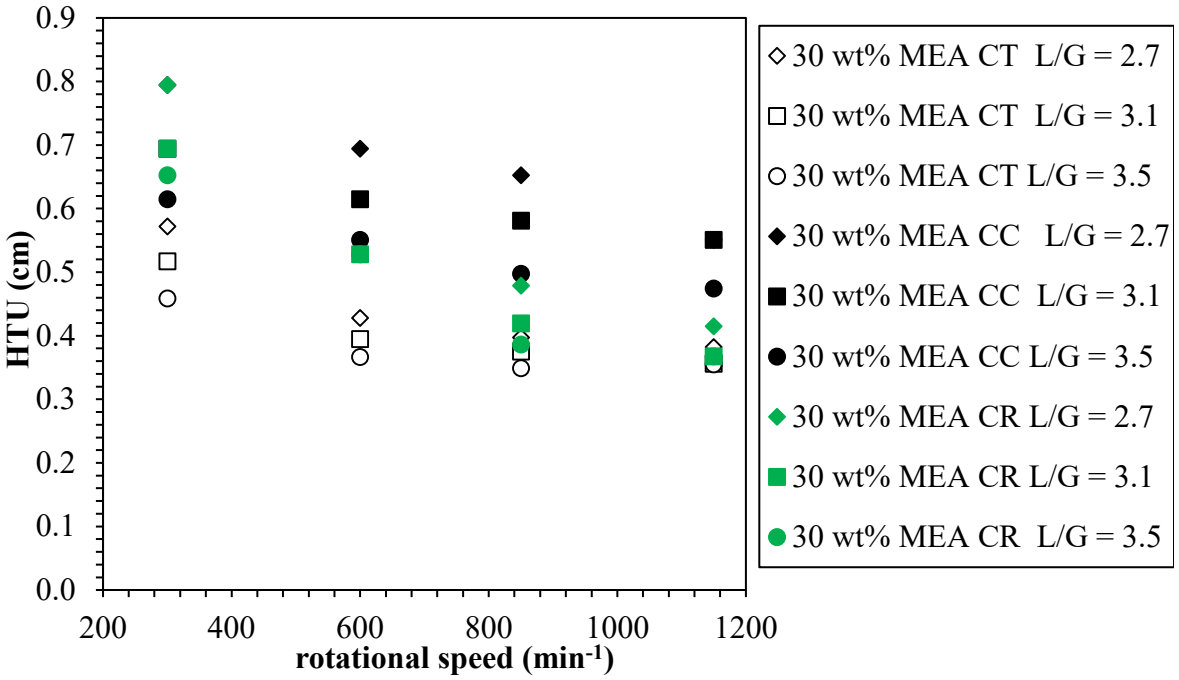

Figure 7.1: HTU results for RPB gas-flow configurations (CT: counter-current, CC: co-current and CR: cross-flow configurations) using 30 wt% MEA solutions.

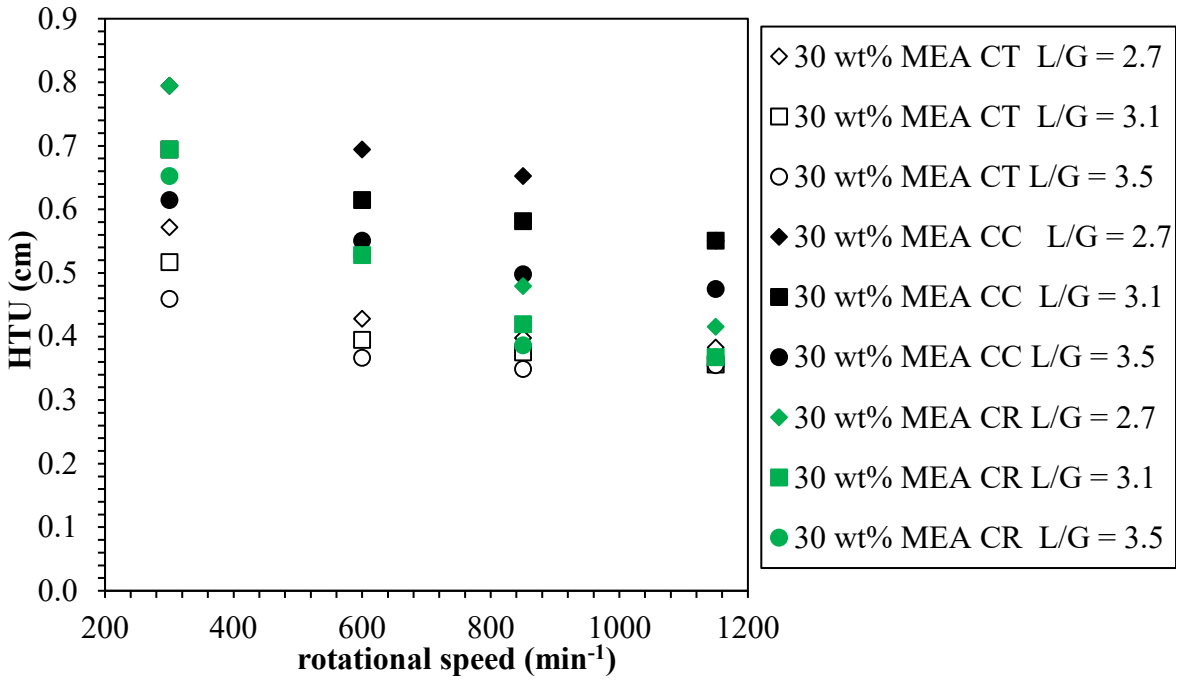

Figure 7.1 shows the trend of decreasing HTU values as the rotational speed increased from 300 rpm to 850 rpm for the three RPB flow configurations. This may be explained by the fact that the increase in rotational speed led to improvement in mixing efficiency and resulted in better mass transfer in the RPBs. As the rotational speed increased to 1150 rpm, the HTU values for cross-flow RPB continued to reduce but it appears that there was no further improvement in HTU values. There were also examples of worsening results for the counter-current and co-current RPBs. This is explained by the fact that increasing the liquid flow rate and rotational speed caused entrainment of the liquid by the gas flow in the the counter-current and co-current RPBs.

According to Lin and Chen (2008), the counter-current and co-current RPB have flooding limitations not present in cross-flow RPB which may be why this did not occur for the cross-flow RPB. In general, the counter-current RPB showed the lowest HTU values and the co-current RPB showed the highest HTU values.

It can also be seen that the RPBs showed different behaviour for HTU results at the different rotational speeds. This is possibly due to the different flow characteristics that occur because of the gas-flow configuration of the RPB. Visual studies of liquid flow in

the counter-current and co-current RPB packing have suggested that at low rotational speeds (300-600rpm), the liquid flows in the form of thread flow and pore flow within the RPB while film flow and droplet flow exists at higher rotational speed above the 600-800 rpm range (Burns and Ramshaw, 1996; Guo *et al.*, 1997). However, it is difficult to find the thread flow and pore flow in the cross-flow RPB. Furthermore, the flow is closer to plug flow (Guo *et al.*, 1997).

For the 50 wt% experiments as shown in Figure 7.2, there was marked drop in the HTU values as the rotational speed increased from 300 rpm to 600 rpm for the three different RPB configurations. This is also the same for the 70 wt% MEA solutions results as shown in Figure 7.3. For example, the counter-current RPB showed a general decreasing trend as rotational speed dropped from 0.32cm at 300 rpm to 0.24 cm for L/G ratio 2.7 for the 50 wt% MEA solution. This can be explained in terms of the reaction kinetics caused by the fact that increasing the MEA concentration provides higher amounts of hydroxide ions per unit volume for better CO_2 absorption at the given L/G ratio. It can be seen that from Figure 7.2 and Figure 7.3 that the counter-current RPB showed the best HTU results. This can be explained by the better mass transfer performance in the counter-current RPB due to the gas and liquid contacting in the counter-current mode (Chu *et al.*, 2014). For the co-current and cross-flow RPBs, there was no improvement in HTU values beyond 850 rpm.

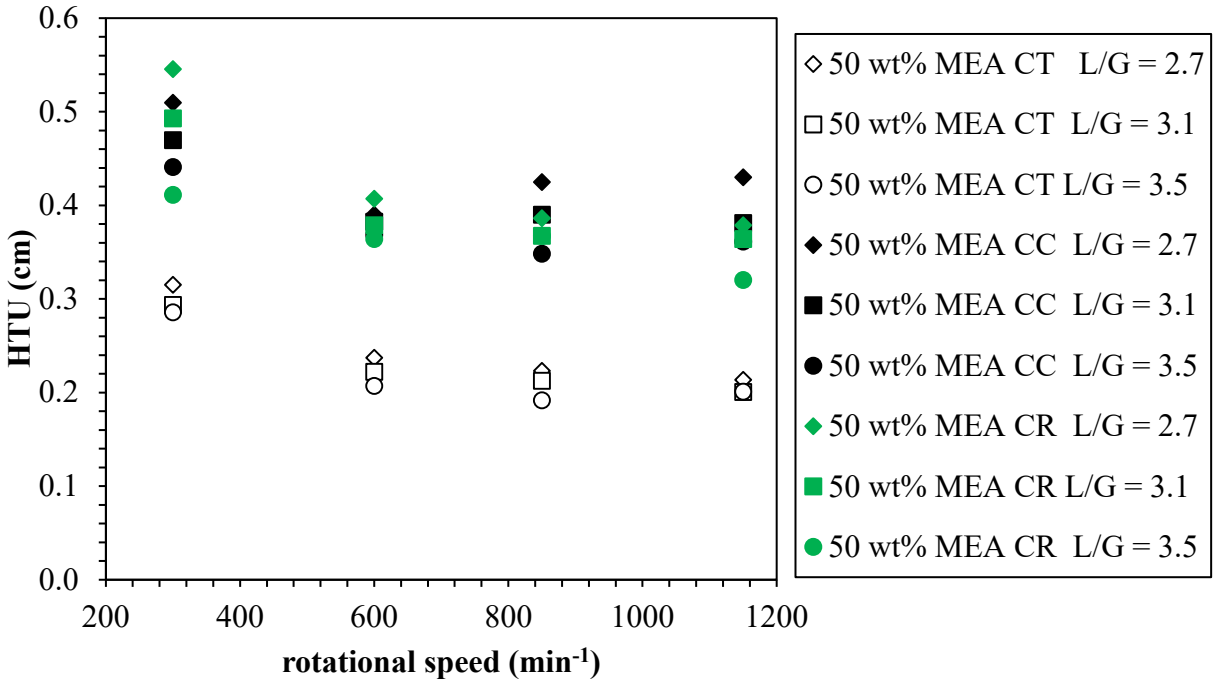

Figure 7.2: HTU results for RPB gas-flow configurations (CT: counter-current, CC: co-current and CR: cross-flow) using 50 wt% MEA solutions.

For the 70 wt% MEA solutions, it is observed from the results presented in Figure 7.3 that the HTU values for the co-current and cross-flow RPB worsened past 850 rpm. This could be due to increased viscosity being more of an issue for these two RPB configurations in comparison to the counter-current RPB. According to Lewis and Whitman (1924), the ratio of the viscosity to density (kinematic viscosity) of the liquid film is a controlling factor in determining the film thickness which affects the rate of diffusion and impacts mass transfer. This is because the viscosity of the MEA solution will influence mass transfer due to CO_2 absorption into MEA solution being a liquid film controlled process with lower viscosity that leads to thinner liquid films (Jassim *et al.*, 2007). In addition, a higher liquid viscosity results in increased difficulty in dispersing the liquid, leading to a smaller gas-liquid interfacial area. This makes it easier for gas to escape through the rotor (Luo *et al.*, 2012b). Moreover, the increase in rotational speed could have had adverse effects on the cross-flow contact between the liquid and gas phase in the cross-flow RPB resulting in a worse performance at the higher MEA

concentration and rotational speed. This is because the increase in rotational speed results in violent collisions between gas and liquid which is more pronounced for the cross-flow RPB because of the angle of contact of the liquid and gas (Luo *et al.*, 2012b).

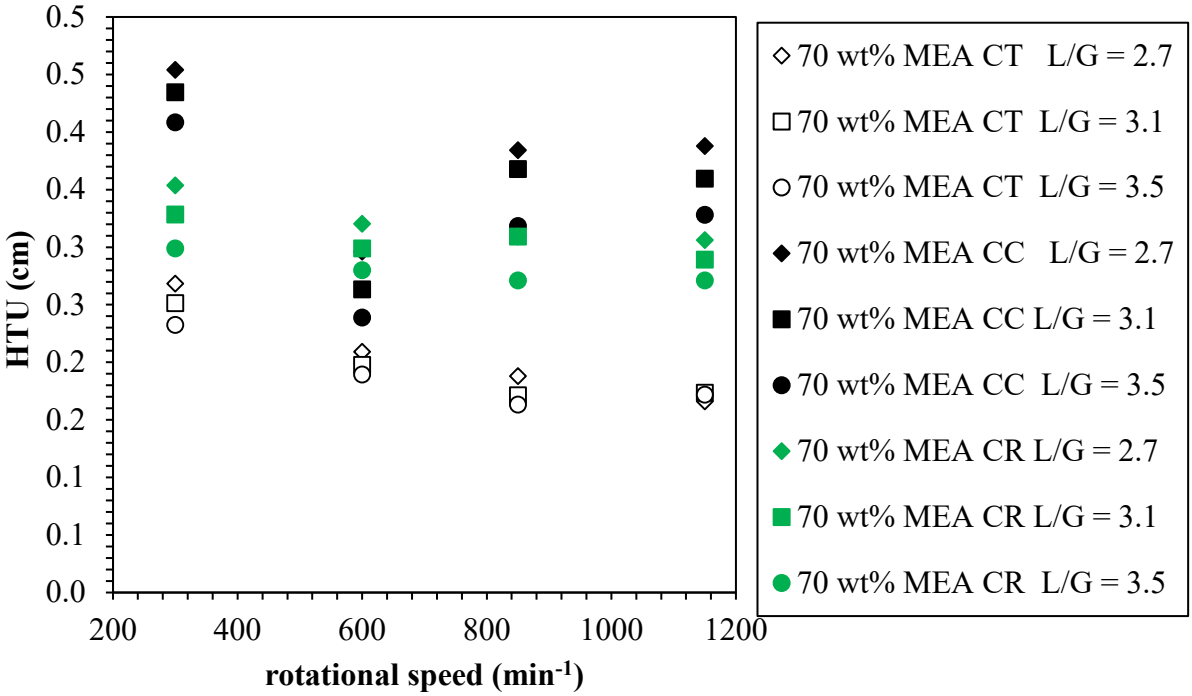

Figure 7.3: HTU results for RPB gas–flow configurations (CT: counter-current, CC: co-current and CR: cross-flow) using 70 wt% MEA solutions.

There appears to be a potential tendency for the gas flow in the cross-flow RPB to deviate from a true cross-flow contact mode at higher rotational speed and instead appear closer to a co-current flow. It can be deduced that the hydrodynamic behaviour influenced the HTU performance in the RPBs studied. This has implications for the scale-up design with respect to the selection of solvent concentrations and optimal rotational speeds.

7.1.2 CO_2 capture efficiency for three RPB configurations

The capture efficiency is important in determining the size of the absorption column especially in terms of meeting the CO_2 emissions making it necessary to be investigated for the RPB configurations. Figure 7.4, Figure 7.5 and Figure 7.6 show the effect of varying the rotational speeds and L/G ratios on the CO_2 capture efficiency for the three

different flow configurations of the RPB for the 30 wt%, 50 wt% and 70 wt% MEA solutions respectively. For the 30 wt% MEA solution results presented in Figure 7.4, there was no marked difference between the three RPB in terms of HTU results.

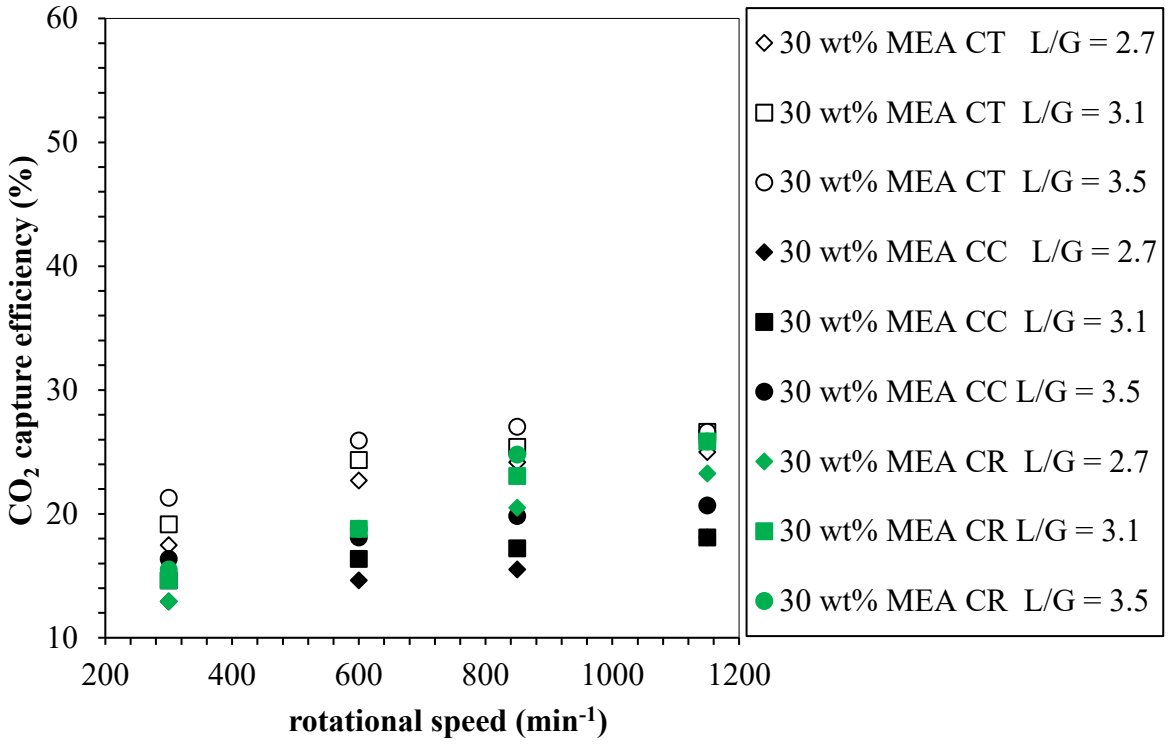

Figure 7.4: CO_2 capture efficiency results for RPB gas-flow configurations (CT: counter-current, CC: co-current and CR: cross-flow) using 30 wt% MEA solutions.

This can be explained by the fact that the MEA concentration was low and so the mass transfer enhancement from increasing the rotational speed and its resultant effects in the different RPBs was very little. The general trend showed that increasing the rotational speed of the RPBs resulted in an increase in the CO_2 capture efficiencies. It is also evident from Figure 7.5 and Figure 7.6 that as the MEA concentration increased, there

was a marked difference in the CO_2 capture efficiency results. The counter-current RPB showing increasingly better results than the other two RPBs.

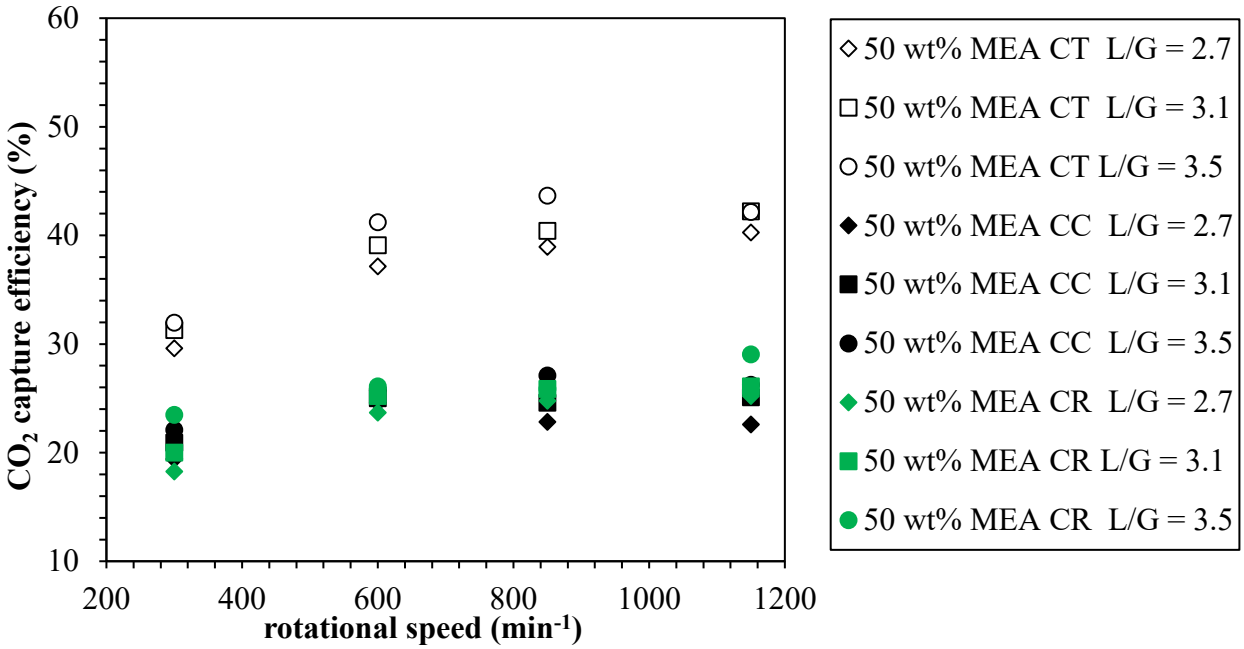

Figure 7.5: CO_2 capture efficiency results for RPB gas-flow configurations (CT: counter-current, CC: co-current and CR: cross-flow) using 50 wt% MEA solutions.

For the 50 wt% and 70 wt% MEA solutions, the counter-current performed considerably better than the co-current and cross-flow in terms of CO_2 capture efficiency. This is due to the better mass transfer performance of the counter-current RPB in terms of the gas-liquid contacting in the counter-current mode. For 50 wt% MEA solutions, the co-current and cross-flow were comparable in terms of CO_2 capture efficiency. For the 70 wt% MEA absorption runs, the counter-current RPB performed better than the other two for capture efficiency while the co-current performed the worst with an exception at 600 rpm. At 600 rpm, the cross-flow RPB had the lowest CO_2 capture efficiency compared to the counter-current and co-current flow RPBs.

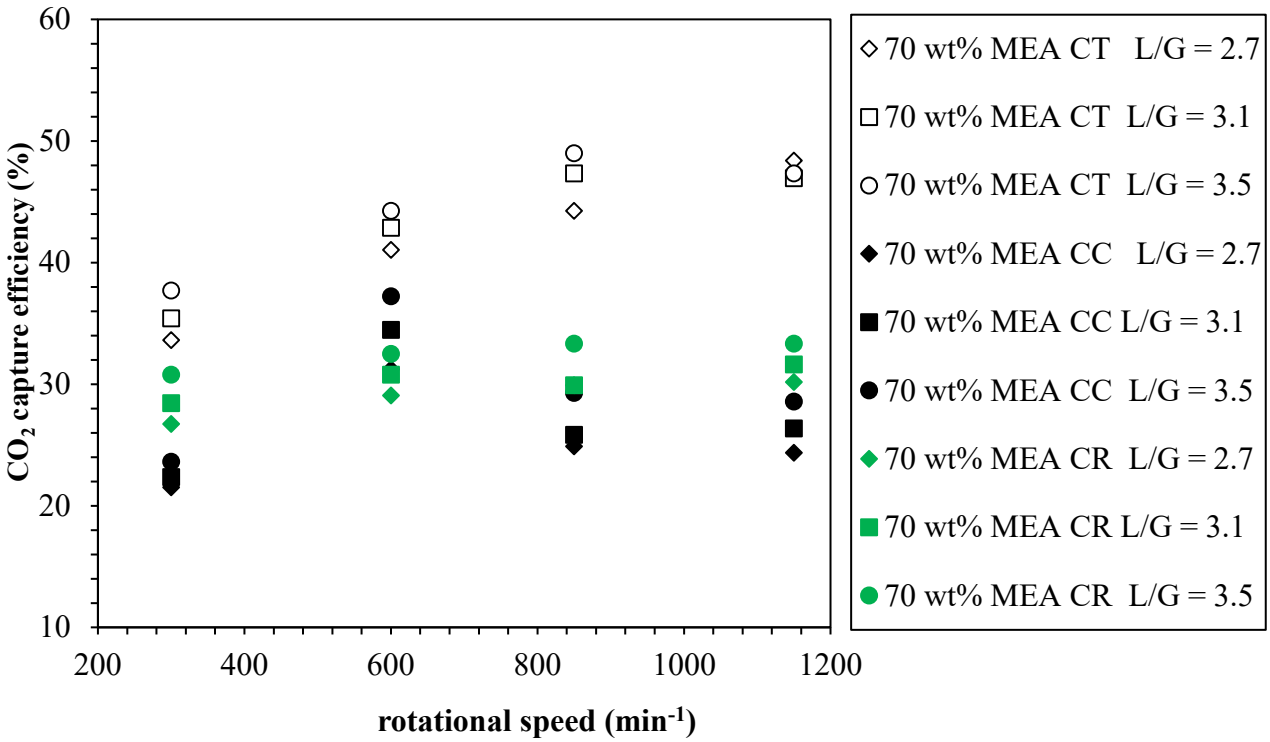

Figure 7.6: CO_2 capture efficiency results for RPB gas-flow configurations (CT: counter-current, CC: co-current and CR: cross-flow) using 70 wt% MEA solutions.

It is interesting to note that the results shown in Figure 7.6 using 70 wt% MEA solutions indicate that the CO_2 capture efficiency performance improved for the other two RPBs as rotational speed went higher but decreased for the co-current RPB beyond 600 rpm. A possible explanation for this phenomenon is that increasing the rotational speeds beyond 600 rpm resulted in shorter contact time in the co-current RPB. This was coupled with the reduced driving force for mass transfer and increased viscosity that may have greater influence on the CO_2 capture efficiency than the expected intensification at higher rotational speeds. This then resulted in the decrease in the CO_2 capture efficiency. Therefore, the optimum rotational speed for the co-current is determined to be at 600 rpm.

7.1.3 Comparison of mass transfer results

Figure 7.7, Figure 7.8 and Figure 7.9 show the overall gas-phase mass transfer results for the counter-current, co-current and cross-flow rotating packed beds as a function of the rotating speed and liquid-gas ratios for 30 wt%, 50 wt% and 70 wt% MEA solutions respectively. It is clear that the overall gas mass transfer values generally increased with rotational speed for the three different RPBs. The counter-current RPB showed the best overall gas mass transfer performance in comparison to the other two RPBs.

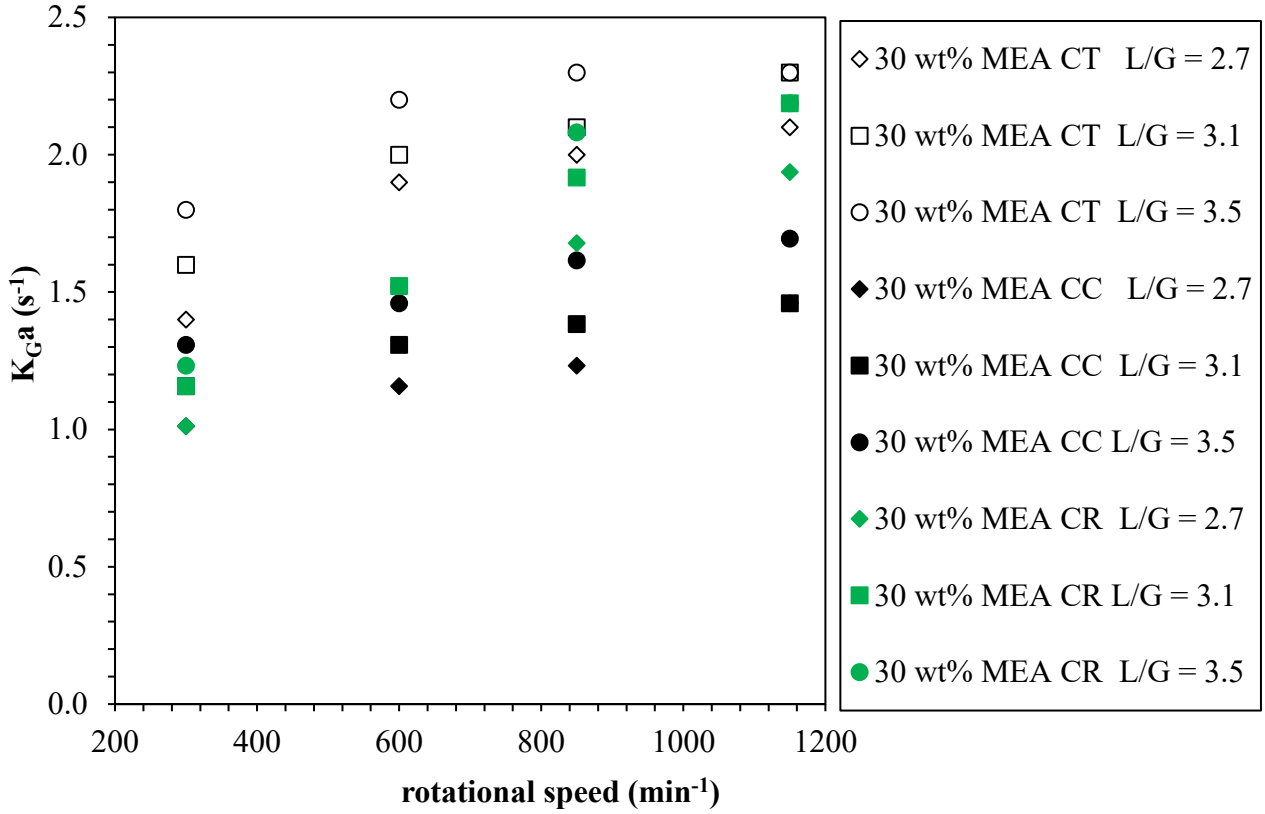

Figure 7.7: K_Ga results for RPB gas-flow configurations (CT: counter-current, CC: co-current and CR: cross-flow) using 30 wt% MEA solutions.

The results for the 30 wt% MEA solutions show that the counter-current RPB had the best overall gas phase mass transfer performance followed by the cross-flow. The co-current showed the worst performance. However, the co-current RPB showed slightly

higher gas mass transfer values than the cross-flow at 300 rpm. The co-current and cross-flow RPBs had comparable results for overall gas mass transfer coefficient for the 50 wt% MEA solutions. The counter-current RPB had the highest values for the overall gas side mass transfer coefficient and these were considerably higher than the co-current and cross-flow RPBs values respectively.

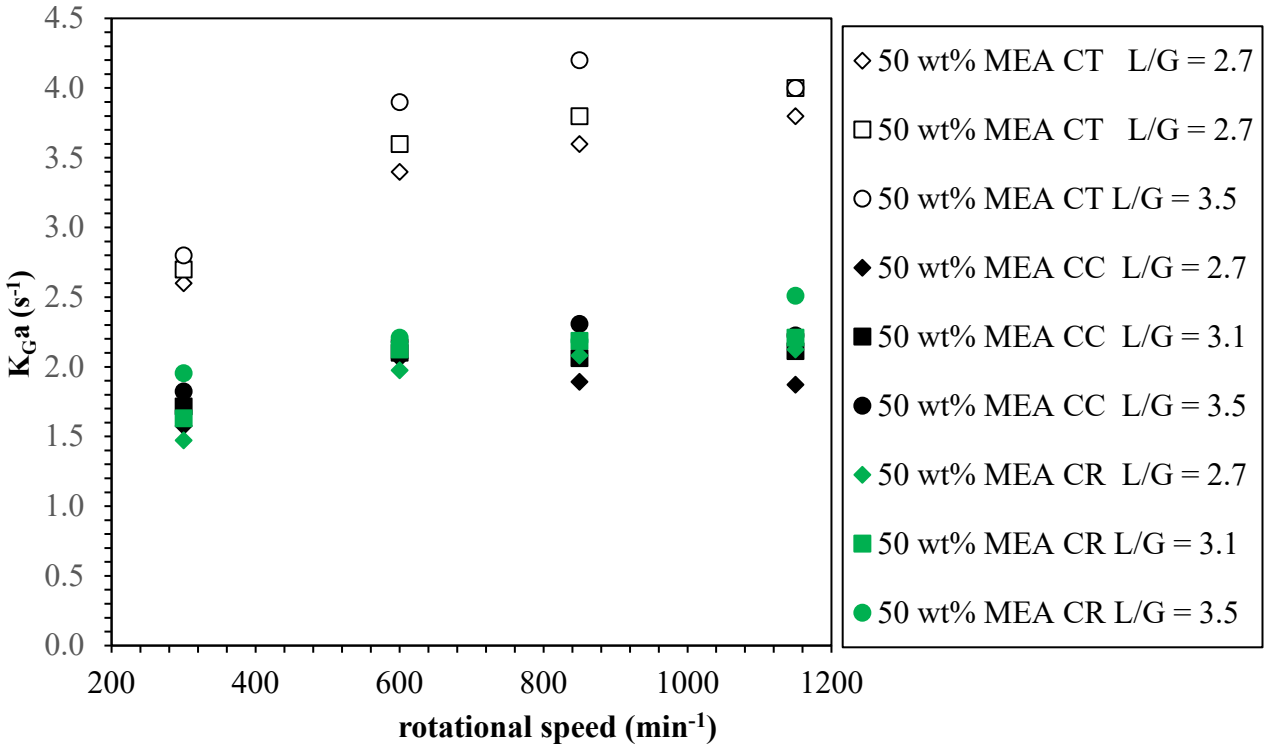

Figure 7.8: K_Ga results for RPB gas-flow configurations (CT: counter-current, CC: co-current and CR: cross-flow)using 50 wt% MEA solutions.

For the 70 wt% MEA solutions, the counter-current RPB also had the highest overall gas mass transfer coefficient values followed by the cross-flow and then the co-current flow. The exception is at 600 rpm where the co-current RPB performed slightly better than the cross-flow RPB. In the work done by Lin *et al.* (2008) on absorption of 10% CO_2 absorption using aqueous NaOH solutions, they found K_Ga values for the cross-flow RPB were higher than those in cross-flow RPB than a comparative counter-current RPB.

However, this is not in agreement with the results obtained in this work as the results shows that the counter-current RPB gives higher $K_G a$ values.

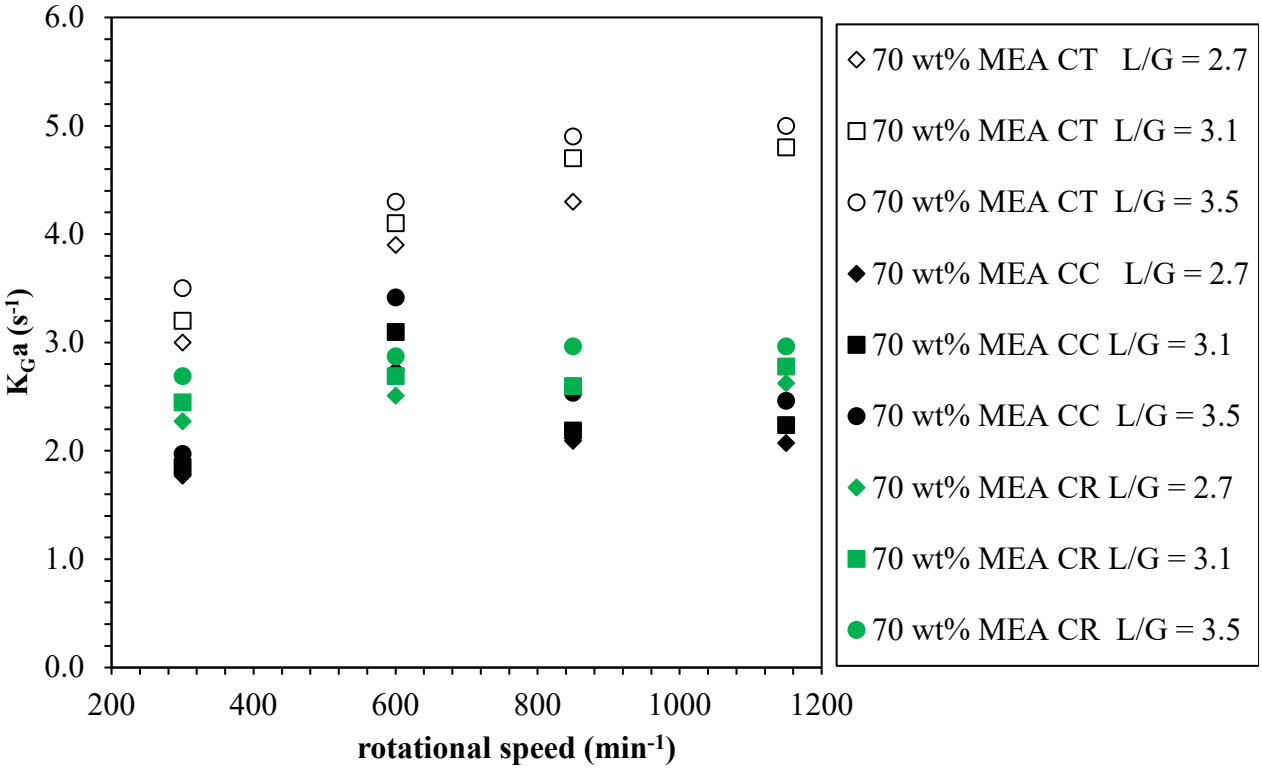

Figure 7.9: $K_G a$ results for RPB gas-flow configurations (CT: counter-current, CC: co-current and CR: cross-flow) using 70 wt% MEA solutions.

Lin *et al.* (2010) suggested in their work there was less contact time in the cross-flow RPB compared to the counter-current RPB. The results obtained in this work show that this may be the case as the $K_G a$ values for the counter-current increasingly become higher than those of the cross-flow as the rotational speed increases from 300 rpm to 600 rpm and are almost double at 850 rpm and 1150 rpm for the 50 wt% and 70 wt% solutions.

7.1.4 Pressure drop for three RPB configurations

Figure 7.10, Figure 7.11 and Figure 7.12 and shows the pressure drop results for the three different RPB configurations. It can be seen that the general trend was that as rotational speed increased, the pressure drop for the counter-current and cross-flow RPBs increased while that of the co-current RPB decreased. Figure 7.10 shows the results for the 30 wt% MEA solutions and it indicates that that the pressure drop for the co-current RPB were highest at 4.4 Pa at 300 rpm while the highest pressure drop of the cross-flow RPB was 1.6 Pa at 1150 rpm.

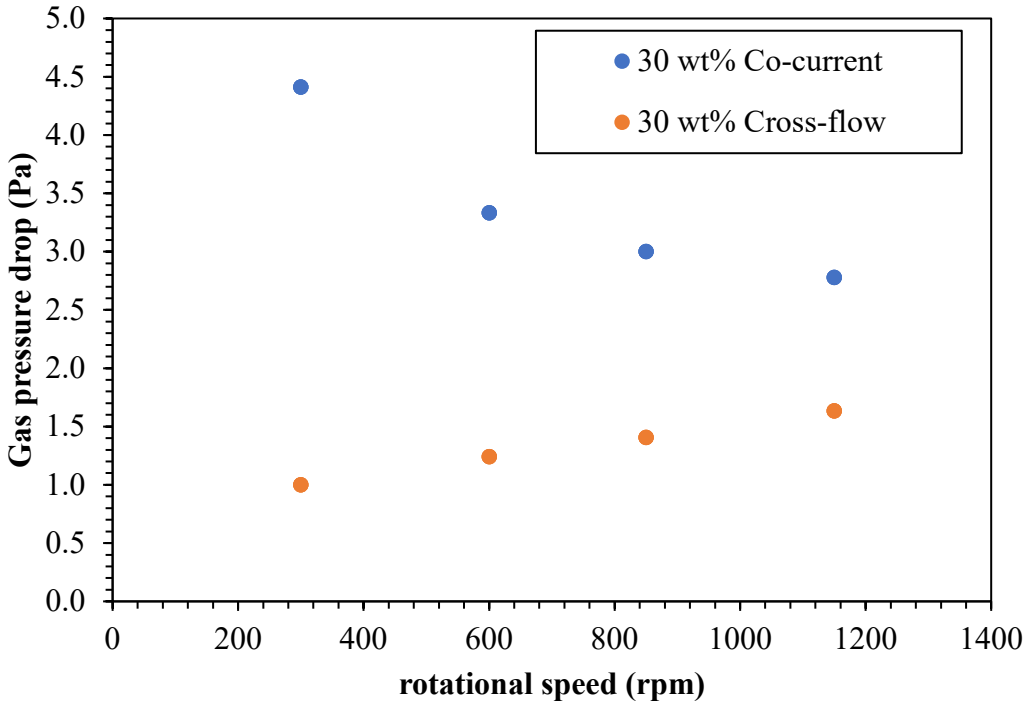

Figure 7.10: Pressure drop results for 30 wt% for co-current and cross-flow RPB configurations.

Figure 7.11 also shows that the pressure drop results for the co-current were the highest, in comparison to the cross-flow RPB. The lowest pressure drop of the co-current RPB was 2.9 Pa at 1150 rpm and the highest value was 6.6 Pa at 300 rpm while the lowest

value of the cross-flow RPB was 1.4 Pa at 300 rpm and highest value was 2.8 Pa at 1150 rpm.

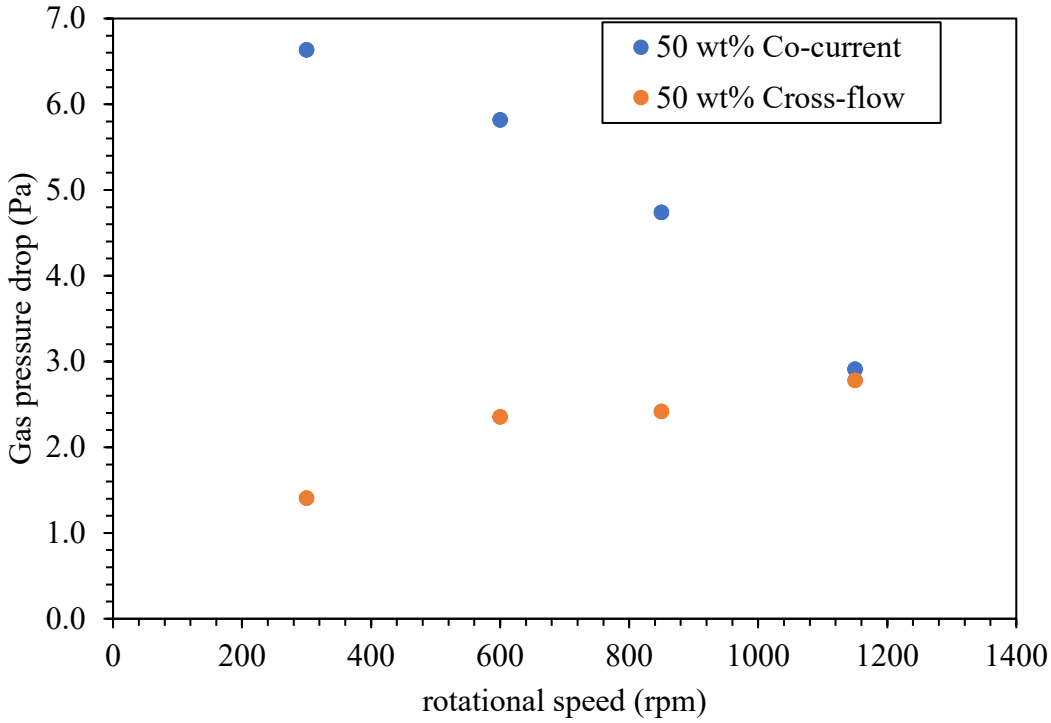

Figure 7.11: Pressure drop for 50 wt% for co-current and cross-flow RPB configurations.

The pressure drop results of the 70 wt% MEA solutions presented in Figure 7.12 for the three RPB configurations using clearly indicate the counter-current RPB had the highest pressure drop values while the cross-flow had the lowest pressure drop readings. The pressure drop values of the counter-current RPB increased with increasing rotational speed with pressure drop readings of 8.8 Pa at 300 rpm that increased to 17.3 Pa at 1150 rpm. The pressure drop values of the co-current RPB increased slightly as rotational speed increased from 300 rpm to 600 rpm then decreased past 600 rpm. The pressure drop of the cross-flow RPB increased slightly from 1.8 Pa at 300 rpm to 4.6 Pa at 1150 rpm.

The results presented for the three RPB configurations at the different MEA concentrations clearly show that the cross-flow RPB had the lowest pressure drop results in comparison to the other RPBs.

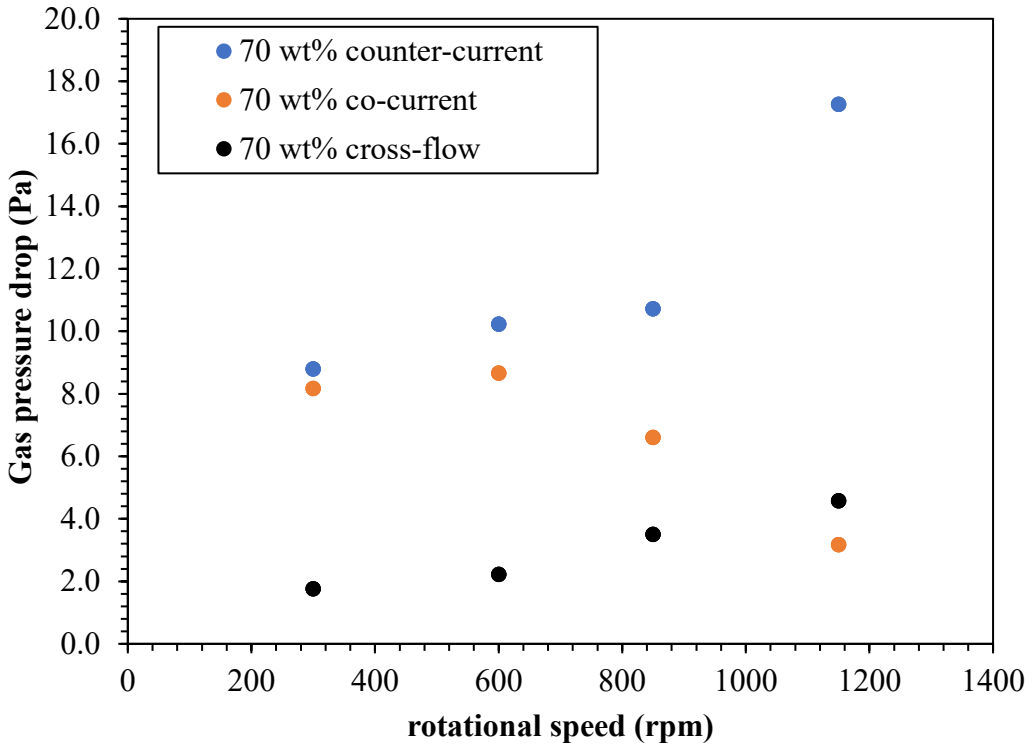

Figure 7.12: Pressure drop for RPB gas-flow configurations (CT: counter-current, CC: co-current and CR: cross-flow) using 70 wt% MEA.

One of the reasons for the development of the cross-flow RPBs was developed was to help tackle the problem of pressure drop when dealing with liquid-gas absorption processes with high gas flow rates (Qi *et al.*, 2016). Qi *et al.* (2016) argued that despite the better mass transfer performance of the counter-current RPB, it is limited in dealing with gas streams of low flow rate and this poses a setback to its industrial development. Therefore, the cross-flow RPB shows potential for reduction of pressure drop for industrial scale CO_2 capture when compared with the other two RPBs.

7.2 Design considerations of RPB scale-up for industrial CO_2 capture

Since the initial introduction of the concept of the RPB by Ramshaw and Mallinson (1981), there have been no reported commercial scale application of the RPB for CO_2 capture. Agarwal *et al.* (2010) attempted to establish a systemic design procedure for RPB unit design for large-scale applications and did case study designs for four industrially relevant process that included CO_2 absorption in diethanolamine (DEA).

Despite the large number of experimental studies on CO_2 capture with alkanolamines using the RPB, the scale-up of RPB for CO_2 capture has not received a great deal of attention. The commercial application of the RPB for CO_2 capture will require demonstration projects that will scale-up the existing experimental RPB sizes. In the following sections, a RPB size design is attempted for a demonstration CO_2 capture to remove 90% CO_2 from simulated flue gas using the three possible RPB configuration. A brief description of the important design parameters are given and a description of the design task is provided.

The basic design parameters of a RPB unit for CO_2 capture process are the outer (r_o) and inner (r_i) packing radii and the axial length (z). These are usually based on the amount of the flue gas feed and the desired capture efficiency. The absorber will also be designed having in mind the specification of the flue gas in terms of the flow rate, composition, temperature and pressure (Agarwal *et al.*, 2010). In selecting the RPB size, this must be done to ensure that there is maximum contact between the gas and liquid feeds to achieve the specified capture efficiency.

7.2.1 Mass transfer considerations

According to Jassim (2002), the overall gas phase mass transfer coefficient for a CO_2 absorption process is expressed as:

$$K_G = \frac{P - P^*}{\frac{1}{k_g} + \frac{H}{Ek_L}} = k_g(P - P^*) \qquad (7.1)$$

Where k_g is the gas-side mass transfer, k_l is the liquid-side mass transfer, H is the Henry's constant, E is enhancement factor.

The difference between the partial pressures of CO_2 in the gas phase and the equilibrium partial pressure of CO_2 (corresponding to the concentration of CO_2 in the liquid phase) is the driving force for the equation 7.1.

The difficulty of separation is expressed in terms of the number of transfer units (NTU) and Colburn (1939) defined the number of overall transfer units based on the change in gas concentration as:

$$NTU_{OG} = \int_{y_1}^{y_2} \frac{dy}{y - y^*} = \ln\left(\frac{y_{CO_{2,in}}}{y_{CO_{2,out}}}\right) \quad (7.2)$$

The assumption of the equation above is that the equilibrium partial pressure of CO_2 is negligible (y^* =0). This holds true if the CO_2 loading (mol CO_2/mol MEA) is low relative to y_{CO_2} (where y_{CO_2} is the equilibrium partial pressure of CO_2 in the feed gas stream). This usually tends to be the case and is due to the fast chemical reaction between CO_2 and the concentrated amine solutions (Jassim *et al.*, 2007). In the work done by Jou *et al.* (1995), the equilibrium pressure of CO_2 at 40 ºC and a loading of 0.33 was approximately 0.04kPa. In Table 7.1, the equilibrium partial pressures at different loadings and at MEA mass concentrations close to those investigated in this work. The lean leading of the MEA used for the CO_2 absorption experiments ranged between 0.10-0.15 (mol CO_2/mol MEA) and the rich loading (mol CO_2/mol MEA) of the MEA carried out in this work was between 0.101-0.188 which satisfies this criteria. In work carried out by Ying *et al.* (2017) on the mass transfer kinetics of CO_2 in loaded aqueous MEA solutions, they suggested that although the equilibrium partial pressure in the lean MEA solutions are not zero as they are already loaded, the CO_2 concentration in the liquid bulk can be assumed to be approximately constant when the residence time is very short. In addition, the CO_2 loading is not significantly increased during the absorption run due to the amount of CO_2 absorbed being little compared to the overall amount of MEA.

7.2.2 RPB outer and inner radius

To calculate the inner radius (r_i), the equation given by Agarwal *et al.* (2010) was used:

$$r_i = \sqrt{\frac{Q_G}{\pi V_{jet}(1 - f_d)} NTU_{OG}} \left(\frac{p\rho_G}{\rho_L}\right)^{0.25} \quad (7.3)$$

Where p is defined as the liquid jet to exit gas kinetic energy ratio (p is recommended to be around the value of 4). The liquid jet velocity (V_{jet}) used in this work is 2 m/s although

a value of between 4-5m/s was recommended by Agarwal *et al.* (2010). Higher values of V_{jet} are discouraged due to the splash back when the liquid jet hits the packing. The values selected should give the optimal kinetic energy fir the liquid jet such that the inner radius of the RPB is as small as possible. Jassim *et al.* (2007) gave the area of transfer unit (ATU) for RPB design as:

$$\pi(r_o^2 - r_i^2) = ATU_{OG}NTU_{OG} = \frac{Q_G}{K_G a_e Z} NTU_{OG} \quad (7.4)$$

Table 7.1: Equilibrium solubility of CO2 in aqueous MEA solutions at different concentrations and 40 ^oC (Aronu et al., 2011).

30 wt% MEA		**45 wt% MEA**		**60 wt% MEA**	
Pco_2 (kPa)	**α_{co_2} (mol/mol)**	**Pco_2 (kPa)**	**α_{co_2} (mol/mol)**	**Pco_2 (kPa)**	**α_{co_2} (mol/mol)**
0.0016	0.102	0.0035	0.141	0.0060	0.173
0.0123	0.206	0.0035	0.148	0.0127	0.242
0.0246	0.250	0.0077	0.195	0.0281	0.306
0.0603	0.337	0.0099	0.217	0.0526	0.344
0.1835	0.401	0.0123	0.234	0.1508	0.394
0.3809	0.433	0.0364	0.300	0.3824	0.427

Rearranging the equation, the outer radius of the RPB is then given as:

$$r_o = \sqrt{r_i^2 + \frac{Q_G}{\pi K_G a_e Z} NTU_{OG}} \quad (7.5)$$

Some important things to take into consideration in design is that in counter-current RPBs, the gas flow rate is limited by the flow area at the eye of the rotor. According to

Cortes Garcia *et al.* (2017), flooding will most likely occur in the eye of the rotor as it is where the velocities of the liquid and the gas are highest.

7.2.3 Axial length

$$\pi(r_o^2 - r_i^2) = \frac{Q_G}{K_G a \quad Z} NTU_{OG} \quad (7.6)$$

The axial length can then after rearranging the equation be expressed as:

$$\frac{Q_G NTU_{OG}}{\pi(r_o^2 - r_i^2) K_G a_e}$$

For the purpose of the RPB scale-up, the axial length of the RPB is calculated assuming 80% of the flooding gas velocity as given as:

$$z = \frac{Q_G}{2\pi r_i 0.8 U_G} \quad (7.7)$$

7.2.4 Selection of packing

To select the packing to be used for a scaled-up industrial RPB, the packing to be used should provide a very large surface area for mass transfer and have high voidage for low pressure drop. Moreover, the packing should be able to withstand constant rotation at high speeds over long periods. It should also be able to balance costs, mass-transfer efficiency and pressure drop (Agarwal *et al.*, 2010). For the experimental study in this work, expamet metal was chosen as metal packing have been shown to satisfy the design criteria. The voidage and surface area of the expamet packing are 0.84 and 694 m^{-1} respectively.

7.2.5 Power consumption

In counter-current rotating packed beds, a mechanical seal is required to prevent the gas flow bypassing or flowing around the rotor (Cortes Garcia *et al.*, 2017). Agarwal *et al.* (2010) suggested that in industrial RPBs where liquid flow rates will be high, the bulk of the power requirements will be for providing kinetic energy to the liquid as well the changes in liquid rotation direction. The power consumption is calculated using the following correlation:

$$W_s = (0.5 S_{out} V_{tip}^2) \qquad (7.8)$$

The power consumption for supplying the gas can also be estimated as:

$$Power\ gas = \frac{mass\ flow_{gas} \Delta P}{\cap_{fan} \rho_{gas}} \quad (7.9)$$

Where μ_{gas} is the viscosity of the gas, ΔP is the pressure drop across the packing (axial length), ρ_{gas} is the density of the gas and $\cap_{fan}$ is the fan efficiency. For a 20 mm axial length, the ΔP is given as: 3/0.02 = 150 Pa/m.

7.2.6 Pressure drop

The gas pressure drop plays a very important role in the choice of packing and the energy consumption of the rotating packed bed and therefore an essential factor for measuring performance (Qi *et al.*, 2016). There have been various experimental studies that have investigated the pressure drop rotating packed beds and several correlations that have been developed to predict the pressure drop in a RPB. Keyvani and Gardner (1989) investigated the gas pressure drop of a counter-current rotating packed bed with a metal aluminium foam packing and found that the gas pressure drop ranged from 0-250 Pa/cm. His findings also showed that the dry gas pressure was much higher than the wet bed pressure and the gas pressure drop increased with increasing gas flow rate. Kumar and Rao (1990) published a correlation to estimate pressure drop within a counter-current rotating packed bed and suggested that the total pressure drop across the rotor arises mainly as a result of the centrifugal and frictional losses and also due to the kinetic energy at the expense of the pressure head.

There have also been some studies done on pressure drop in cross-flow rotating packed beds. Jiao *et al.* (2010) investigated a cross-flow rotating packed bed with stainless steel porous plate packing and plastic corrugated plate packing and obtained a correlation for the pressure drop by modelling with MATLAB. Sandilya *et al.* (2001) also studied pressure drop in a counter-current RPB with wire-gauze packing and reported that the gas in the RPB undergoes a solid-body like rotation in the rotor due to the drag by the packing. They also presented a method to evaluate the friction factor required to estimate the frictional pressure drop.

Figure 7.13 shows gas flow pathway (1-2-3-4) in a counter-current gas flow rotating packed bed. The gas enters the rotor through the outer periphery at uniform velocity and flow into the eye of the rotor. The pressure drop, (ΔP_t) is the pressure difference across points 1 and 4 and it depends on the type of packing used, the type of liquid distributor used. The liquid flow rates have been shown to have only minor effects on the total gas pressure drop (Sandilya *et al.*, 2001; Qi *et al.*, 2016). The gas flow can be considered to be one-dimensional and of similar flow pattern as in conventional packed columns except for the flow area (Rao *et al.*, 2004). The Ergun equation is used to estimate the pressure drop across the packed section of the rotor and is expressed as in equation 1.11

$$\frac{dP}{dr}\frac{\epsilon^3 d_p \rho_g}{(1-\epsilon)G^2} = \frac{150(1-\epsilon)}{Re_p} + 1.75 \qquad (7.10)$$

Where ϵ is the porosity of the packing, d_p is the equivalent particle diameter of the packing ($6[1-\epsilon]/\alpha_{p,}\, m$), G is the gas mass flow rate (kg/s), Re_p is the particle Reynolds number defined as Gd_p/μ_g (μ_g is the gas viscosity). It is important to note that the gas velocity varies in the direction of the flow and equation 7.10 can be integrated to give:

$$\frac{\mathrm{dP}}{\mathrm{dr}}\frac{\epsilon^3 \mathrm{d_p}\rho_g}{(1-\epsilon)G^2} = \frac{150(1-\epsilon)}{\mathrm{Re_p}} + 1.75 \qquad (7.10) \qquad \Delta P$$

The gas within the RPB undergoes a solid-body rotation within the packing and the tangential slip velocity between the gas and packing is considered to be negligible (Rao *et al.*, 2004; Neumann *et al.*, 2017).

The components of the total gas pressure drop has been expressed in different form in literature. Rao *et al.* (2004) suggested that the total pressure drop is the sum of four individual components: ΔP_m the pressure drop that was due to the momentum gain, ΔP_f the frictional pressure drop, $\Delta P_{c,}$ the centrifugal pressure drop in the region and $\Delta P_{o,}$ which is the pressure drop as a result of expansion and contraction in the gas flow pathway. Sandilya *et al.* (2001) resolved the total pressure drop into two broad categories which are ΔP_a and $\Delta P_{o.}$ The centrifugal pressure drop, frictional loss and the momentum pressure drop make up ΔP_a while ΔP_o was defined as the entry and exit losses at the inner and outer periphery of the rotor. ΔP_o is generally considered to be negligible compared to the other pressure drops (Sandilya *et al.*, 2001).

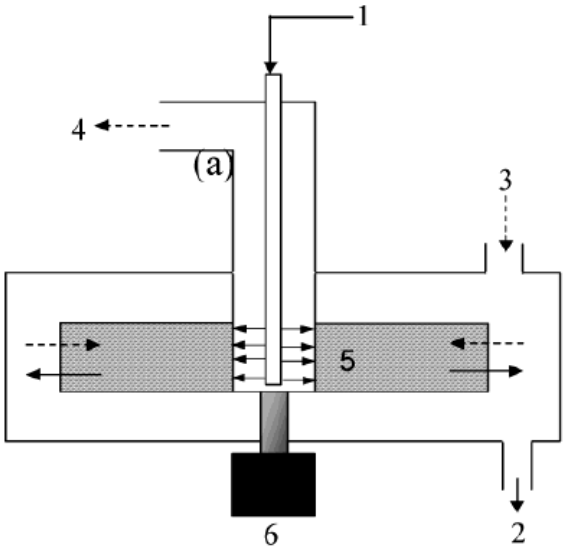

Figure 7.13: Schematic diagram of a RPB where 1 is liquid feed inlet; 2 is liquid outlet; 3 is gas inlet; 4 is gas outlet; 5 is packing and 6 is motor (Rao *et al.*, 2004).

Therefore, the pressure drop expression reduces to ΔP_a, which will be the sum of the centrifugal pressure drop, frictional loss and the momentum pressure drop. This gas pressure drop across the rotor is represented by a equation of motion for radial flow of a fluid (frictionless) in a RPB as obtained from the work of Chandra *et al.* (2005) and expressed as:

$$-\frac{dP}{dr} = -\rho\,\frac{dv_r{}^2}{dr} - \rho\frac{V_\theta{}^2}{r} - \frac{1}{2}f_r\left(\frac{v_r{}^2}{dh}\right)_f \qquad (7.12)$$

Where dp/dr is the differential radial pressure in the RPB rotor, $V_r = \frac{Q_G}{2\pi r\epsilon Z}$ and is the gas radial velocity, V_θ is the gas tangential velocity and f_r is the radial friction factor and d_h is the hydraulic dimeter. In equation 7.13, the first term represents the momentum pressure drop, the second term represents the centrifugal pressure drop and the third term accounts for the frictional pressure drop. ΔP_a can be calculated if V_r and V_θ are known. V_r is found from the continuity equation as:

$$V_r = \frac{Q_G}{2\pi r\epsilon Z} \qquad (7.13)$$

where Q_G is the volumetric gas flow rate, Z is the axial length and ϵ is the porosity of the RPB.

The pressure due to the momentum gain, $\Delta P_{m,}$ can then be obtained by integrating term two of equation 7.13:

$$\Delta P_m = \rho \int_{r_i}^{r_0} \frac{{v_r}^2}{r} dr \qquad (7.14)$$

Substituting equation 7.14 into equation 7.13 and integrating the equation, the following expression is obtained:

$$\Delta P_m = \frac{1}{2}\rho \left(\frac{Q_G}{2\pi\epsilon Z}\right)^2 \left(\frac{1}{{r_0}^2} - \frac{1}{{r_i}^2}\right) \qquad (7.15)$$

The centrifugal pressure drop, $\Delta P_{c,}$ can then be evaluated by integrating the following expression:

$$\Delta P_c = \rho \int_{r_i}^{r_0} \frac{{v_\theta}^2}{r} dr \qquad (7.16)$$

Due to the assumption that the gas is in a solid body rotation with the packing, $V_\theta = \omega r$ and equation 7.17 can then be resolved to get:

$$\Delta P_c = \frac{1}{2}\rho\omega^2({r_i}^2 - {r_o}^2) \qquad (7.17)$$

There have been suggestions that a parameter, A, which is a constant be added to the equation for the centrifugal pressure drop, ΔP_c (Kumar and Rao, 1990; Kelleher and Fair, 1996). This then makes equation 1.18 to be expressed as:

$$\Delta P_c = A\frac{1}{2}\rho\omega^2({r_o}^2 - {r_i}^2) \quad (7.18)$$

Sandilya *et al.* (2001) in the findings showed that including this constant was necessary as their work had a 20% overestimation when comparing experimental and calculated centrifugal pressure drop values. Rao *et al.* (2004) suggested that this value should be unity if the gas undergoes a solid body rotation as assumed in this work. The values used for A in literature tend to range from 0.5 to 2 and appears to show that the rotor acts either as a blower or an expander in the RPB (Rao *et al.*, 2004).

The frictional pressure drop, ΔP_f, can be integrated

$$\Delta P_f = \int_{r_i}^{r_0} f_r \frac{{v_r}^2}{2d_h} dr \tag{7.17}$$

The radial friction factor, f_r is given as:

$$f_r = \frac{\alpha}{Re_f} + \beta \tag{7.20}$$

Where α and β are coefficients that depend on the liquid rate, L and the rotational speed, respectively and the Re_f is the Reynold's number of the friction factor which is expressed as:

$$Re_f = \frac{v_r d_h \rho}{\mu_g} \tag{7.21}$$

Where v_r is the radial velocity of the gas, μ_g is the gas viscosity. Substituting equation 7.20 and 7.21 into equation 7.19, and integrating from r_i to r_o gives:

$$\Delta P_f = \frac{\rho}{2\epsilon^2 d_h}\left(\frac{Q_G}{2\pi Z}\right)^2 \left[\alpha \frac{2\pi Z \mu_g}{Q_G d_h} \ln\frac{r_o}{r_i} + \beta\left(\frac{1}{{r_i}^2} - \frac{1}{{r_o}^2}\right)\right] \tag{7.22}$$

Where d_h is the hydraulic diameter and is given as $4\epsilon/a_p$ (m). The frictional pressure drop ΔP_f is obtained by subtracting the calculated ΔP_c and ΔP_m from the experimental pressure drop measurements and then the coefficients α and β may then obtained. It then follows that ΔP_c, ΔP_m and ΔP_f can then be predicted using their equations and the total

predicted pressure obtained from their sum. It is important to note that this is a pressure drop model that is based on the tangential velocity of the gas flow.

Rao *et al.* (2004) suggested that the frictional pressure drop can be estimated from Ergun's equation as there is negligible effect of liquid flow on the total pressure drop when flooding has not been reached. They also argued that the slip velocity is also negligible in the rotor and the flow predominantly radial.

The Ergun's equation is given as:

$$\Delta P = \frac{(1-\epsilon)}{\epsilon^3} \frac{Q_g}{2\pi h d_p} \left[\frac{150(1-\epsilon)\mu_g}{d_p} \ln\frac{r_o}{r_i} + 1.75\frac{Q_g\rho_g}{2\pi h}\left(\frac{1}{r_i}-\frac{1}{r_o}\right)\right] \qquad (7.23)$$

It can be seen when comparing with Ergun's equation form with equation 1.22 that the β in equation 7.22 can be represented by $1.75\frac{Q_g\rho_g}{2\pi h}$.

For the cross-flow RPB, the following equations are used for the pressure drop.

$$-\frac{dP}{dr} = -\rho\frac{V\theta^2}{r} + PV_r\frac{dv_r}{dr} \qquad (7.24)$$

Where P is pressure, v_r is the radial velocity and V_θ is the tangential velocity. This then gives:

$$\frac{dP}{dr} = -P\frac{d({v_r}^2)}{dr} + P\frac{V\theta^2}{r} \qquad (7.25)$$

$$\frac{dP}{dr} = P\frac{v_r|v_r|}{r} + P\omega^2 r - \left(\frac{dp}{dr}\right)_f \qquad (7.26)$$

7.3 Design procedure

The case study develops a RPB absorber for a design problem details presented in Table 7.2 for capturing CO_2 from simulated flue gas in a CO_2 capture demonstration plant. The flue gas feed at 650 kg s^{-1} containing 12 mol % CO_2 as would be expected from flue gas from a coal-fired boiler (Rochelle, 2009). The expected capture efficiency will also be 90% CO_2 capture according to the US DOE post-combustion CO_2 capture goal (DOE/NETL, 2010).

Table 7.2: CO_2 absorption using MEA design specification.

Gas feed specification Gas flow rate Gas mole fraction Pressure	 650 kg s^{-1} 0.12 CO_2, 0.64 N_2, 0.10 H_2O 1 atm
Percentage capture	90% CO_2 capture
Molar flow ratio	4.0
Lean loading	0.1 mol CO_2/mol MEA
Liquid jet velocity	5 m s^{-1}
NTU_{OG} (for desired separation)	2.2

7.3.1 Gas and liquid flow rate

The expected feed flue gas composition should be made up of carbon dioxide (CO_2), nitrogen (N_2), oxygen (O_2) and water vapour (H_2O) and their mole fractions calculated as 0.12, 0.64, 0.17 and 0.07 respectively (with SO_2 less than 10 ppm as recommended by Rochelle (2009)). The gas feed temperature was set at 40ºC (313K) at pressure of 1 atm. The gas density and mass flow rate of the gas was calculated to be 1.16 kg m^{-3} and 650 kg s^{-1}. The liquid flow rates for the MEA solutions (shown in table 7.3) were calculated based on the MEA strength scenario (30 wt%, 50 wt% and 70 wt%) with molar ratio fixed at 4.0 for this case study.

Table 7.3: Design mass flow rates.

Weight percentage (wt%)	**Mass flow MEA solution (kg s^{-1})**
30 50 70	2125.2 1275.1 910.8

7.3.2 Design of diameter of eye of the rotor and axial length

The equation by Agarwal *et al.* (2010) was then used to calculate the radius of the eye of the rotor for the gas flow rate as given in equation 7.29 using a liquid jet velocity is 2 m s^{-1} and the fraction of the eye occupied by the liquid distributor f_d was assumed to be 0.25 (Agarwal *et al.*, 2010)

$$r_i = \sqrt{\frac{Q_G}{\pi V_{jet}(1 - f_d} NTU_{OG} \left(\frac{p\rho_G}{\rho_L}\right)^{0.25} \qquad (7.27)$$

From equation 7.29, inner radius calculated for both the counter-current and the co-current rotating packed beds was 2.84 m. The voidage and surface area selected for the packing were 0.84 and 694 m^{-1} respectively (based on characteristics of packing used in this work) and the angular velocity calculated using equation 7.30:

$$\omega = \left(\frac{2\pi rpm}{60}\right) \qquad (7.28)$$

The Sherwood X-axis and Y-axis parameter were then calculated using equation 1.31 and 1.32 respectively (Jassim *et al.*, 2007)

$$X_s = \left(\frac{S}{F}\right)\sqrt{\frac{\rho_G}{\rho_L}} \qquad (7.29)$$

$$Y_s = Exp\left[-3.01 - 1.4Log(X_s) - 0.15\,(Log(X_s))^2\right] \qquad (7.30)$$

Where S is the total liquid mass flow to the RPB and F is the mass flow rate of the gas feed. The gas velocity at flooding (m/s) is given by:

$$U_G = \sqrt{Y_s\left(\frac{\rho_G}{\rho_L}\right)\left(\frac{\epsilon^3}{aP}\right)\omega^2 r_i} \qquad (7.31)$$

The axial length of the rotor is then calculated at 80% of the flooding gas velocity as:

$$z = \frac{Q_G}{2\pi r_i 0.8U_G} \qquad (7.32)$$

Where Q_G is given as the gas flow rate at feed conditions.

7.3.3 Design of the outer radius of the RPB

The outer molar flow rate of CO_2 and of gas was calculated assuming a 90% CO_2 removal using equation 7.35 and 7.36 respectively

$$F_{CO_2\,out} = 0.1F_{CO_2\,in} \quad (7.33)$$

$$F_{out} = \left(\frac{F}{M}\right)\left(1 - yF_{CO_2}\right) + F_{CO_2\,out} \quad (7.34)$$

The mole fraction composition at the outlet of the constituents of the gas stream is given by:

$$y_{out} = \left\{\frac{F_{CO_2\,out}}{F_{out}}, \frac{\left(\frac{F}{M}\right)yF_{N_2}}{F_{out}}, \frac{\left(\frac{F}{M}\right)yF_{O_2}}{F_{out}}, \frac{\left(\frac{F}{M}\right)yF_{H_2O}}{F_{out}}\right\} \quad (7.35)$$

The number of transfer units required is then calculated assuming that the concentration of CO_2 in the solvent is zero (Lin *et al.*, 2003)

$$NTU_{og} = Log\left(\frac{yF_{CO_2}}{y_{out_{CO_2}}}\right) \quad (7.36)$$

Selecting the appropriate $K_G a$ for the MEA concentration used, the outer radius diameter is calculated using equation 7.39 given by Jassim *et al.*
(2007)

$$r_o = \sqrt{r_i^2 + \frac{Q_G}{\pi K_G a_e Z} NTU_{OG}} \quad (7.37)$$

For the cross flow RPB, the smallest diameter for the counter-current was selected and the inner radius calculated based on the assumption of no flooding within the RPB and the design gas flow rate.

7.3.4 Design of motor power

Equation 7.40 is used to calculate the outlet loading,

$$\frac{\left(\frac{S\,XF_{CO_2}}{M_{CO_2}}\right) + \left(F_{CO_2\,in} - F_{CO_2\,out}\right)}{\frac{S\,XF_{MEA}}{M_{MEA}}} \quad (7.8)$$

The mass flow rate of the liquid leaving the rotor is then given by:

$$S_{out} = S + \left(F_{CO_2\,in} - F_{CO_2\,out}\right)M_{CO_2} \quad (7.39)$$

Where S is the total liquid mass flow fed into the RPB. The mass fraction composition of the solvent leaving the rotor is then calculated using equation 7.42

$$X_{out} = \left\{\frac{S\,XF_{CO_2} + \left(F_{CO_2\,in} - F_{CO_2\,out}\right)M_{CO_2}}{S_{out}}, \frac{S\,XF_{MEA}}{S_{out}}, \frac{S\,XF_{H_2O}}{S_{out}}\right\} \quad (7.40)$$

The motor power is expressed as:

$$W_s = \left(0.5 S_{out} {V_{tip}}^2\right) \quad (7.42)$$

Where the tip speed is then calculated as:

$$V_{tip} = \omega r_o \quad (7.42)$$

7.4 Evaluation of RPB absorber design sizes

The RPB absorber design units are reported in Table 7.4. 7.5 and 7.6 for the counter-current, co-current and cross-flow RPBs respectively. The fixed inner diameter for the counter-current and co-current RPB was calculated to be 2.84 m using a liquid jet velocity of 2 m s^{-1}. For the cross-flow RPB, the inner radius was calculated to be 1.60 m using a recommended fluid velocity of 1.8 m s^{-1} and the absorber size results are presented in

Table 7.6. For the results for the counter-current RPB shown in Table 7.4, it can be seen that the outer diameter size of the RPB decreased as the concentration of the MEA solution increased from 30 wt% to 70 wt%. The same trend is also observed for the axial length of the counter-current RPB. Moreover, the power required for rotating the RPB increased with the rotating speed showing that running that RPB at higher rotating speed will result into greater power consumption. The motor power also decreased as the solution concentration increased with the 70 wt% MEA solutions showing the lowest motor power consumption, which is followed by the 50 wt% solutions and finally the 30 wt% solution. This may be due to the reduced liquid flow rates as a result using higher concentration MEA solutions. Therefore, using higher concentration MEA solutions will result in lower power consumption for the liquids.

Similarly, for the co-current RPB, the results as displayed in .

Table 7.5 showed a trend where the axial length decreased with increase in rotational

MEA (wt%)	Experimental motor speed (rpm)	Rotor speed at scale-up (rpm)	KGa /s-1	d0 /m	z /m	Power (liquid) /W
30	300	55	1.2	15.4	6.6	2.22 X 106
	600	110	1.3	19.8	3.3	1.48 X 107
	850	155	1.4	22.7	2.3	3.88 X 107
	1150	210	1.5	25.6	1.7	8.27 X 107
50	300	55	1.7	14.0	5.6	1.15 X 106
	600	110	2.1	17.2	2.8	7.00 X 106
	850	155	2.1	20.3	2.0	1.96 X 107
	1150	210	2.1	23.2	1.5	4.65 X 107
70	300	55	1.9	14.0	5.1	8.65 X 105
	600	110	3.1	15.1	2.5	4.01 X 106
	850	155	2.2	20.7	1.8	1.50 X 107
	1150	210	2.2	23.6	1.3	3.57 X 107

speed. In terms of absorber sizes, it also indicates that using higher concentration monoethanolamine solutions leads to a reduction in the absorber sizes to be used for CO_2 capture from flue gas. The results for the cross-flow rotating packed bed show that the inner diameter is 1.6 m and the outer diameter sizes required reduced with increasing MEA solution concentration. It can also be seen that operating the RPB at higher rotational speeds will reduce the axial length requirement. For the 70 wt% MEA solutions, the axial length requirement decreased from 5.1 m to 2.0 m as the rotational speed increased from 55 rpm to 210 rpm. The trend also showed that the liquid power requirements increased as rotational speed increased and decreased as the solution concentration was increased.

Table 7.4: Table showing design parameters for counter-current flow configuration.

MEA (wt%)	Experimental motor speed (rpm)	Rotor speed at scale-up	K_Ga /s^{-1}	d_0 /m	z /m	Power (liquid) /W
30	300	55	1.6	13.6	6.6	1.73 X 10^6
	600	110	2.0	16.2	3.3	9.90 X 10^6
	850	155	2.1	18.6	2.3	2.59 X 10^7
	1150	210	2.3	20.8	1.7	5.96 X 10^7
50	300	55	2.7	11.6	5.6	7.90 X 10^5
	600	110	3.6	13.6	2.8	4.38 X 10^6
	850	155	3.8	15.5	2.0	1.14 X 10^7
	1150	210	4.0	17.3	1.5	2.58 X 10^7
70	300	55	3.2	11.3	5.1	5.60 X 10^5
	600	110	4.1	13.4	2.5	3.17 X 10^6
	850	155	4.7	14.7	1.8	7.60 X 10^6
	1150	210	4.8	16.6	1.3	1.77 X 10^7

Table 7.5: Table showing design parameters for co-current flow configuration.

MEA (wt%)	Experimental motor speed (rpm)	Rotor speed at scale-up (rpm)	K_Ga /s^{-1}	d_0 /m	z /m	Power (liquid) /W
30	300	55	1.2	15.4	6.6	2.22 X 10^6
	600	110	1.3	19.8	3.3	1.48 X 10^7
	850	155	1.4	22.7	2.3	3.88 X 10^7
	1150	210	1.5	25.6	1.7	8.27 X 10^7
50	300	55	1.7	14.0	5.6	1.15 X 10^6
	600	110	2.1	17.2	2.8	7.00 X 10^6
	850	155	2.1	20.3	2.0	1.96 X 10^7
	1150	210	2.1	23.2	1.5	4.65 X 10^7
70	300	55	1.9	14.0	5.1	8.65 X 10^5
	600	110	3.1	15.1	2.5	4.01 X 10^6
	850	155	2.2	20.7	1.8	1.50 X 10^7
	1150	210	2.2	23.6	1.3	3.57 X 10^7

Table 7.6: Table showing design parameters for cross-flow configuration.

MEA (wt%)	Rotor speed (rpm)	$K_G a$ /s^{-1}	d_i /m	d_0 /m	z /m	Power (liquid) /W
30	300	1.2	1.6	5.65	7.4	1.73×10^6
	600	1.5	1.6	5.65	5.6	6.92×10^6
	850	1.9	1.6	5.65	4.5	1.39×10^7
	1150	2.2	1.6	5.65	4.1	2.54×10^7
50	300	1.6	1.6	5.65	7.3	7.90×10^5
	600	2.1	1.6	5.65	5.6	3.15×10^6
	850	2.2	1.6	5.65	5.4	6.32×10^6
	1150	2.2	1.6	5.65	5.4	1.16×10^7
70	300	2.4	1.6	5.65	5.1	5.60×10^5
	600	2.7	1.6	5.65	4.6	2.24×10^6
	850	2.6	1.6	5.65	4.7	4.48×10^6
	1150	2.8	1.6	5.65	4.5	8.21×10^6

Although Agarwal (2010) recommended operating the RPB unit at as high rpm as possible, the experimental results for overall gas-side mass transfer in this work have shown that the there is no considerable improvement in the by increasing the rotational speed beyond 600 rpm. Moreover, operating the rotating packed bed at higher rotational speeds also increases the power consumption. In view of this, it was deemed reasonable to make a comparison of the absorber sizes for the three different RPB configurations at 600 rpm as a design rpm as shown in Table 7.7. It can be seen that for the cross-flow RPB has the lowest inner diameter compared to the counter-current and co-current RPBs. The cross-flow RPB has no flooding limitation, therefore higher gas flow rates could potentially be used whereas flooding may occur in the counter-current RPB (Lin *et al.*, 2008).

Table 7.7: Scale up parameters at 600 rpm.

MEA concentration (wt%)	Flow configuration	K_Ga /s^{-1}	d_i /m	d_0 /m	z /m	Power /W
30	Counter-current	2.0	2.84	16.2	3.3	9.9 X 10^6
	Co-current	1.3	2.84	19.8	3.3	1.48 X 10^7
	Cross-flow	1.5	1.60	5.65	3.9	9.9 X 10^6
50	Counter-current	3.6	2.84	13.6	2.8	4.38 X 10^6
	Co-current	2.1	2.84	17.2	2.8	7.00 X 10^6
	Cross-flow	2.1	1.60	5.65	4.0	4.38 X 10^6
70	Counter-current	4.1	2.84	13.4	2.5	3.17 X 10^6
	Co-current	3.1	2.84	15.1	2.5	4.01 X 10^6
	Cross-flow	2.7	1.60	5.65	3.2	3.17 X 10^6

It can be seen from Table 7.7 that the cross-flow RPB gives the most compact size in terms of the RPB absorber size as it has the lowest inner and outer diameter with a comparable power consumption to the counter-current RPB. Although the overall gas-side mass transfer results for the counter-current RPB were higher, the cross-flow RPB size required to achieve out the 90% CO_2 is of smaller dimensions than the counter-current and co-current RPBs. This shows that the cross-flow has a great deal of potential for greatly reducing the required equipment sizes and it has the advantage of relaxed flooding limit. However, the cross-flow RPB is more complicated to design. The co-current RPB on the other hand had the largest outer diameter size and highest amount of power consumption that is likely due to the high gas side pressure drop present in the co-current RPB. The absorber sizing estimation did not take into consideration the power consumption due to the air feed and the pressure drop.

Chapter 8. Conclusions and recommendations for future work

8.1 Conclusions

This thesis has presented the performance results for CO_2 capture using RPBs in counter-current, co-current and cross-flow configurations with aqueous MEA solutions. The RPB performance was investigated with respect to overall gas mass transfer, HTU, CO_2 capture efficiency and pressure drop. The review of the literature on CO_2 capture using RPBs showed that there has not been an experimental study investigating the three different RPB configurations for CO_2 capture. There has been especially limited work done on the cross-flow and co-current RPBs using high MEA concentrations. Little experimental work had been done to investigate the pressure drop of the three different RPBs when carrying out CO_2 absorption with MEA solutions.

In this work, a new pilot-scale test RPB rig for CO_2 absorption has been constructed and validated. CO_2 absorption experiments were carried out with 30 wt%, 50wt% and 70 wt% MEA solutions from simulated flue gas. The effects of varying rotational speed, liquid-gas (L/G) ratios, pressure drop and amine concentration were investigated and this covered the range of interest for industrial application of CO_2 capture from flue gas. The novelty of the work was the systematic study of the three RPB configurations for CO_2 capture and the comparison of the three RPB configurations. The gas phase was also saturated to closely simulate flue gas. In addition, the mass transfer results and CO_2 efficiency results were used in the scale-up design of a RPB facility for industrial CO_2 capture with aqueous MEA solutions.

The counter-current RPB showed the best overall gas-side mass transfer performance in the range of 1.8 s^{-1} – 6.2 s^{-1} compared to the co-current and cross-flow which were 1.0 s^{-1} - 3.1 s^{-1} and 1.0 s^{-1} -3.0 s^{-1} respectively. The counter-current RPB also had the lowest height of transfer unit (HTU) in the range 0.13 cm – 0.50 cm compared to 0.24 cm -0.8 cm for the co-current and 0.28 cm - 0.79 cm cross-flow RPB. The results indicate that the hydrodynamics within the RPB plays an important role with regards to the mass transfer performance of the RPB gas-flow configurations. It is pivotal in deciding the rotational speed and L/G ratio to be used in industrial scale-up. Furthermore, the effect of

increasing viscosity as the MEA concentration increased was shown to be important for the co-current and cross-flow RPBs.

The counter-current RPB showed the best performance for CO_2 capture efficiency although its advantage was demonstrated clearly with the higher concentration MEA solutions. This shows that the advantages of the RPB will be mostly harnessed when using higher concentration MEA solutions due to the short contact times within the RPB especially at higher rotational speeds. The results showed that the RPBs generally performed better in terms of CO_2 capture efficiency at higher rotational speed due to the transformation of the type of liquid flow within the RPB.

It was found that the cross-flow RPB had the lowest gas pressure drop of the three RPB configurations while the counter-current RPB showed the highest pressure drop results. This makes the cross-flow RPB very attractive for CO_2 capture especially as it theoretically has no flooding limitations. The effect of rotational speed was the most important as the pressure drop values of the counter-current and cross-flow RPB increased as rotational speed increased while the pressure drop values of the co-current RPB decreased as the rotational speed increased.

The scale-up design showed that the cross-flow RPB would give the most compact RPB size with the lowest pressure drop for CO_2 capture and a comparable power consumption to the counter-current RPB. The counter-current RPB provided the best mass transfer performance although with a larger absorber size and greater pressure drop. However, one of the challenges for scaling up the cross-flow RPB is its technical difficulty especially in achieving a liquid-gas cross-flow contact at a larger size and higher rotational speed. Furthermore is the possibility of the flow changing from a cross-flow contact of the gas-liquid to appear like co-current flow. The co-current RPB showed the worst mass transfer performance but had a better pressure drop performance than the counter-current RPB, with the pressure drop decreasing as rotational speed went higher.

8.2 Recommendations for future work

There are still some knowledge gaps required to be fully understood before full commercial deployment of the RPB for CO_2 capture can be realised. The following are suggestions for further investigation of CO_2 capture using RPB absorbers:

- The designing of an intensified stripper for CO_2 stripping and having full intensified absorption and stripping rig for post-combustion CO_2 capture. A considerable amount of work had been done in the study of stand-alone intensified absorbers but only two studies have been reported in open literature that have attempted to investigate intensified regenerator (Jassim *et al.*, 2007; Cheng *et al.*, 2013). However, the regenerators used in both studies have not been fully intensified (Wang *et al.*, 2015) . It is important that the integrated absorption and stripping process be studied for the successful scale-up of intensified CO_2 capture using the RPB. This will provide a better understanding of the entire process of intensified CO_2 capture and will aid in conducting technical and economic analysis for the intensified CO_2 capture process.
- Testing other packing materials with different specific surface areas and porosities and comparing the performance of such packing materials is very important as the selection of packing plays a pivotal role in the design consideration of the rotating packed bed. The decision of the packing to use on a commercial scale RPB will have to be based on experimental studies that enable the best decision that balances packing cost with pressure drop and mass transfer efficiency.
- Investigating the effect of using split packing within the RPB and comparing its performance with that of the single-block rotating packed bed. The use of split packing is suggested to increase the angular slip velocity between the liquid and gas (Chandra *et al.*, 2005).
- A detailed investigation of the power consumption for the RPB using a more accurate and reliable method is also essential. There will also be the need to investigate the power consumption of the entire capture process including the absorber and stripper. There have been very limited work done to investigate the power consumption of the entire intensified CO_2 capture process.

- Testing MEA, its blends and other novel solvents such as phase change solvents at different concentrations for fully intensified CO_2 capture process using RPBs. This will be very important in deciding the best solvents to use for the intensified CO_2 capture process. Due to the short residence time within the rotating packed bed, important factors that would need to be considered are the reaction kinetics and absorption capacity of potential solvents to be used. In addition, the required energy for regeneration will also be important together with solvent degradation.

References

Addington, L. and Ness, C. (2010) 'An Evaluation of General “Rules of Thumb” in Amine Sweetening Unit Design and Operation', *Proceedings of the Annual Convention- Gas Processors Association* 2018(1), pp. 119-135.

Agarwal, L., Pavani, V., Rao, D.P. and Kaistha, N. (2010) 'Process Intensification in HiGee Absorption and Distillation: Design Procedure and Applications', *Industrial & Engineering Chemistry Research*, 49(20), pp. 10046-10058.

Aghaie, M., Rezaei, N. and Zendehboudi, S. (2018) 'A systematic review on CO_2 capture with ionic liquids: Current status and future prospects', *Renewable and Sustainable Energy Reviews*, 96, pp. 502-525.

Arstad, B., Blom, R. and Swang, O. (2007) 'CO_2 Absorption in Aqueous Solutions of Alkanolamines: Mechanistic Insight from Quantum Chemical Calculations', *The Journal of Physical Chemistry A*, 111(7), pp. 1222-1228.

Astarita, G. (1967) *Mass transfer with chemical reaction*. London, UK: Elsevier.

Astarita, G., Savage, D.W. and Bisio, A. (1983) *Gas treating with chemical solvents*. New York, United States: John Wiley.

Bašić, A. and Duduković, M.P. (1995) 'Liquid holdup in rotating packed beds: Examination of the film flow assumption', *AIChE Journal*, 41(2), pp. 301-316.

Bernhardsen, I.M. and Knuutila, H.K. (2017) 'A review of potential amine solvents for CO_2 absorption process: Absorption capacity, cyclic capacity and pKa', *International Journal of Greenhouse Gas Control*, 61, pp. 27-48.

Biliyok, C., Lawal, A., Wang, M. and Seibert, F. (2012) 'Dynamic modelling, validation and analysis of post-combustion chemical absorption CO_2 capture plant', *International Journal of Greenhouse Gas Control*, 9, pp. 428-445.

Bishnoi, S. and Rochelle, G.T. (2000) 'Absorption of carbon dioxide into aqueous piperazine: Reaction kinetics, mass transfer and solubility', *Chemical Engineering Science*, 55(22), pp. 5531-5543.

Buhre, B.J.P., Elliott, L.K., Sheng, C.D., Gupta, R.P. and Wall, T.F. (2005) 'Oxy-fuel combustion technology for coal-fired power generation', *Progress in Energy and Combustion Science*, 31(4), pp. 283-307.

Burns, J.R., Jamil, J.N. and Ramshaw, C. (2000) 'Process intensification: operating characteristics of rotating packed beds — determination of liquid hold-up for a high-voidage structured packing', *Chemical Engineering Science*, 55(13), pp. 2401-2415.

Burns, J.R. and Ramshaw, C. (1996) 'Process intensification: Visual study of liquid maldistribution in rotating packed beds', *Chemical Engineering Science*, 51(8), pp. 1347-1352.

Chakravarti S., Gupta A. and B., H. (2001) 'Advanced technology for the capture of carbon dioxide from flue gases', *1st National Conference on Carbon Sequestration*. Washington DC, United States, 2001. Praxair Technology, Inc.

Chamber, H.H. and Wall, M.A. (1954) 'Some factors affecting the design of centrifugal absorbers', *Trans. Inst. Chem. Eng.*, 32, pp. 96-107.

Chandra, A., Goswami, P.S. and Rao, D.P. (2005) 'Characteristics of flow in a rotating packed bed (HIGEE) with split packing', *Industrial and Engineering Chemistry Research*, 44(11), pp. 4051-4060.

Chen, Y.-S., Lin, C.-C. and Liu, H.-S. (2005) 'Mass Transfer in a Rotating Packed Bed with Viscous Newtonian and Non-Newtonian Fluids', *Industrial & Engineering Chemistry Research*, 44(4), pp. 1043-1051.

Cheng, H.-H., Lai, C.-C. and Tan, C.-S. (2013) 'Thermal regeneration of alkanolamine solutions in a rotating packed bed', *International Journal of Greenhouse Gas Control*, 16(0), pp. 206-216.

Cheng, H.-H. and Tan, C.-S. (2006) 'Reduction of CO_2 concentration in a zinc/air battery by absorption in a rotating packed bed', *Journal of Power Sources*, 162(2), pp. 1431-1436.

Cheng, H.-H. and Tan, C.-S. (2009) 'Carbon dioxide capture by blended alkanolamines in rotating packed bed', *Energy Procedia*, 1(1), pp. 925-932.

Cheng, H.H. and Tan, C.S. (2011) 'Removal of CO_2 from indoor air by alkanolamine in a rotating packed bed', *Separation and Purification Technology*, 82(1), pp. 156-166.

Chiang, C.-Y., Chen, Y.-S., Liang, M.-S., Lin, F.-Y., Tai, C.Y.-D. and Liu, H.-S. (2009) 'Absorption of ethanol into water and glycerol/water solution in a rotating packed bed', *Journal of the Taiwan Institute of Chemical Engineers*, 40(4), pp. 418-423.

Chu, G.-W., Luo, Y., Shan, C.-Y., Zou, H.-K., Xiang, Y., Shao, L. and Chen, J.-F. (2014) 'Absorption of SO_2 with Ammonia-Based Solution in a Co-current Rotating Packed Bed', *Industrial & Engineering Chemistry Research*, 53(40), pp. 15731-15737.

Chung, B.T.F., Fan, L.T. and Hwang, C.L. (1971) 'Surface renewal and penetration models in the transient state', *AIChE Journal*, 17(1), pp. 154-160.

Colburn, A.P. (1939) *The Simplified Calculation of Diffusional Processes: General Consideration of Two-film Resistances*. New York, United States: American Society of Mechanical Engineers.

Cortes Garcia, G.E., van der Schaaf, J. and Kiss, A.A. (2017) 'A review on process intensification in HiGee distillation', *Journal of Chemical Technology & Biotechnology*, 92(6), pp. 1136-1156.

Crooks, J.E. and Donnellan, J.P. (1989) 'Kinetics and mechanism of the reaction between carbon dioxide and amines in aqueous solution', *Journal of the Chemical Society, Perkin Transactions 2*, (4), pp. 331-333.

D'Alessandro, D.M., Smit, B. and Long, J.R. (2010) 'Carbon Dioxide Capture: Prospects for New Materials', *Angewandte Chemie International Edition*, 49(35), pp. 6058-6082.

Da Silva, E.F. and Svendsen, H.F. (2004) 'Ab initio study of the reaction of carbamate formation from CO_2 and alkanolamines', *Industrial and Engineering Chemistry Research*, 43(13), pp. 3413-3418.

Danckwerts, P.V. (1965) 'The Absorption of Gases in Liquids', *Pure and Applied Chemistry*, 10(4), pp. 625-642.

Danckwerts, P.V. (1971) *Gas-liquid reactions*. New York, United States: McGraw-Hill Book Co.

Danckwerts, P.V. and Kennedy, A.M. (1997) 'Kinetics of liquid-film process in gas absorption. Part I: Models of the absorption process', *Chemical Engineering Research and Design*, 75, pp. 101-104.

Dang, H. and Rochelle, G.T. (2003) 'CO2 Absorption Rate and Solubility in Monoethanolamine/Piperazine/Water', *Separation Science and Technology*, 38(2), pp. 337-357.

Davidson, R. (2007) *Post-combustion carbon capture from coal fired plants: solvent scrubbing*. London, United Kingdom: IEA Clean Coal Centre.

DOE/NETL (2010) *DOE/NETL Carbon Dioxide Capture and Storage RD&D Roadmap*. US Department of Energy/National Energy Technology Laboratory DOE/NETL. [Online]. Available at: http://www.netl.doe.gov/File%20Library/Research/Carbon%20Seq/Reference%20Shelf/CCSRoadmap.pdf (Accessed: 27/03/19).

Dubois, L. and Thomas, D. (2012) 'Screening of Aqueous Amine-Based Solvents for Postcombustion CO_2 Capture by Chemical Absorption', *Chemical Engineering & Technology*, 35(3), pp. 513-524.

Eimer, D.A. (2014) 'Rotating Packed Beds', in *Gas Treating*. Chichester, United Kingdom: John Wiley & Sons, Ltd, pp. 181-191.

Eldardiry, H. and Habib, E. (2018) 'Carbon capture and sequestration in power generation: review of impacts and opportunities for water sustainability', *Energy Sustainability and Society*, 8(1), p. 6.

Elsenhans, A. (1906) *Apparatus for purifying gas*. US820772.

Feron, P. (2016) *Absorption-Based Post-Combustion Capture of Carbon Dioxide*. Cambridge, United Kingdom: Woodhead Publishing.

Florin, N. and Fennell, P. (2010) *Review of Advanced Carbon Capture Technologies. Work stream 2, Report 5A of the AVOID programme (AV/WS2/D1/R05A)*. London, United Kingdom: GIIC. [Online]. Available at: www.avoid.uk.net (Accessed: 01/12/18).

Gao, X.-Y., Liu, L., Hu, M.-L., Xiang, Y., Chu, G.-W., Zou, H.-K., Sun, B.-C. and Chen, J.-F. (2016) 'Numerical simulation for mass transfer characteristics of CO_2 capture in a rotating packed bed', *Chemical Engineering and Processing: Process Intensification*, 109, pp. 68-79.

Garg, B., Verheyen, T.V., Pearson, P., Feron, P. and Cousins, A. (2018) 'A technology review for regeneration of sulfur rich amine systems', *International Journal of Greenhouse Gas Control*, 75, pp. 243-253.

GCCSI (2017) *The Global Status of CCS 2017*. Melbourne, Australia: Global CCS Institute GCCSI. [Online]. Available at: https://www.globalccsinstitute.com/ (Accessed: 27/03/19).

Greenblatt, J.B., Brown, N.R., Slaybaugh, R., Wilks, T., Stewart, E. and McCoy, S.T. (2017) 'The Future of Low-Carbon Electricity', *Annual Review of Environment and Resources*, 42(1), pp. 289-316.

Guo, F., Zheng, C., Guo, K., Feng, Y. and Gardner, N.C. (1997) 'Hydrodynamics and mass transfer in cross-flow rotating packed bed', *Chemical Engineering Science*, 52(21-22), pp. 3853-3859.

Guo, K., Guo, F., Feng, Y., Chen, J., Zheng, C. and Gardner, N.C. (2000) 'Synchronous visual and RTD study on liquid flow in rotating packed-bed contactor', *Chemical Engineering Science*, 55(9), pp. 1699-1706.

Guo, K., Zhang, Z., Luo, H., Dang, J. and Qian, Z. (2014) 'An Innovative Approach of the Effective Mass Transfer Area in the Rotating Packed Bed', *Industrial & Engineering Chemistry Research*, 53(10), pp. 4052-4058.

Hassan-beck, H.M. (1997) *Process Intensification: mass transfer and pressure drop for counter-current rotating packed bed*. Ph.D thesis. Newcastle University, United Kingdom.

Horvath, I.R. and Chatterjee, S.G. (2018) 'A surface renewal model for unsteady-state mass transfer using the generalized Danckwerts age distribution function', *Royal Society Open Science*, 5(5:172423).

HSE (2018) *General hazards of carbon dioxide*. Available at: http://www.hse.gov.uk/carboncapture/carbondioxide.htm (Accessed: 01/11/18).

Hu, D.D., Zhu, G.W. and Shan, W.Y. (2013) 'The Research Progress on Pressure Drop of Rotating Packed Bed', *Key Engineering Materials*, 561, pp. 646-651.

IEA (2016) *Energy,climate change & environment: 2016 Insights*. Paris: International Energy Agency IEA.

IEA/OECD (2016) *World Energy Outlook 2016*. Paris, France: IEA. [Online]. Available at: https://doi.org/10.1787/weo-2016-en. (Accessed: 27/03/19).

IEAGHG (2014) *Assessment of emerging CO_2 capture technologies and their potential to reduce costs* Cheltenham, United Kingdom: IEAGHG.

IEAGHG (2015) *Integrated Carbon Capture and Storage Project at SaskPower Boundary Dam Power Station*. Cheltenham, United Kingdom: IEAGHG.

IPCC (2014) *Climate Change 2014: Mitigation of Climate Change* Cambridge, United Kingdom and New York, NY, USA.: Cambridge University Press.

Iranshahi, D., Golrokh, A., Pourazadi, E., Saeidi, S. and Gallucci, F. (2018) 'Progress in spherical packed-bed reactors: Opportunities for refineries and chemical industries', *Chemical Engineering and Processing - Process Intensification*, 132, pp. 16-24.

Jassim, M.S. (2002) *Process Intensification:Absorption and Desorption of carbon dioxide from monoethanolamine solutions using Higee Technology*. PhD Thesis thesis. Newcastle University, United Kingdom.

Jassim, M.S., Rochelle, G., Eimer, D. and Ramshaw, C. (2007) 'Carbon Dioxide Absorption and Desorption in Aqueous Monoethanolamine Solutions in a Rotating Packed Bed', *Industrial & Engineering Chemistry Research*, 46(9), pp. 2823-2833.

Jiao, W., Luo, S., He, Z. and Liu, Y. (2017) 'Applications of high gravity technologies for wastewater treatment: A review', *Chemical Engineering Journal*, 313, pp. 912-927.

Jiao, W.Z., Liu, Y.Z. and Qi, G.S. (2010) 'Gas Pressure Drop and Mass Transfer Characteristics in a Cross-flow Rotating Packed Bed with Porous Plate Packing', *Industrial & Engineering Chemistry Research*, 49(8), pp. 3732-3740.

Jou, F.-Y., Mather, A.E. and Otto, F.D. (1995) 'The solubility of CO_2 in a 30 mass percent monoethanolamine solution', *The Canadian Journal of Chemical Engineering*, 73(1), pp. 140-147.

Karimi, F. and Khalilpour, R. (2015) 'Evolution of carbon capture and storage research: Trends of international collaborations and knowledge maps', *International Journal of Greenhouse Gas Control*, 37, pp. 362-376.

Kasikamphaiboon, P., Chungsiriporn, J., Bunyakan, C. and Wiyaratn, W. (2013) *Simultaneous removal of CO2 and H2S using MEA solution in a packed column absorber for biogas upgrading*.

Kelleher, T. and Fair, J.R. (1996) 'Distillation Studies in a High-Gravity Contactor', *Industrial and Engineering Chemistry Research*, 35(12), pp. 4646-4655.

Keyvani, M. and Gardner, N.C. (1989) 'Operating characteristics of rotating packed beds', *Chemical Engineering Progress September*, pp. 48-52.

Khan, F.M., Krishnamoorthi, V. and Mahmud, T. (2011) 'Modelling reactive absorption of CO2 in packed columns for post-combustion carbon capture applications', *Chemical Engineering Research and Design*, 89(9), pp. 1600-1608.

Kristiansen, J. (2003) 'The Guide to Expression of Uncertainty in Measurement Approach for Estimating Uncertainty', *An Appraisal*, 49(11), pp. 1822-1829.

Kumar, M.P. and Rao, D.P. (1990) 'Studies on a high-gravity gas-liquid contactor', *Industrial & Engineering Chemistry Research*, 29(5), pp. 917-920.

Lawal, A., Wang, M., Stephenson, P. and Obi, O. (2012) 'Demonstrating full-scale post-combustion CO_2 capture for coal-fired power plants through dynamic modelling and simulation', *Fuel*, 101, pp. 115-128.

Lee, J., Kolawole, T. and Attidekou, P. (2017) 'Carbon Capture from a Simulated Flue Gas Using a Rotating Packed Bed Absorber and Monoethanolamine (MEA)', *Energy Procedia*, 114, pp. 1834-1840.

Leonard, G. (2013) *Optimal design of a CO_2 capture unit with assessment of solvent degradation*. Ph.D thesis. University of Liege, Belgium.

Lewis, W.K. and Whitman, W.G. (1924) 'Principles of Gas Absorption', *Industrial & Engineering Chemistry*, 16(12), pp. 1215-1220.

Li, W., Liu, H., Li, S., Li, W., Chen, Y., Gao, J. and Cao, Y. (2016) 'Removal of hydrophobic volatile organic compounds with sodium hypochlorite and surfactant in a co-current rotating packed bed', *Journal of Environmental Sciences*.

Li, Y., Ji, J., Xu, Z., Wang, G., Li, X. and Liu, X. (2013) 'Pressure drop model on rotating zigzag bed as a new high-gravity technology', *Industrial and Engineering Chemistry Research*, 52(12), pp. 4638-4649.

Li, Z.H. and Hao, G.J. (2013) 'Study on pressure drop and mass transfer in cocurrent flow rotating packed bed', *Journal of Chemical Industry & Engineering* 34, pp. 50-54.

Lin, C.-C. and Chen, B.-C. (2008) 'Characteristics of cross-flow rotating packed beds', *Journal of Industrial and Engineering Chemistry*, 14(3), pp. 322-327.

Lin, C.-C. and Chen, B.-C. (2011a) 'Carbon dioxide absorption in a cross-flow rotating packed bed', *Chemical Engineering Research and Design*, 89(9), pp. 1722-1729.

Lin, C.-C., Chen, B.-C., Chen, Y.-S. and Hsu, S.-K. (2008) 'Feasibility of a cross-flow rotating packed bed in removing carbon dioxide from gaseous streams', *Separation and Purification Technology*, 62(3), pp. 507-512.

Lin, C.-C. and Lin, H.-T. (2013) 'Removal of Carbon Dioxide from Indoor Air Using a Cross-Flow Rotating Packed Bed', *Energy Procedia*, 37, pp. 1187-1193.

Lin, C.-C., Lin, Y.-H. and Tan, C.-S. (2010) 'Evaluation of alkanolamine solutions for carbon dioxide removal in cross-flow rotating packed beds', *Journal of Hazardous Materials*, 175(1), pp. 344-351.

Lin, C.-C., Liu, W.-T. and Tan, C.-S. (2003) 'Removal of Carbon Dioxide by Absorption in a Rotating Packed Bed', *Industrial & Engineering Chemistry Research*, 42(11), pp. 2381-2386.

Lin, C.-C., Wei, T.-Y., Hsu, S.-K. and Liu, W.-T. (2006) 'Performance of a pilot-scale cross-flow rotating packed bed in removing VOCs from waste gas streams', *Separation and Purification Technology*, 52(2), pp. 274-279.

Lin, C.C. and Chen, B.C. (2011b) 'Carbon dioxide absorption in a cross-flow rotating packed bed', *Chemical Engineering Research and Design*, 89(9), pp. 1722-1729.

Lin, C.C. and Chen, Y.W. (2011c) 'Performance of a cross-flow rotating packed bed in removing carbon dioxide from gaseous streams by chemical absorption', *International Journal of Greenhouse Gas Control*, 5(4), pp. 668-675.

Liu, H.-S., Lin, C.-C., Wu, S.-C. and Hsu, H.-W. (1996) 'Characteristics of a Rotating Packed Bed', *Industrial & Engineering Chemistry Research*, 35(10), pp. 3590-3596.

Liu, H., Gao, H., Idem, R., Tontiwachwuthikul, P. and Liang, Z. (2017) 'Analysis of CO_2 solubility and absorption heat into 1-dimethylamino-2-propanol solution', *Chemical Engineering Science*, 170, pp. 3-15.

Luo, Y., Chu, G.-W., Zou, H.-K., Wang, F., Xiang, Y., Shao, L. and Chen, J.-F. (2012a) 'Mass Transfer Studies in a Rotating Packed Bed with Novel Rotors: Chemisorption of CO2', *Industrial & Engineering Chemistry Research*, 51(26), pp. 9164-9172.

Luo, Y., Chu, G.-W., Zou, H.-K., Xiang, Y., Shao, L. and Chen, J.-F. (2012b) 'Characteristics of a two-stage counter-current rotating packed bed for continuous distillation', *Chemical Engineering and Processing: Process Intensification*, 52, pp. 55-62.

Luo, Y., Chu, G.-W., Zou, H.-K., Zhao, Z.-Q., Dudukovic, M.P. and Chen, J.-F. (2012c) 'Gas–Liquid Effective Interfacial Area in a Rotating Packed Bed', *Industrial & Engineering Chemistry Research*, 51(50), pp. 16320-16325.

Lv, B., Guo, B., Zhou, Z. and Jing, G. (2015) 'Mechanisms of CO_2 Capture into Monoethanolamine Solution with Different CO_2 Loading during the Absorption/Desorption Processes', *Environmental Science & Technology*, 49(17), pp. 10728-10735.

Ma, H.-J. and Chen, Y.-S. (2016) 'Evaluation of effectiveness of highly concentrated alkanolamine solutions for capturing CO_2 in a rotating packed bed', *International Journal of Greenhouse Gas Control*, 55, pp. 55-59.

Masohan, A., Ahmed, M., Nirmal, S.K., Kumar, A. and Garg, M.O. (2009) 'A simple pH-based method for estimation of CO_2 absorbed in alkanolamines ', *Indian Journal of Science and Technology* 2(4), pp. 59-64.

McDonough, J. (2013) *Carbon capture using a rotating packed bed: An investigation into pressure drop, liquid distribution and power consumption*. M.Eng thesis. Newcastle university, United Kingdom.

Metz, B., Davidson, O., De Coninck, H., Loos, M. and Meyer, L. (2005) *Carbon Dioxide Capture and Storage*. Cambridge, United Kingdom: IPCC.

Neumann, K., Hunold, S., Skiborowski, M. and Górak, A. (2017) 'Dry Pressure Drop in Rotating Packed Beds—Systematic Experimental Studies', *Industrial & Engineering Chemistry Research*, 56(43), pp. 12395-12405.

Normann, F., Andersson, K., Leckner, B. and Johnsson, F. (2009) 'Emission control of nitrogen oxides in the oxy-fuel process', *Progress in Energy and Combustion Science*, 35(5), pp. 385-397.

Oko, E., Wang, M. and Joel, A.S. (2017) 'Current status and future development of solvent-based carbon capture', *International Journal of Coal Science & Technology*, 4(1), pp. 5-14.

Olivier, J.G.J., Janssens-Maehout, G., Muntean, M. and Peters, J.A.H.W. (2016) *Trends in global CO_2 emissions: 2016 Report*. The Hague, Netherlands: PBL Netherlands Environmental Assessment Agency.

Pachauri, R.K. and Reisinger, A. (2007) *Climate Change 2007 Synthesis Report.Contribution of working groups I,II and III to the fourth assessment report of the intergovernmental panel on Climate change*. Geneva,Switzerland: IPCC.

Pan, S.-Y., Wang, P., Chen, Q., Jiang, W., Chu, Y.-H. and Chiang, P.-C. (2017) 'Development of high-gravity technology for removing particulate and gaseous pollutant emissions: Principles and applications', *Journal of Cleaner Production*, 149, pp. 540-556.

Peng, Y., Zhao, B. and Li, L. (2012) 'Advance in Post-Combustion CO_2 Capture with Alkaline Solution: A Brief Review', *Energy Procedia*, 14(0), pp. 1515-1522.

Perlmutter, D.D. (1961) 'Surface-renewal models in mass transfer', *Chemical Engineering Science*, 16(3), pp. 287-296.

Peters, G.P., Andrew, R.M., Canadell, J.G., Fuss, S., Jackson, R.B., Korsbakken, Jan I., Le Quéré, C. and Nakicenovic, N. (2017) 'Key indicators to track current progress and future ambition of the Paris Agreement', *Nature Climate Change*, 7, p. 118.

Pilo, C. and Dahlbeck, S.W. (1960) *Apparatus for intimatecontacting of two fluid media having different specific weight*. US294187.

Putta, K.R., Knuutila, H. and Svendsen, H.F. (2014) 'Activity Based Kinetics and Mass Transfer of CO_2 Absorption Into MEA Using Penetration Theory', *Energy Procedia*, 63, pp. 1196-1205.

Putta, K.R., Pinto, D.D.D., Svendsen, H.F. and Knuutila, H.K. (2016) 'CO_2 absorption into loaded aqueous MEA solutions: Kinetics assessment using penetration theory', *International Journal of Greenhouse Gas Control*, 53, pp. 338-353.

Qi, G.S., Wang, H., Liu, Y.Z., Zhu, Z.W., Tian, J.X. and Fu, J. (2016) 'Characteristics of gas pressure drop of a countercurrent-flow rotating packed bed', *Indian Journal of Chemical Technology*, 23, pp. 59-64.

Qian, Z., Xu, L.B., Li, Z.H., Li, H. and Guo, K. (2010) 'Selective absorption of H_2S from a gas mixture with CO_2 by aqueous N -methyldiethanolamine in a rotating packed bed', *Industrial and Engineering Chemistry Research*, 49(13), pp. 6196-6203.

Rafiee, A., Rajab Khalilpour, K., Milani, D. and Panahi, M. (2018) 'Trends in CO_2 conversion and utilization: A review from process systems perspective', *Journal of Environmental Chemical Engineering*, 6(5), pp. 5771-5794.

Rahimi, M.R. and Mosleh, S. (2015) 'CO_2 Removal from Air in a Countercurrent Rotating Packed Bed, Experimental Determination of Height of Transfer Unit', *Advances in Environmental Technology*, 1(1), pp. 25-30.

Ramshaw, C. and Mallinson, R.H. (1981) *Mass Transfer Process*. Office, U.S.P. US4283255 A.

Rao, D.P., Bhowal, A. and Goswami, P.S. (2004) 'Process Intensification in Rotating Packed Beds (HIGEE): An Appraisal', *Industrial & Engineering Chemistry Research*, 43(4), pp. 1150-1162.

Reay, D. (2008) 'The role of process intensification in cutting greenhouse gas emissions', *Applied Thermal Engineering*, 28(16), pp. 2011-2019.

Reay, D., Ramshaw, C. and Harvey, A. (2011) *Process Intensification: Engineering for Efficiency, Sustainability and Flexibility*. Oxford, United Kingdom: Butterworth-Heinemann Publishers.

Rochelle, G.T. (2009) 'Amine Scrubbing for CO_2 Capture', *Science*, 325(5948), pp. 1652-1654.

Rogelj, J., den Elzen, M., Höhne, N., Fransen, T., Fekete, H., Winkler, H., Schaeffer, R., Sha, F., Riahi, K. and Meinshausen, M. (2016) 'Paris Agreement climate proposals need a boost to keep warming well below 2 °C', *Nature*, 534, p. 631.

Sandilya, P., Rao, D.P., Sharma, A. and Biswas, G. (2001) 'Gas-Phase Mass Transfer in a Centrifugal Contactor', *Industrial & Engineering Chemistry Research*, 40(1), pp. 384-392.

Sang, L., Luo, Y., Chu, G.-W., Zhang, J.-P., Xiang, Y. and Chen, J.-F. (2017) 'Liquid flow pattern transition, droplet diameter and size distribution in the cavity zone of a rotating packed bed: A visual study', *Chemical Engineering Science*, 158, pp. 429-438.

Schmidt, P. (1913) *Gas washer*. S1051016.

Sheng, M., Sun, B., Zhang, F., Chu, G., Zhang, L., Liu, C., Chen, J.-F. and Zou, H. (2016) 'Mass-Transfer Characteristics of the CO_2 Absorption Process in a Rotating Packed Bed', *Energy & Fuels*, 30(5), pp. 4215-4220.

Shivhare, M.K., Rao, D.P. and Kaistha, N. (2013) 'Mass transfer studies on split-packing and single-block packing rotating packed beds', *Chemical Engineering and Processing: Process Intensification*, 71, pp. 115-124.

Songolzadeh, M., Soleimani, M., Takht Ravanchi, M. and Songolzadeh, R. (2014) 'Carbon Dioxide Separation from Flue Gases: A Technological Review Emphasizing Reduction in Greenhouse Gas Emissions', *The Scientific World Journal*, 2014, p. 34.

Sreenivasulu, B., Gayatri, D.V., Sreedhar, I. and Raghavan, K.V. (2015) 'A journey into the process and engineering aspects of carbon capture technologies', *Renewable and Sustainable Energy Reviews*, 41, pp. 1324-1350.

Stanger, R., Wall, T., Spörl, R., Paneru, M., Grathwohl, S., Weidmann, M., Scheffknecht, G., McDonald, D., Myöhänen, K., Ritvanen, J., Rahiala, S., Hyppänen, T., Mletzko, J., Kather, A. and Santos, S. (2015) 'Oxyfuel combustion for CO_2 capture in power plants', *International Journal of Greenhouse Gas Control*, 40, pp. 55-125.

Sun, B., Zou, H., Chu, G., Shao, L., Zeng, Z. and Chen, J. (2012) 'Determination of Mass-Transfer Coefficient of CO_2 in NH_3 and CO_2 Absorption by Materials Balance in a Rotating Packed Bed', *Industrial & Engineering Chemistry Research*, 51(33), pp. 10949-10954.

Tan, C.-S. and Chen, J.-E. (2006) 'Absorption of carbon dioxide with piperazine and its mixtures in a rotating packed bed', *Separation and Purification Technology*, 49(2), pp. 174-180.

Toftegaard, M.B., Brix, J., Jensen, P.A., Glarborg, P. and Jensen, A.D. (2010) 'Oxy-fuel combustion of solid fuels', *Progress in Energy and Combustion Science*, 36(5), pp. 581-625.

Vaidya, P.D. and Kenig, E.Y. (2007a) 'Absorption of into aqueous blends of alkanolamines prepared from renewable resources', *Chemical Engineering Science*, 62(24), pp. 7344-7350.

Vaidya, P.D. and Kenig, E.Y. (2007b) 'CO2-Alkanolamine Reaction Kinetics: A Review of Recent Studies', *Chemical Engineering & Technology*, 30(11), pp. 1467-1474.

Veerapandian, S.K.P., Leys, C., De Geyter, N. and Morent, R. (2017) 'Abatement of VOCs Using Packed Bed Non-Thermal Plasma Reactors: A Review', *Catalysts*, 7(4), p. 113.

Wang, C., Xu, Z., Lai, C. and Sun, X. (2018) 'Beyond the standard two-film theory: Computational fluid dynamics simulations for carbon dioxide capture in a wetted wall column', *Chemical Engineering Science*, 184, pp. 103-110.

Wang, G.Q., Xu, Z.C. and Ji, J.B. (2011a) 'Progress on Higee distillation—Introduction to a new device and its industrial applications', *Chemical Engineering Research and Design*, 89(8), pp. 1434-1442.

Wang, M., Joel, A.S., Ramshaw, C., Eimer, D. and Musa, N.M. (2015) 'Process intensification for post-combustion CO_2 capture with chemical absorption: A critical review', *Applied Energy*, 158, pp. 275-291.

Wang, M., Lawal, A., Stephenson, P., Sidders, J. and Ramshaw, C. (2011b) 'Post-combustion CO_2 capture with chemical absorption: A state-of-the-art review', *Chemical Engineering Research and Design*, 89(9), pp. 1609-1624.

Wenzel, D. and Górak, A. (2018) 'Review and analysis of micromixing in rotating packed beds', *Chemical Engineering Journal*, 345, pp. 492-506.

Wilcox, J., Rochana, P., Kirchofer, A., Glatz, G. and He, J. (2014) 'Revisiting film theory to consider approaches for enhanced solvent-process design for carbon capture', *Energy & Environmental Science*, 7(5), pp. 1769-1785.

Wojtasik, J., Gładyszewski, K., Skiborowski, M., Górak, A. and Piątkowski, M. (2018) 'Enzyme-enhanced CO_2 absorption process in rotating packed bed', *Chemical Papers*, pp. 1–9.

Xie, P., Lu, X., Ding, H., Yang, X., Ingham, D., Ma, L. and Pourkashanian, M. (2019) 'A mesoscale 3D CFD analysis of the liquid flow in a rotating packed bed', *Chemical Engineering Science*, 199, pp. 528-545.

Xie, P., Lu, X., Yang, X., Ingham, D., Ma, L. and Pourkashanian, M. (2017) 'Characteristics of liquid flow in a rotating packed bed for CO_2 capture: A CFD analysis', *Chemical Engineering Science*, 172, pp. 216-229.

Yan, Y. and Chen, C.-C. (2010) 'Thermodynamic modeling of CO_2 solubility in aqueous solutions of NaCl and Na_2SO_4', *The Journal of Supercritical Fluids*, 55(2), pp. 623-634.

Yang, K., Chu, G., Zou, H., Sun, B., Shao, L. and Chen, J.-F. (2011) 'Determination of the effective interfacial area in rotating packed bed', *Chemical Engineering Journal*, 168(3), pp. 1377-1382.

Ying, J. (2013) *Mass Transfer Kinetics of carbon dioxide into concentrated aqueous solutions of monoethanolamine*. PhD thesis. Telemark University College, Norway

Ying, J. and Eimer, D.A. (2013) 'A Study of Mass Transfer Kinetics of Carbon Dioxide in (Monoethanolamine + Water) by Stirred Cell', *Energy Procedia*, 37(0), pp. 2180-2187.

Ying, J., Knutsen, A.R. and Eimer, D.A. (2017) 'Mass Transfer Kinetics of CO_2 in Loaded Aqueous MEA Solutions', *Energy Procedia*, 114, pp. 2088-2095.

Yu, C.H., Cheng, H.H. and Tan, C.S. (2012) 'CO_2 capture by alkanolamine solutions containing diethylenetriamine and piperazine in a rotating packed bed', *International Journal of Greenhouse Gas Control*, 9(0), pp. 136-147.

Yu, C.H. and Tan, C.S. (2013) 'Mixed alkanolamines with low regeneration energy for CO_2 capture in a rotating packed bed', *11th International Conference on Greenhouse Gas Control Technologies*, 37, pp. 455-460.

Yu, C.H., Wu, T.W. and Tan, C.S. (2013) 'CO_2 capture by piperazine mixed with non-aqueous solvent diethylene glycol in a rotating packed bed', *International Journal of Greenhouse Gas Control*, 19(0), pp. 503-509.

Zhao, B., Tao, W., Zhong, M., Su, Y. and Cui, G. (2016) 'Process, performance and modeling of CO_2 capture by chemical absorption using high gravity: A review', *Renewable and Sustainable Energy Reviews*, 65, pp. 44-56.

Zhao, H., Shao, L. and Chen, J.-F. (2010) 'High-gravity process intensification technology and application', *Chemical Engineering Journal*, 156(3), pp. 588-593.